Holistic Modeling, Design & Analysis of Integrated Stirling and Auxiliary Clean Energy Systems for Combined Heat and Power Applications

Amrit Om Nayak

A thesis

submitted in partial fulfillment of the

requirements for the degree of

Master of Science in Mechanical Engineering

University of Washington

2015

Committee:

Brian C. Fabien

John C. Kramlich

Igor Novosselov

Program Authorized to Offer Degree:

Mechanical Engineering

University of Washington

Abstract

Holistic Modeling, Design & Analysis of Integrated Stirling and Auxiliary Clean Energy Systems for Combined Heat and Power Applications

Amrit Om Nayak

Chair of the Supervisory Committee:

Professor Brian C. Fabien

[Associate Dean, Academic Affairs

College of Engineering]

Department of Mechanical Engineering

The research revolves around the development of a model to design and analyze Stirling systems. Lack of a standard approach to study Stirling systems and difficulty in generalizing existing approaches pose stiff challenges. A stable mathematical model (integrated second order adiabatic and dynamic model) is devised and validated for general use. The research attempts to design compact combined heat and power (CHP) system to run on multiple biomass fuels and solar energy. Analysis is also carried out regarding the design of suitable auxiliary systems like thermal energy storage system, biomass moisture removal system and Fresnel solar collector for the CHP Stirling system.

TABLE OF CONTENTS

LIST OF TABLES

LIST OF FIGURES

GLOSSARY

TPES – Total primary energy supply

Mtoe – Million tonne of oil equivalent (1 toe ≈ 42 gigajoules)

PV – Photovoltaic

CSP – Concentrated Solar Power

AC – Alternating Current

DC – Direct Current

GWth – Gigawatt Thermal

CHP – Combined Heat and Power

HP – Horsepower

RHP – Right Half Plane

LHS – Left hand side

FPSE – Free Piston Stirling Engine

PCM – Phase Change Material

TESS – Thermal Energy Storage System

BMRS – Biomass Moisture Removal System

CSP – Concentrated Solar Power

LFCSP – Linear Fresnel Concentrated Solar Power

IC – Internal combustion

EC- External combustion

STE-SPP – Hybrid solar thermal energy Stirling power plant

MSPH – Mini Stirling plant – hybrid

NOMENCLATURE

For dynamic analysis

Symbol	Description
A	Cylinder Area
A_p	Working Piston Area
D	Damping Constant
F_p	Pressure Forces
F_{sl}	Sliding Friction Force
i	$\sqrt{-1}$
K	Spring Constant
m	Mass of Component
m_{tg}	Total mass of gas
p	Pressure
p_s	Pressure due to spring
P_o	Mean cycle pressure
P	Power
Q	Stored energy/energy dissipated per cycle
R	Gas constant
s	Laplace transform variable
t	Time
T_c	Cold end temperature
T_h	Hot end temperature
T_r	Regenerator effective temperature
V	Phasor, volume
V_c	Compression space volume
V_e	Expansion space volume

V_h	Heater volume
V_k	Cooler volume
V_r	Regenerator void volume
V_{cs}	Compression space swept volume
V_{es}	Expansion space swept volume
W	Work
x	Displacement
$\dot{x}$	Velocity
$\ddot{x}$	Acceleration
$\hat{x}$	Transformed displacement (laplacian)
X	Amplitude, phasor
Φ	Phase angle (piston to displacer)
θ	Phasor angle
Ω	Frequency (rad/s)
Subscripts	
c	Cylinder, Operating conditions
d	Displacer
p	Working piston
s	Spring
v_d	Viscous damping
s_d	Spring damping

<u>For adiabatic analysis</u>

2 x R2= stroke of power piston, in cm

3 x RC= stroke of displacer, in cm

AL=phase lag

DB= displacer diameter, in cm

DC= diameter inside engine cylinder, in cm

Dp= change in pressure, in MPa

f=crank angle

gAck=mass flow from compression space to cold end heat exchanger space

gAhe= mass flow from hot end heat exchanger space to expansion space

gAkr= mass flow from cold end heat exchanger to regenerator space

gArh= mass flow from regenerator space to hot end heat exchanger space

h= clearance between cylinder top/bottom and displacer top/bottom when displacer is at topmost/bottommost position respectively.

LC= cold end heat exchanger length

LH= hot end heat exchanger length

M= total mass of working gas present in the engine, in gram mole

mc=compression space mass

me=expansion space mass

mec=cold end heat exchanger mass

meh=hot end heat exchanger mass

mr=regenerator mass

p=instantaneous pressure

R= universal gas constant= 8.314 J/gmol-K

r=C_p/C_v for the working gas

Tc=compression space temperature

Tce=cold end heat exchanger temperature

Te=expansion space temperature

The=hot end heat exchanger temperature

Tr=regenerator temperature

Vc=Cold end volume

Vcd=cold end dead volume

Vce=cold end heat exchanger volume

Vd=cold end maximum displacer volume

Ve=Maximum Hot end volume

Vhd=hot end dead volume

Vhe=Hot end heat exchanger volume

Vp=cold end maximum piston volume

Vr=regenerator volume

DVc= change in volume in compression space

DVe= change in volume in expansion space

Dmc= change in mass in compression space

Dme= change in mass in expansion space

Dmce= change in mass in cold end heat exchanger space

Dmhe= change in mass in hot end heat exchanger space

Dmr= change in mass in regenerator space

Tck, The= conditional temperatures varying as per instantaneous mass flow direction

ACKNOWLEDGEMENTS

I would like to acknowledge the immense contribution of the following people during the course of my research.

• Prof. Brian Fabien for his patience, guidance and unending support.

• Prof. John Kramlich for his vast knowledge and expert views on thermal cycles.

• Prof. Igor Novosselov for his support and the wonderful brainstorming sessions & suggestions during the weekly meetings in combustion laboratory.

• Mr. Nitish Hirve, graduate student and fellow researcher for his ideas, patience and support during the entire process.

• Dr. James Klett from Oakridge National Laboratory (ORNL), the inventor of 'graphite foam', for his valuable inputs on regenerator design and permitting us to use his research in our work.

• Mr. Eamon McQuaide and Mr. Veasna for their invaluable knowledge & expertise in various manufacturing processes and system designs in the Mechanical workshop.

• Millions of people around the globe without access to energy or electricity who have constantly inspired me to stay focused in my work!

• And last but most importantly, my mother & father for their unending love and support.

CHAPTER ONE

1. Introduction

1.1 World Energy Requirement

Energy drives the modern world. Rising populations and our insatiable thirst for development has been consistently increasing the demand for cheap energy and power. However, unprecedented growth in the 20th and 21st centuries has had its fair share of risks and problems. Energy is at the core of many of the greatest issues and challenges facing the world today. Environmental pollution and global warming are huge issues that promise to change the face of the planet in unimaginable and irreversible ways. It is necessary that governments and industries around the globe join hands to reverse this trend.

Cheap energy is the foundation of industrial growth. Fossil fuels have satisfied our need for cheap power for over a century and half. Half of the world's electricity production is from cheap but environmentally harmful coal. A major portion of our energy needs are also met by petroleum based fossil fuels which release harmful gases and toxic particulate matter when combusted. The following diagram illustrates this trend with better clarity. The pie chart shows the contribution of different fuel sources in the total primary energy supply in the years 1973 and 2012 [1]. One cannot help but notice the slight decrease in dependence on oil but an increase in coal usage. We also notice a 54% increase in total primary energy supply. This helps us shed light on the fact that dependence on oil has increased by 1.5 times while that on coal has increased by an astonishing 2.6 times! Rapid

industrialization and monopoly of vested interests in the oil and coal industry are undermining the growth of other clean energy technologies.

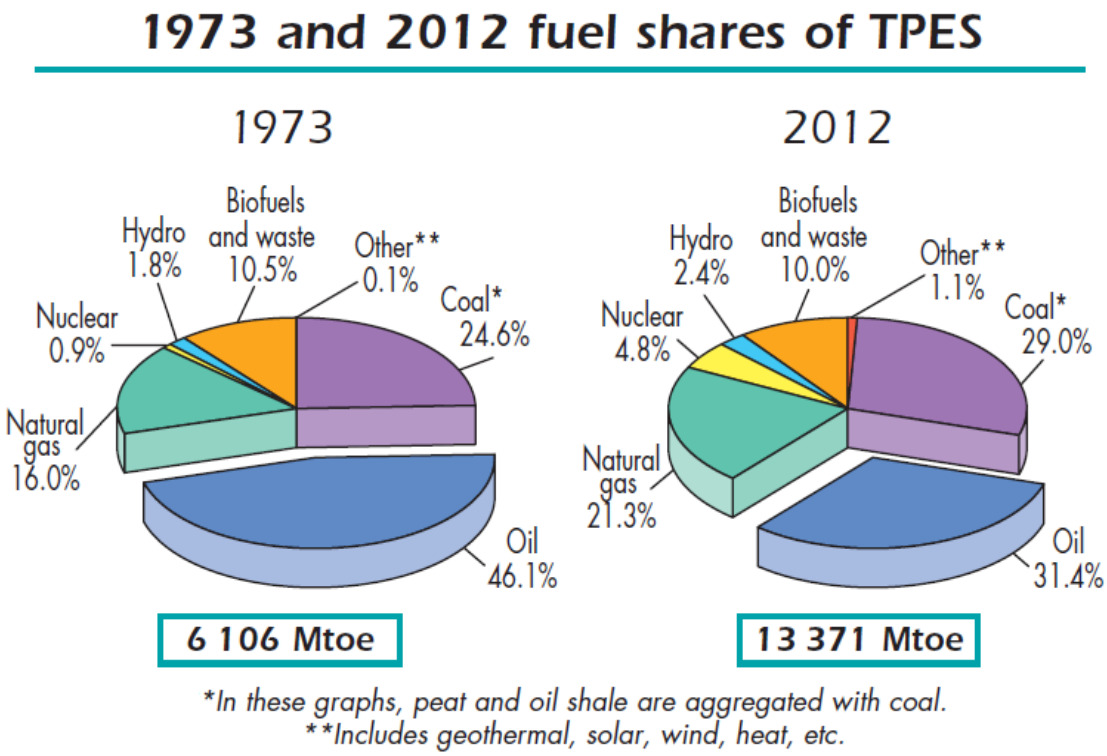

Figure 1 Fuel shares of total primary energy supply in 1973 and 2012 [1]

Renewable energy sources are the need of the hour. It is imperative to steadily increase our dependence on clean energy sources to strive for a sustainable future. Growth will not be possible unless cost of energy from renewable resources is on par or comparable with fossil fuel driven systems. Typically, lower operating costs due to lack of specific fuel requirements, flexibility of input heat source, greater security of supply, independence from foreign fuel suppliers and immunity to fuel price fluctuations make up for the disadvantages of higher costs. Renewable energy technologies are in use all around the world today and there is a steady increase in their usage.

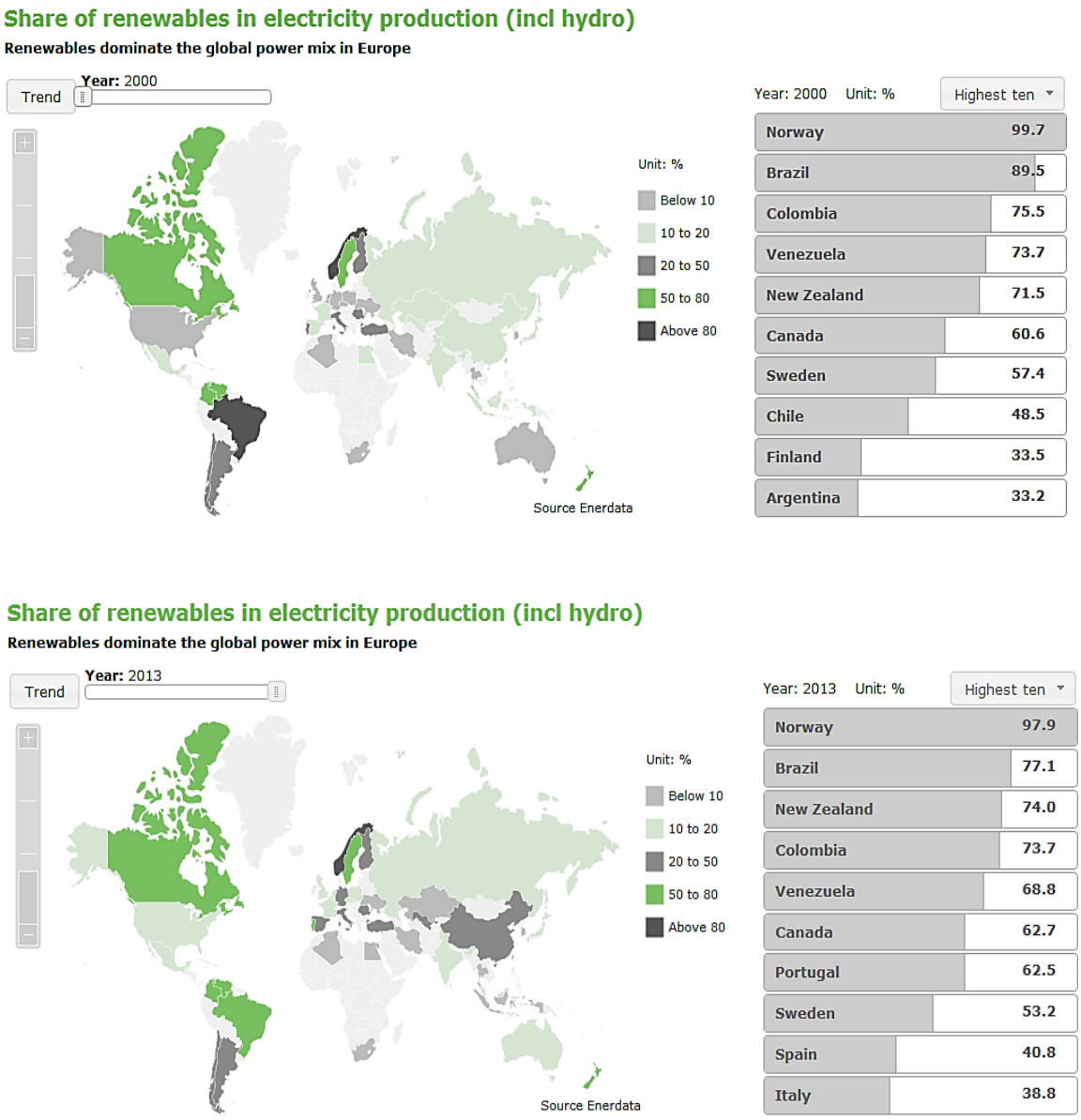

Figure 2 Share of Renewables in electricity production (including hydro power) [7]

1.2 Comparing Stirling systems and competing renewable energy technologies

Si. No.	Wind power	Solar PV	Solar CSP	Stirling system
Advantages:				
1	Little Pollution	Pollution free during use	Pollution free during use	High working efficiency and flexible input heat source.
2	Long term potential	Grid connected solar electricity reduces transmission/distribution losses	Grid connected solar electricity reduces transmission/distribution losses	Huge long term potential
3	Low capital and operating Cost	Low operating costs and little maintenance needed after initial set up.	Low operating costs and little maintenance needed after initial set up.	Low capital cost and running costs
4	Clearing of woods often unnecessary	The amount of solar energy intercepted by the Earth every minute	The amount of solar energy intercepted by the Earth every minute	Hybrid nature of the device allows for use of plentiful solar energy and

		is greater than the amount of fossil fuel the world uses every year.	is greater than the amount of fossil fuel the world uses every year.	biomass which is abundant and cheap.
5	Scalable in size	Scalable in size	Scalable in size	Compact size and scalable to any size based on requirement
Disadvantages:				
1	Highly taxed	Large capital costs	Large capital costs	Policy dependent
2	Hazard to birds and ecosystem	Intermittency	Intermittency	CO_2 & CO emissions
3	Noisy	Low energy output in high altitudes & cloudy region	Low energy output in high altitudes & cloudy regions	Depends heavily on commercialization of biomass
4	Depreciation of property value	AC to DC conversion	AC to DC conversion	Conversion losses
5	Variable efficiency	Limited power density	Limited power density	Material constraints
6	Land intensive	Land intensive	Land intensive	Depends on input heat source

Table 1 Comparison between Stirling systems and competing technologies

Parameter	Solar CSP	Solar PV	Wind Power	Stirling systems	Biomass Power Generation Systems
Pollution	1	1	1	1	1
Capex & Opex	0	0	1	1	1
Maintenance	1	1	1	1	0
Reliability	1	1	1	1	0
Growth Potential	1	1	1	1	1
Land Req.	0	0	0	1	1
Installation	0	1	1	1	1
Scalability	1	1	1	1	0
Dependence (Taxes & Laws)	0	0	0	0	0
Levelized Cost Of Energy	0	0	0	1	1
Dependence (Environmental)	0	0	0	1	1

Efficiency	0	0	1	1	1
TOTAL (Out Of 12)	5	6	8	11	8

Table 2 Decision matrix to compare Stirling systems and competing technologies

We observe that Stirling systems have an edge over parallel competing technologies as evident from the above two comparison tables.

1.3 Biomass as a clean fuel for Stirling systems

Combustion of organic matter invariably leads to emission of greenhouse gases like carbon dioxide and carbon monoxide. Biomass combustion therefore by definition must also pollute the environment as biomass is organic matter. However, recent research indicates otherwise. A study by Evan Hughes [8] lists the following reasons in support of biomass as a clean and green fuel.

1) Biomass results in emissions of CO_2 and other green-house gases. However, CO_2 derived from plant biomass was removed from the atmosphere within the recent past, typically one year to a few decades. By contrast, fossil fuels locked up their carbon over millions of years, a process now being reversed over a period of centuries.
2) As a substitution for fossil fuels, biomass mitigates global warming even in the absence of any renewed CO_2 fixation. If energy crops are used, biomass burned needs to be replaced in a reasonable time (typically one to ten years) with new

biomass. In a typical energy crop operation, biomass is used at the same rate it is produced.

3) Biomass power uses combustion technology, and hence is perceived by some as not green. Today, combustion systems operate with highly controlled emissions. Current developments include gasification technologies (for both biomass and coal). Gasifiers provide higher efficiency power generation and achieve higher emissions control than direct combustion technologies.
4) Most biomass fuels are significantly lower in air pollutants than most coals. Biomass has virtually no sulfur (often less than 1/100 that of coal), low nitrogen (less than 1/5 that in coal), and low-ash content. Exceptions can be identified and controlled. Compared to natural gas, however, biomass cannot claim any inherent advantage in terms of emissions, except for greenhouse gas emissions.

1.4 Research focus

The research primarily focusses on the development of a stable mathematical model which integrates in depth second order adiabatic and dynamic analysis. An integrated code is formulated in MATLAB in order to design and analyze Stirling engines of various configurations. The code is validated for general usage to design Stirling systems. Attempts are made to design a small hybrid CHP system which will run on multiple biomass fuels and solar energy. Preliminary analysis is carried out to design suitable auxiliary systems for the same. These systems include a thermal energy storage system using heat storage fluids, Fresnel solar collector and a biomass moisture removal system.

CHAPTER TWO

2. Stirling Engine

2.1 Background

Robert Stirling invented the Stirling engine in 1816 [2]. Stirling engines were safe as they would not explode unlike steam engines, due to lower operating pressure. A Stirling engine operates on a closed loop thermodynamic cycle. Difference in temperature causes compression and expansion of the gaseous working medium. This work is tapped by different arrangements of pistons, which reciprocate with the changes in the internal pressure. The flow of the working medium is controlled by changes in the volume of the hot and cold spaces, without the use of valves.

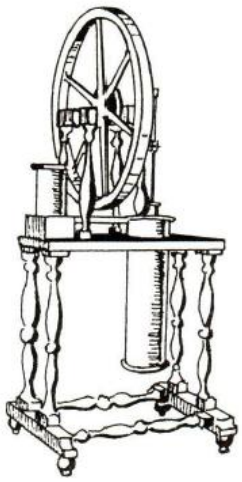

Figure 3 First working Stirling engine (ϒ - type) from 1815 [9]

Robert Stirling applied for patents for this engine and the economizer in 1816. The "economizer" or regenerator is the most important part of the patent that Robert Stirling received. This patent was outstanding as it predated much of the study of thermodynamics. It is believed that the reason for Robert Stirling's efforts were

driven by his concerns regarding the extensive use of relatively unstable steam engines back then.

The growth of Stirling engines was overshadowed by the gasoline internal combustion engine because of the time it takes for a Stirling engine to heat up enough to get moving. Lately, environmental issues, the need for cleaner alternatives and depleting fossil fuel reserves has revived interest in Stirling engine.

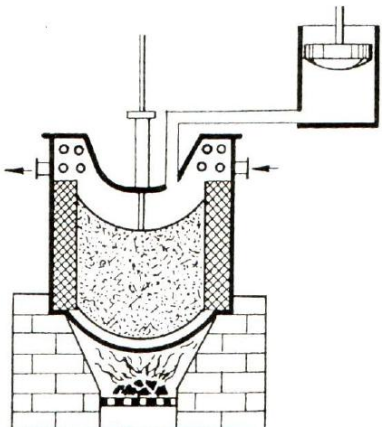

Figure 4 Pressurized cycle engine by Stirling brothers in 1845 [9]

The full potential of Stirling engine has largely remained unused to date. The beauty of Stirling engine lies in the fact that it can theoretically run on any fuel or heat source. However, we focus only on heat energy derived from renewable sources here.

2.2 The ideal Stirling cycle

The ideal Stirling cycle consists of four processes which together form a closed cycle: two isothermal and two isochoric processes. Area under the P-v diagram is the work done and the area under the T-s diagram is the heat. Depending on the

direction of integration, the work and heat will either be added to or subtracted from the system. Only the isothermal processes produce work. To facilitate the exchange of work to and from the system a flywheel or a spring system (in case of free piston Stirling systems) must be integrated into the design which will store energy during the working stroke and give it back to the system during the non-working stroke for completion of the full cycle. Heat transfer takes place during all the processes.

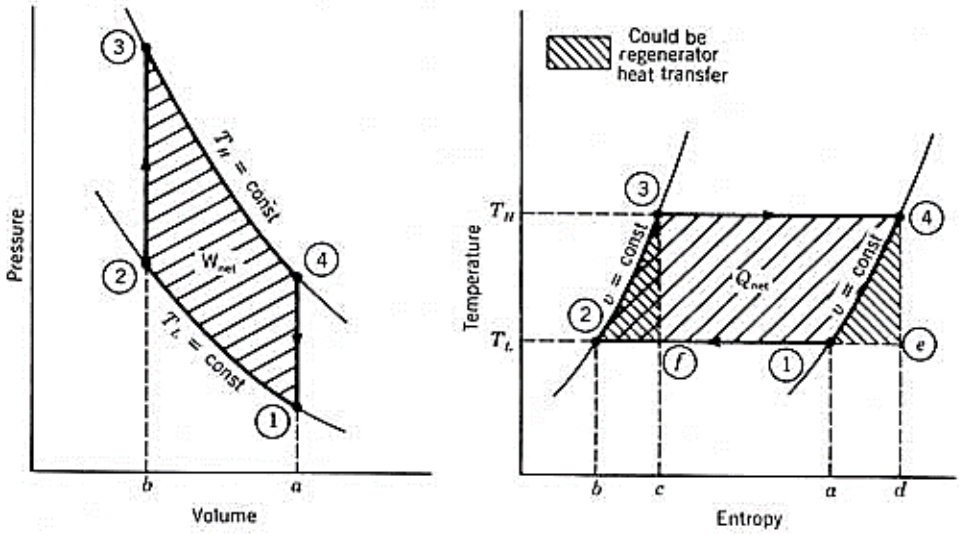

Figure 5 P-V & T-S graphs of ideal Stirling cycle [10]

Area 1-2-3-4 on the P-V diagram represents the net work produced by the closed ideal Stirling cycle. From the first law of thermodynamics, net work output must equal the net heat input represented by the area 1-2-3-4 on the T-s diagram. The Stirling cycle can best approximate the Carnot cycle out of all gas powered engine cycles by integrating a regenerator into the design. The regenerator will take heat from the working gas in process 4-1 and return the heat in process 2-3 of the cycle.

Process 1-2 (Isothermal Compression):

Heat rejection to low temperature heat sink

$_1Q_2$ = area *1-2-b-a* on T-s diagram

Work is done on the working fluid (energy exchange from flywheel/spring system)

$_1W_2$ = area *1-2-b-a* on P-v diagram

Process 2-3 (Isochoric heat addition):

Heat addition (energy exchange from regenerator)

$_2Q_3$ = area *2-3-c-b* on T-s diagram

$_1W_2$ = 0 (No work is done)

Process 3-4 (Isothermal Expansion):

Heat addition from high temperature heat sink

$_3Q_4$ = area *3-4-d-c* on T-s diagram

Work is done by the working fluid (energy exchange to flywheel/spring system)

$_3W_4$ = area *3-4-a-b* on P-v diagram

Process 4-1 (Isochoric heat rejection):

Heat rejection (energy exchange to regenerator)

$_4Q_1$ = area *1-4-d-a* on T-s diagram

$_4W_1$ = 0 (No work is done)

2.3 The real Stirling engine cycle

The real Stirling engine cycle is shown below. Here, work is done during processes 2-3 and 4-1 unlike the zero work in the ideal cycle. One of the major causes for inefficiency of the real Stirling cycle involves the regenerator. The regenerator adds friction to the flow of

the working gas. For the real cycle to approximate the Carnot cycle, the regenerator would have to reach the temperature of the high temperature thermal sink so that $T_R=T_H$. A measure of the regenerator effectiveness is given by

$$e = \frac{T_R - T_L}{T_H - T_L}$$ with the value of e=1 being ideal.

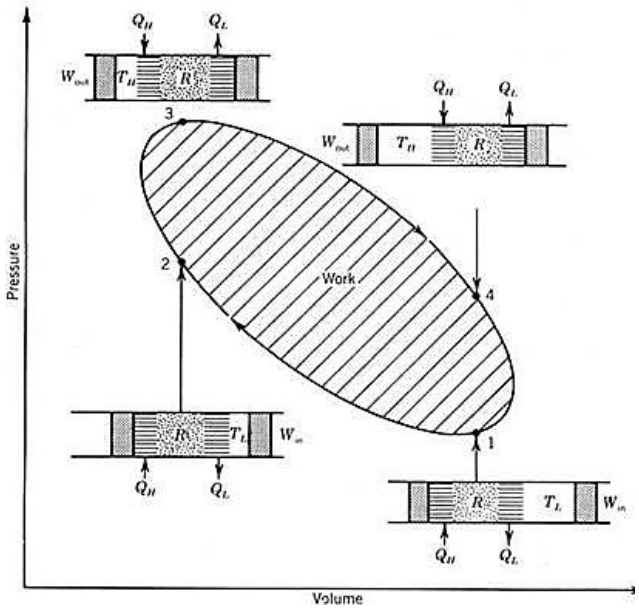

Figure 6 Real Stirling engine cycle [10]

A major cause for inefficiencies is dead volume or the part of working gas that doesn't participate or contribute to work output. This involves the volume that does not participate in the swept volume of the piston stroke. Martini (2004) [11] states that the relationship between the percentage of dead volume in the system to the decrease in work done per cycle is linear. Hence, an engine with 20% dead volume will have a power output of 80% of the maximum total power with zero dead volume. However, dead volume cannot be completely eliminated because addition of internal heat exchangers, clearances, regenerators etc. are required to improve heat exchange or heat transfer efficiency of the real system.

2.4 Types of Stirling engine designs

Stirling engines require their heat sources and sinks to be oriented to ensure that sufficient volume of working fluid is heated and cooled at the appropriate point in the cycle. These orientations have been classified into different engine design types, designated alpha, beta, and gamma [12].

Alpha type engines differ by the method of separation of hot expansion and cold compression chambers. The hot and cold chambers are distinctly separated from one another, usually in separate cylinders [16]. The pistons are linked to the same crankshaft. The two piston volumes are linked with the regenerator placed in the path of the fluid between them [13]. The clear separation of heat source and sink prevents premature mixing of hot and cold working fluid. However, need for connections between the pistons increases the number of parts resulting in increased chance of leakage around joints and connections. Intense heat at the expansion chamber can cause leaks.

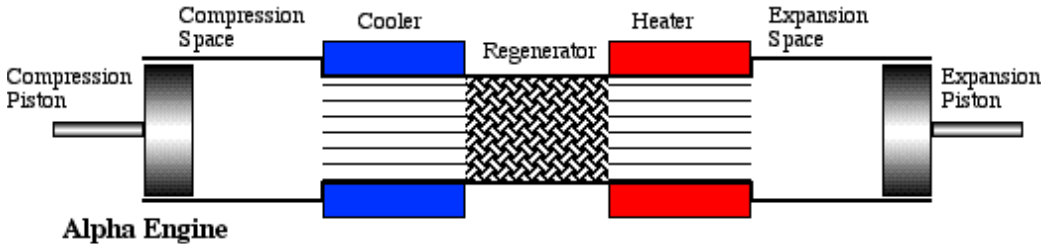

Figure 7 Simplified α - Stirling engine

Beta type engines lack separate chambers for the hot expansion and cold compression stages of the cycle. The expansion and compression actions are performed in the same cylinder with only a single piston to derive power from the engine. A displacer (a loosely fit non-sealing piston) is also inside the cylinder in

line with the power piston. Displacer forces the working fluid to flow around it between the expansion and compression sections of the cylinder. Expansion and contraction of the working fluid drives the power piston, which in turn drives the displacer, restarting the cycle. Beta type engines do not have a hot seal, with the only seal being around the power piston in the compression section of the cylinder. Hence, it is much easier to contain leaks. However, regulating interference between the cycles is more difficult in the beta type design because heating and cooling occur in the same cylinder [16].

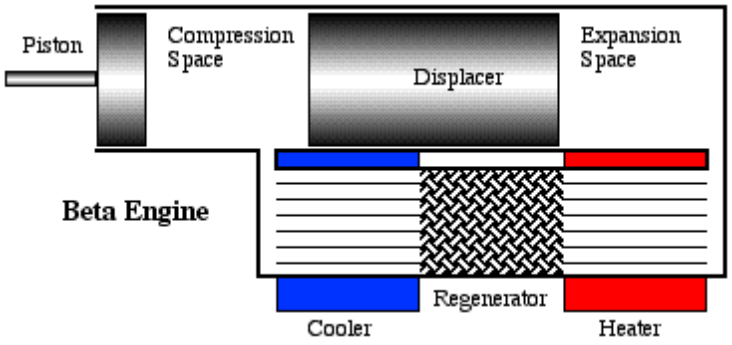

Figure 8 Simplified β - type Stirling engine [14]

Gamma type engines are similar to beta type engines, with the hot expansion and cold compression stages occurring in the same cylinder and a displacer forcing the working fluid to flow between the sections. But the power piston in gamma type engines is not in line with the displacer. The power piston is in a separate cylinder that is connected to the compression section of the first cylinder. This configuration allows the power piston to not be limited by the displacer orientation or size. Gamma type engines have same benefits as beta types in avoiding hot seals, and the same concerns with regulating interference between the cycles. The additional cylinder in gamma types translated into greater dead volume (working fluid which

doesn't contribute to the expansion or compression stages). This results in low compression ratio and lower power output [16].

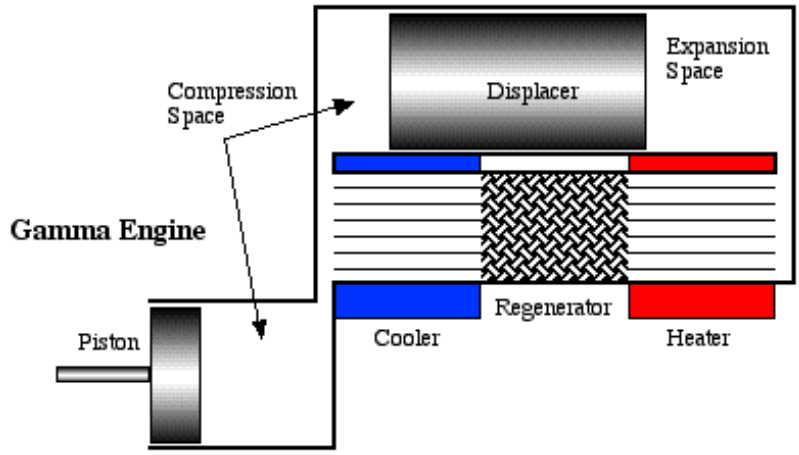

Figure 9 Simplified ϒ - type Stirling engine [15]

Modern Stirling systems are classified as: the kinematic and the Free-Piston Stirling engine (invented by Prof. William Beale). The kinematic engines have mechanical devices, like a crankshaft, or swash plate, that coordinate piston movement through connecting rods. Free piston Stirling engines, have no mechanical devices to control piston motion. The pistons are moved by pneumatic forces created by the internal pressure variations within the engine. Since piston motion cannot be controlled by an external mechanical device, optimum performance of these engines is difficult to achieve. Free Piston Stirling engines can be hermetically sealed, thereby, reducing the seal problem possessed by kinematic engines [17].

Depending on the arrangement and type, Stirling engines have a wide variety of applications. Table 3 shows some of the characteristics of Stirling engines and their applications.

Stirling Engine Characteristics and Applications.

APPLICATION AREA	EXTERNAL HEAT SOURCE	QUIETNESS AND SMOOTH-NESS	HIGH EFFICIENCY	REJECT HEAT AVAIL-ABILITY	VERY LONG LIFE/HIGH RELIABIL-ITY
Artificial heart power	essential	essential	important	essential	essential
Underwater power unit	essential	important	important	important	important
Space power	essential	important	essential		essential
Remote small power sources	essential		essential		essential
Military ground power	important	essential			important
Heat pump driver	important	important	important	important	
Automotive engine	important	important	essential		important
Solar thermal conversion	essential		important		

Table 3 Stirling Engine characteristics and applications (Reproduced from Walker, Stirling engines [18])

2.5 Advances in Stirling technology

Several design advancements have been made since the revised Stirling design in 1845. Innovations like the open cycle engine (Ericsson, 1860) were made, which replenished the hot air in each cycle with fresh cold air. This eliminated cooling difficulties but caused great heat losses at an efficiency of just over 2% [9]. Efforts were made to increase heat transfer area by use of a toothed displacer arrangement (Young and Kirk, 1865). Experiments regarding discontinuous displacer motion (Lauberau, 1869) failed due to mechanical complexity [9]. Swedish inventor, John Ericsson built the first solar powered Stirling Engine in 1870. Its performance is unknown though Ericsson is recorded as saying that "A solar engine of one horse-power demands the concentration of solar heat from an area of 10 square feet."

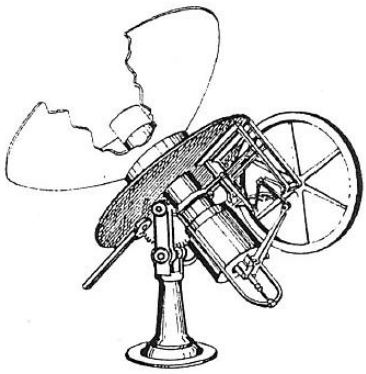

Figure 10 First solar Stirling engine by John Ericsson in 1870 [9]

Rider-engine, built in 1875 by the Rider Ericsson Engine Company, was the first recorded α-type Stirling Engine. A.E.H. Robinson, in 1880, devised a new design which featured an air pre-heater. It channeled incoming combustion air around the hot exhaust in order to pre-heat it, resulting in an improvement in overall efficiency by almost three times [9]. After 1937, the Philips Corporation developed a number of engine ranging in power output from 6 Watts to 1 HP [29]. During World War II, a patent was granted for the double-acting Stirling Engine, named as Type 19 by Philips. Subsequently, the type 20 engine was designed, a 4-cylinder double-acting engine with a swept volume of 2.9 litres and a target power output of 50 HP. It was fast and smooth, had good torque and a respectable efficiency of 15% [29].

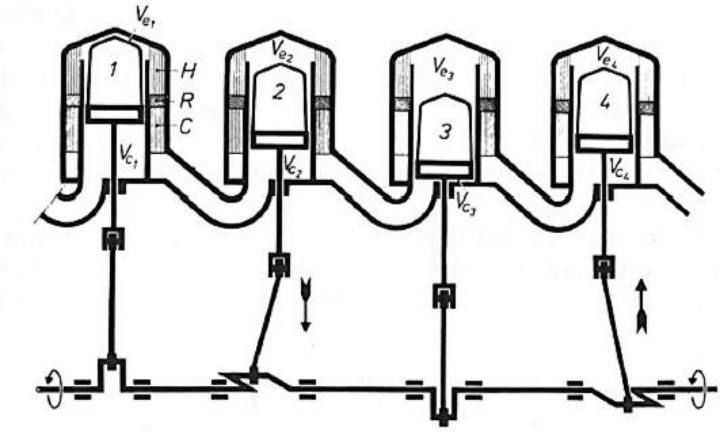

Figure 11 Phillips 4-cylinder Type 19 double acting engine [29]

Philips invented the rhombic-drive mechanism in 1953. It was demonstrated in a small beta-type engine solving the problem of balancing a small displacer-type engine, with better piston sealing due to lack of side-loading forces. Another major benefit was being able to pressurize the engine working gas without pressurizing the crankcase, meaning a significant weight and cost reduction. This was possible due to perfect seals around the piston rod as no lateral thrust acted upon them [29]. Advantages included higher possible working pressures, fewer vibrations and a compact design.

In 1978, a new Stirling was designed to power a submarine. A Stirling engine is suitable for this as they are silent and vibration free (making the submarines harder to detect), they don't require air for combustion (depending on heat source) and they are surrounded by a very effective heat sink, the sea.

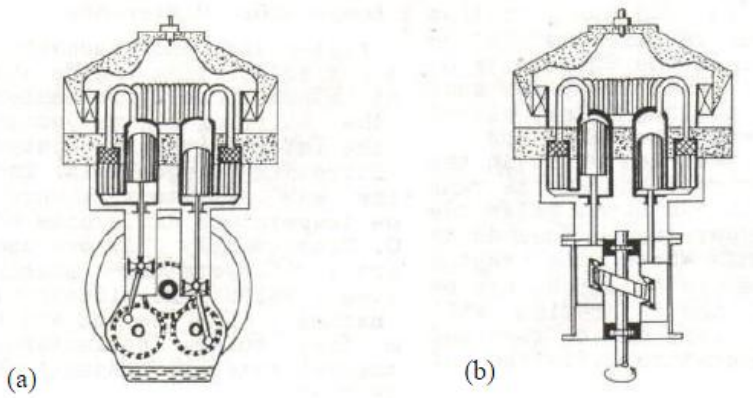

Figure 12 a) United Stirling submarine engine and (b) later improved version (right) with wobble-plate drive [9]

McDonnell Douglas designed a large solar parabolic mirror setup in 1985, which could track the sun focusing its energy on a centrally mounted Stirling engine that could reach up to 1430°C [9]. They used Stirling engines made by United Stirling,

which could produce 25kW of electrical power with a thermal to electric efficiency of 31% [9].

Figure 13 McDonnell Douglas Solar Stirling engine system [31]

These large parabolic mirrors were used in 2005 in a joint venture between Southern California Edison and Stirling Energy Systems. 20,000 solar Stirling dishes were installed into a 1,800 ha area of the Mojave Desert, for a total power generating capacity of 500 MW – the largest of its type in the world at the time of the agreement (until the 900 MW project in Imperial County, Southern California was announced). The project was expanded up to 34,000 dishes totaling 850 MW. The advantages of solar Stirling systems is high efficiency (exceeding that of parabolic troughs and non-concentrated photovoltaic), relatively low cost per kW compared with other solar technology and high life expectancy (the Stirling engine used is the 25kW unit same as that pictured in Figure 18 (a), and has been tested for 26,000 hours of continuous operation) [32].

CHAPTER THREE

3. Design of Stirling engine for the CHP system

Free piston Stirling engine configuration is chosen for the CHP system design. Potential advantages of free piston Stirling engine are: high efficiency, few moving parts, multi–fuel capability and the possibility of generating power over a wide range of source temperatures [27]. It allows for hermetically sealing the engine and hence is not subject to problems arising out of dirt ingress or leakage. Linear dynamics is applied to the system to understand the requirements for oscillation and the general behavior under load.

3.1 Dynamic analysis of the simplified free piston Stirling engine design

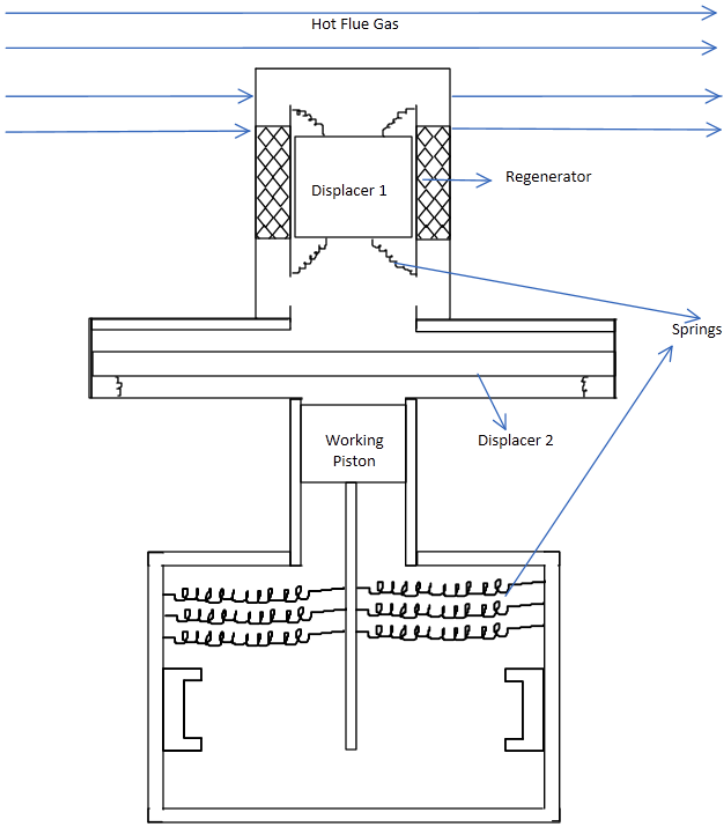

Figure 14 Schematic of simplified free piston Stirling engine

We assume the displacer 2 to be non-existent to simplify our present analysis. We also assume that the same type of springs are used throughout. The orientations of the springs are symmetric or parallel subject to their placement in the design.

Equations of motion

Displacer 1

Force balance is given by:

$$F_{total} = -F_{vd} + F_{net(gas\ \&\ spring)} - F_{sd} \qquad \text{[Equation 3.1]}$$

We now get our initial equation of motion as:

$$m_{d1}\ddot{x}_{d1} = -D_{d1}\dot{x}_{d1} + A_{d1}(p_{s1} - p) \qquad \text{[Equation 3.2]}$$

Here, D_{d1} is damping on displacer due to viscous forces on the moving gas. For 'n' number of springs attached to the displacer, we get:

$$m_{d1}\ddot{x}_{d1} = -D_{d1}\dot{x}_{d1} + A_{d1}(np_{s1} - p) \qquad \text{[Equation 3.3]}$$

But we know that here 'p_{s1}' acts over the entire area A_{d1} and its 'Sin ϒ' component acts over the displacer.

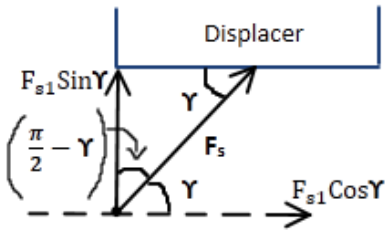

Also from above spring orientation diagram, we get

$$x_{s1} = x_{d1}Sin\ \Upsilon \qquad \text{[Equation 3.4]}$$

Actual spring pressure on displacer 1 = $np_{s1}\text{Sin}\,\Upsilon = \frac{nK_{s1}x_{s1}\,\text{Sin}\,\Upsilon}{A_{d1}} = \frac{nK_{s1}x_{d1}\text{Sin}^2\Upsilon}{A_{d1}}$

[Equation set 3.5]

We now get,

$$m_{d1}\ddot{x}_{d1} = -D_{d1}\dot{x}_{d1} + A_{d1}\left(\frac{nK_{s1}x_{d1}13\text{Sin}^2\Upsilon}{A_{d1}} - p\right) \quad \text{[Equation 3.6]}$$

Now, we generalize the above equation for any orientation of the springs and replace '$\text{Sin}^2\Upsilon$' by 'δ_1' to represent the angular component and get:

$$m_{d1}\ddot{x}_{d1} = -D_{d1}\dot{x}_{d1} + A_{d1}\left(\frac{nK_{s1}x_{d1}\delta_1}{A_{d1}} - p\right) \quad \text{[Equation 3.7]}$$

Again, considering spring damping and other factors, we rewrite [Equation 3.3] as:

$$m_{d1}\ddot{x}_{d1} = -D_{d1}\dot{x}_{d1} - D_{s1}\dot{x}_{d1}\delta_1 + A_{d1}\left(np_{s1}\delta_1 + \frac{m_{d1}}{m_c}p - p\right)$$

[Where $D_{s1} = 2\xi\sqrt{m_{d1}K_{s1}}$ and ξ = damping ratio]

[Equation set 3.8]

Hence, the equation of motion for displacer 1 is given by:

$$m_{d1}\ddot{x}_{d1} = (-D_{d1} - D_{s1}\delta_1)\dot{x}_{d1} + A_{d1}(np_{s1}\delta_1 + \frac{m_{d1}}{m_c}p - p) \quad \text{[Equation 3.9]}$$

Linearizing the above equation, we get,

$$m_{d1}\ddot{x}_{d1} = (-D_{d1} - D_{s1}\delta_1)\dot{x}_{d1} + A_{d1}\left[\left(n\frac{\partial p_{s1}}{\partial x_{d1}}\delta_1 + \frac{m_{d1}}{m_c}\frac{\partial p}{\partial x_c} - \frac{\partial p}{\partial x_{d1}}\right)x_{d1} - \frac{\partial p}{\partial x_p}x_p\right]$$

[Equation 3.10]

Taking Laplace transform of [Equation 3.10], we get:

$$[m_{d1}s^2 + (D_{d1} + D_{s1}\delta_1)s + K_{d1}]\hat{x}_{d1} = -\left(\frac{\partial p}{\partial x_p}A_{d1}\right)\hat{x}_p + (\text{initial conditions})_{d1}$$

[Equation 3.11]

Now, we rewrite [Equation 3.11] as:

$$m_{d1}\left[s^2 + \frac{\omega_{d1}}{2\pi}\left(\frac{1}{Q_{d1}} + \frac{\delta_1}{Q_{s1}}\right)s + \omega_{d1}^2\right]\hat{x}_{d1} + \alpha_p\hat{x}_p + D_{d1,p}s\hat{x}_{d1} = (as + b)_{d1}$$

[Equation 3.12]

Where,

$(as + b)_{d1}$ = initial conditions and a = $f(x_{d1,o})$ and b = $f(x_{p,o})$;

ω_{d1} = undamped resonance frequency = $\sqrt{\frac{K_{d1}}{m_{d1}}}$;

And $K_{d1} = K_{ext,d1}\left(1 + \frac{m_{d1}}{m_c}\right) + A_{d1}\left(\frac{\partial p_c}{\partial x_{d1}} - \frac{m_{d1}}{m_c}\frac{\partial p_c}{\partial x_c} - n\delta_1\frac{\partial p_{s1}}{\partial x_{d1}}\right)$

*Note: m_c is mass of cylinder and x_c is displacement of cylinder.

But practically, by order of magnitude analysis:

$$K_{d1} \approx A_{d1}\left(\frac{\partial p_c}{\partial x_{d1}} - \frac{m_{d1}}{m_c}\frac{\partial p_c}{\partial x_c} - n\delta_1\frac{\partial p_{s1}}{\partial x_{d1}}\right)$$

Q_{d1} = (stored displacer 1 energy/energy loss per cycle at ω_{d1}) = $\frac{\omega_{d1}}{2\pi}\frac{m_{d1}}{D_{d1}}$;

Δp = drop in pressure across the heat exchanger loop;

$D_{d1,p}$ = displacer/piston viscous coupling

D_{ext} = incidental damping (Ns/m) and we assume $Dd_1 = D_{dd1}$

$D_{d1} = D_{dd1} - D_{dc}\frac{m_{d1}}{m_c}$; $D_{dd1} = D_{ext,d1} - A\frac{\partial \Delta p}{\partial \dot{x}_{d1}}$; $D_{d1,c} = -D_{extd,d1} - A\frac{\partial \Delta p}{\partial \dot{x}_c}$; $D_{d1,p} = -A\frac{\partial \Delta p}{\partial \dot{x}_p}$;

Now, $\alpha_p = A_{d1}\left(\frac{\partial p}{\partial x_p} - \frac{m_p}{m_c}\frac{\partial p}{\partial x_c}\right) + K_{ext,d1}\frac{m_p}{m_c} \rightarrow \alpha_p \approx A_{d1}\left(\frac{\partial p}{\partial x_p} - \frac{m_p}{m_c}\frac{\partial p}{\partial x_c}\right)$

Also we take $p = p_c$. [Equation set 3.12]

Now let,

$$T_{d1}(s) = m_{d1}\left[s^2 + \frac{\omega_{d1}}{2\pi}\left(\frac{1}{Q_{d1}} + \frac{\delta_1}{Q_{s1}}\right)s + \omega_{d1}^2\right]\hat{x}_{d1} + D_{d1,p}s\hat{x}_{d1} \qquad \text{[Equation 3.13]}$$

Hence, we now get,

$$T_{d1}(s)\hat{x}_{d1} + \alpha_p\hat{x}_p = (as + b)_{d1} \qquad \text{[Equation 3.14]}$$

Equation of motion for the working piston

The linearized unbalanced pressure force on the working piston, F_p, is given by:

$F_p = -F_{d1,p} - F_{net} = -F_{d1,p} - (F_g - F_{s2})$ [Equation 3.15]

Where F_g = force due to gaseous working medium

On linearizing, we get,

$$F_p = -A_p\left[\frac{\partial p}{\partial x_{d1}}x_{d1} + \left(\frac{\partial p}{\partial x_{d1}} - n\frac{\partial p_{s2}}{\partial x_p}\delta_2\right)x_p\right] \qquad \text{[Equation 3.16]}$$

(This is the working piston equation of motion)

Here, δ_2 = Angular component based on spring orientation in the working piston chamber.

The first term in the above equation represents a thermodynamic coupling between piston force and displacer motion. Considering damping forces on the piston:

$-D_p\dot{x}_p$ = damping force on piston from electric generator (or other useful load)

$-D_{s2}\dot{x}_p\delta_2$ = damping force on piston due to attached springs

And $K_p \approx A_p\left(\frac{\partial p_c}{\partial x_p} - \frac{m_p}{m_e}\frac{\partial p_c}{\partial x_e} - n\delta_2\frac{\partial p_{s2}}{\partial x_p}\right)$; [Equation 3.16]

On taking Laplace transform of the working piston equation of motion we get:

$$m_p\left[s^2 + \frac{\omega_p}{2\pi}\left(\frac{1}{Q_p} + \frac{\delta_2}{Q_{S2}}\right)s + \omega_p^2\right]\hat{x}_p + \alpha_p\hat{x}_{d1} + D_{d1,p}s\hat{x}_p = (ys + z)_p$$

[Equation 3.17]

Where,

$(ys + z)_p$ = initial conditions and $y = f(x_{p,o})$ and $z = f(x_{d1,o})$;

ω_p = undamped resonance frequency = $\sqrt{\frac{K_p}{m_p}}$;

And $K_p = K_{ext,p}\left(1 + \frac{m_p}{m_e}\right) + A_p\left(\frac{\partial p_c}{\partial x_p} - \frac{m_p}{m_c}\frac{\partial p_c}{\partial x_c} - n\delta_2\frac{\partial p_{s2}}{\partial x_p}\right)$

But practically, by order of magnitude analysis:

$K_p \approx A_p\left(\frac{\partial p_c}{\partial x_p} - \frac{m_p}{m_c}\frac{\partial p_c}{\partial x_c} - n\delta_2\frac{\partial p_{s2}}{\partial x_p}\right)$

Q_p = (stored working piston energy/energy loss per cycle at ω_p) = $\frac{\omega_{d1}}{2\pi}\frac{m_{d1}}{D_{d1}}$;

Δp = drop in pressure across the heat exchanger loop;

$D_{d1,p}$ = displacer/piston viscous coupling

Now, $\alpha_T = A_p\left(\frac{\partial p}{\partial x_{d1}} - \frac{m_{d1}}{m_c}\frac{\partial p}{\partial x_c}\right) + K_{ext,p}\frac{m_{d1}}{m_c} \rightarrow \alpha_T \approx A_p\left(\frac{\partial p}{\partial x_{d1}} - \frac{m_{d1}}{m_c}\frac{\partial p}{\partial x_c}\right)$

[Equation set 3.18]

Now let, $T_p(s) = m_p\left[s^2 + \frac{\omega_p}{2\pi}\left(\frac{1}{Q_p} + \frac{\delta_2}{Q_{S2}}\right)s + \omega_p^2\right]\hat{x}_p + D_{d1,p}s\hat{x}_p$ [Equation 3.19]

Hence, we now get, the following two equations:

1) Equation of motion of displacer 1: $\boxed{T_{d1}(s)\hat{x}_{d1} + \alpha_p\hat{x}_p = (as + b)_{d1}}$

2) Equation of motion of working piston: $\boxed{T_p(s)\hat{x}_p + \alpha_T\hat{x}_{d1} = (ys + z)_p}$

[Equation set 3.20]

Solving for roots

Now solutions of $x_{d1}(t)$ and $x_p(t)$ are given by (locating in the complex plane) the 4 roots of:

$$T_{d1}(s)T_p(s) - \alpha_p\alpha_T = 0$$ [Equation 3.21]

We take $D_{d1,p} = 0$ here for simplicity.

Note:

For oscillation, at least 2 roots must be in the Right Half Plane (RHP). We check for the existence of such roots by examining the graph of the complex plane of LHS of above equation where, 's' moves along the 'Bromwich contour' in a clockwise sense. Since the LHS has no RHP poles, number of clockwise rotations about the origin in the graph is equal to the number of RHP roots of the above equation. We know that in reality, $\alpha_T < 0$ (as pressure decreases when the displacer moves up). We infer that number of RHP roots of the above equation is equal to the number of rotations of the point $-|\alpha_p\alpha_T| + i(0)$ in a graph of $T_{d1}(s)T_p(s)$ where 's' moves along the 'Bromwich contour'.

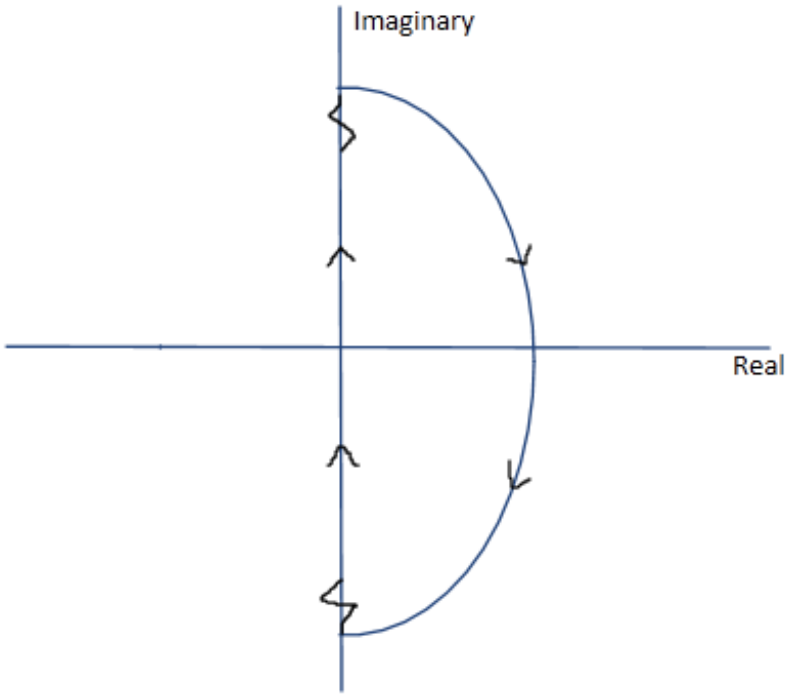

Figure 15 Bromwich contour

Hence we now get:

$$\boxed{T_{d1}(s)T_p(s) = (s - \lambda_+)(s - \lambda_-)(s - \beta_+)(s - \beta_-)} \qquad \text{[Equation 3.22]}$$

Where λ and β are the zeroes or roots of $T_{d1}(s) = 0$ and $T_p(s) = 0$ respectively.

Using quadratic formula, we now get after making considerations for practical machines:

$$\boxed{\begin{aligned} \lambda_+, \lambda_- &= \omega_{d1}\left\{-\frac{1}{4\pi}\left(\frac{1}{Q_{d1}} + \frac{\delta_1}{Q_{s1}}\right) \pm i\right\} \\ \beta_+, \beta_- &= \omega_p\left\{-\frac{1}{4\pi}\left(\frac{1}{Q_p} + \frac{\delta_2}{Q_{s2}}\right) \pm i\right\} \end{aligned}} \qquad \text{[Equation set 3.23]}$$

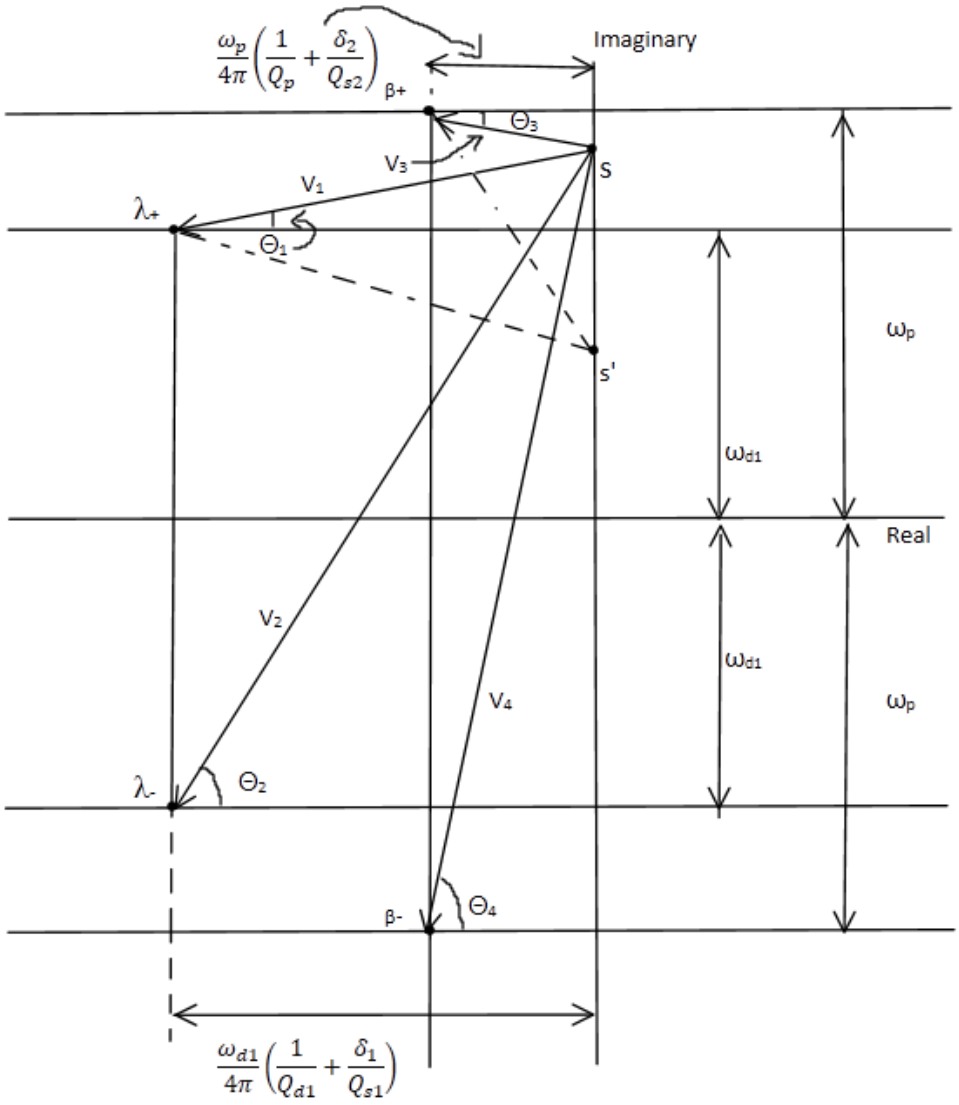

Figure 16 Locations of roots in complex plane (V1, V2, V3 and V4 are volume phasors)

Deriving the oscillation criterion

Now, we start mapping the locus of 's' at s = 0 and get:

$\theta_1 + \theta_2 + \theta_3 + \theta_4 = 0$ [Equation 3.24]

And $[T_{d1}(0)T_p(0)]$ is real and positive.

Note:

If 's' moves up along the imaginary axis, then θ_2 and θ_4 decrease while θ_1 and θ_3 (initially negative) decrease up to a point and then become positive & increase steadily after that. As $s \rightarrow i(\infty)$, then $(\theta_1 + \theta_2 + \theta_3 + \theta_4) \rightarrow 2\pi$

Clearly, this graph circles the origin counterclockwise and returns to the real axis at +infinity. Now, the contour traverses an infinite RHP semi-circle. For 's' moving from $+\infty$ to $-\infty$ in clockwise direction, $(\theta_1 + \theta_2 + \theta_3 + \theta_4)$ decreases from 2π to -2π and the locus of $T_{d1}(s)T_p(s)$ is given by 2 circles of infinite radius in clockwise direction. Here, both the positions for RHP roots are shown in the same diagram for simplicity. One position has no roots while the other one has 2 RHP roots.

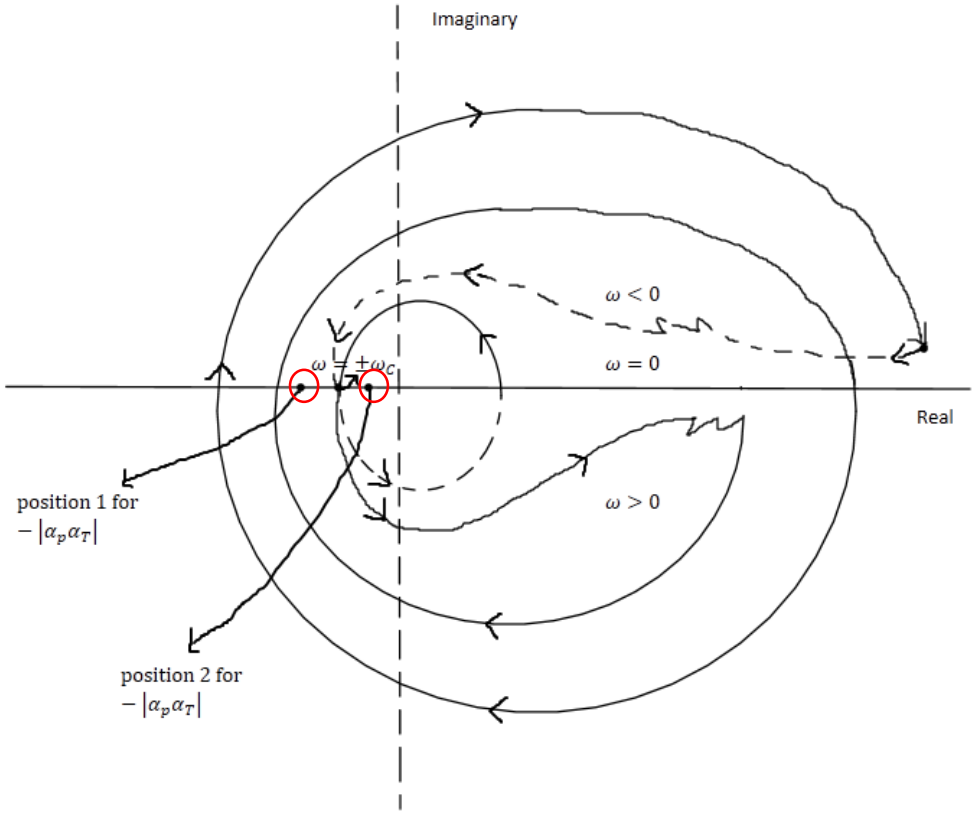

Figure 17 RHP roots' positions

For position 1, 2 RHP roots exist → 2 clockwise encirclements of $-\left|\alpha_p \alpha_T\right|$

For position 2, no RHP roots exist → 2 clockwise and 2 counterclockwise encirclements and hence no net rotation and hence they are not RHP roots of the equation.

Clearly locus of the final part of the contour is negative imaginary axis from -$i\infty$ to origin. In this part the graph is a complex conjugate of the graph in the positive imaginary axis part.

Hence we get, $\theta_1(\omega_c) + \theta_2(\omega_c) + \theta_3(\omega_2) + \theta_4(\omega_c) = \pi$ [Equation 3.25]

Hence a necessity for oscillation in our system is :

$\boxed{T_{d1}(i\omega_c)T_p(i\omega_c) < \left|\alpha_p \alpha_T\right|}$ OSCILLATION CRITERION [Equation 3.26]

Operating frequency equation

Also, from our diagram, we get,

$\omega_p < \omega_c < \omega_d$

Hence, $\theta_1(\omega_c) = -\theta_3(\omega_c)$

For practical cases, @ $\omega = \omega_c$, $\theta_2 + \theta_4 \approx \pi$

Now, on solving, we get,

$$\boxed{\omega_c \approx \frac{\omega_p \omega_{d1}\{Q_{d1}Q_{s1}(Q_{s2} + \delta_2 Q_p) + Q_p Q_{s2}(Q_{s1} + \delta_1 Q_{d1})\}}{\omega_p \omega_{d1} Q_{s1}(Q_{s2} + \delta_2 Q_p) + \omega_{d1} Q_p Q_{s2}(Q_{s1} + \delta_1 Q_{d1})}}$$

[Equation 3.27]

If $Q_{d1} \gg Q_p \rightarrow \omega_c \approx \omega_{d1}$

And if $Q_p \gg Q_{d1} \rightarrow \omega_c \approx \omega_p$

Also we get the 'General Criterion for Oscillation of the System':

$$m_{d1}m_p\begin{pmatrix}\omega_c\\+\omega_{d1}\end{pmatrix}\begin{pmatrix}\omega_c\\+\omega_p\end{pmatrix}\left[+\left\{\frac{\omega_{d1}}{4\pi}\left(\frac{1}{Q_{d1}}+\frac{\delta_1}{Q_{s1}}\right)\right\}^2+\frac{(\omega_c-\omega_{d1})^2}{(\omega_c-\omega_{d1})^2}\right]^{\frac{1}{2}}\left[+\left\{\frac{\omega_p}{4\pi}\left(\frac{1}{Q_p}+\frac{\delta_2}{Q_{s2}}\right)\right\}^2+\frac{(\omega_c-\omega_p)^2}{(\omega_c-\omega_p)^2}\right]^{\frac{1}{2}}<|\alpha_p\alpha_T|$$

[Equation 3.28]

If $\omega_c = \omega_p = \omega_{d1}$, then we get,

$$\frac{m_{d1}m_p\omega^4}{4\pi^2}\left(\frac{1}{Q_{d1}}+\frac{\delta_1}{Q_{s1}}\right)\left(\frac{1}{Q_p}+\frac{\delta_2}{Q_{s2}}\right)<|\alpha_p\alpha_T|$$

[Equation 3.29]

Root loci

We infer the locus of roots of equation 3.21 as $|\alpha_p\alpha_T|$ varies with the help of equation 3.25 and the fact that the starting points for the root loci, for $|\alpha_p\alpha_T| = 0$ are the roots of $T_{d1}(s) = 0$ and $T_p(s) = 0$ as seen in equation set 3.23.

Given below is the resultant locus for a typical case where $Q_p > Q_{d1}$ [27].

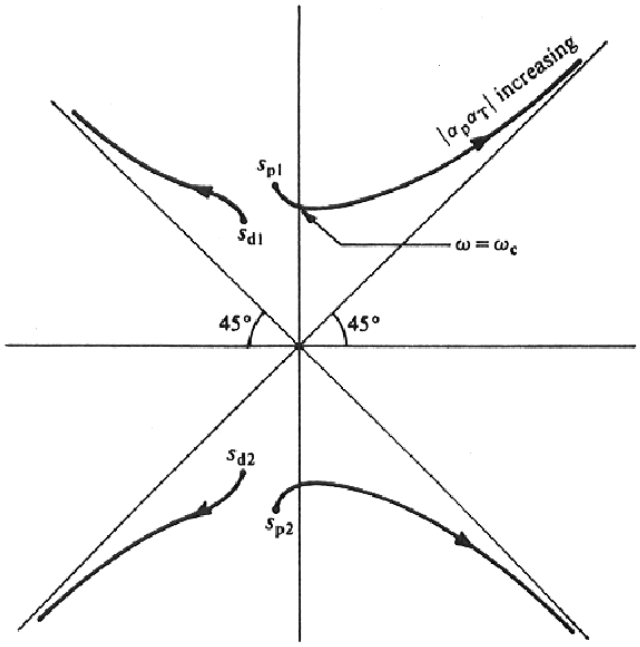

Figure 18 Root locus with $|\alpha_p\alpha_T|$ as parameter (Redlich et al 1985) [27]

As α_T increases (due to increase in hot end temperature), one conjugate pair of roots moves from ±β to $-i\omega$ axis, eventually reaching it at a value of $\alpha_p\alpha_T$, predicted by the stability criterion. Oscillation begins here. The other two roots are conjugate pair in the LHP and are associated with dynamic evanescence [27].

In real life systems, oscillation amplitude is limited by non linearities, either artificially induced by means of closed loop mechanisms that control Q_p or Q_{d1} in response to piston amplitude or inherent in the working gas flow processes or both. Their effect is to decrease the positive real part of the conjugate root pair associated with oscillation as amplitude increases, untill the roots eventually reach the imaginary axis at an equilibrium amplitude as shown below for a situation where Q_p decreases with amplitude [27].

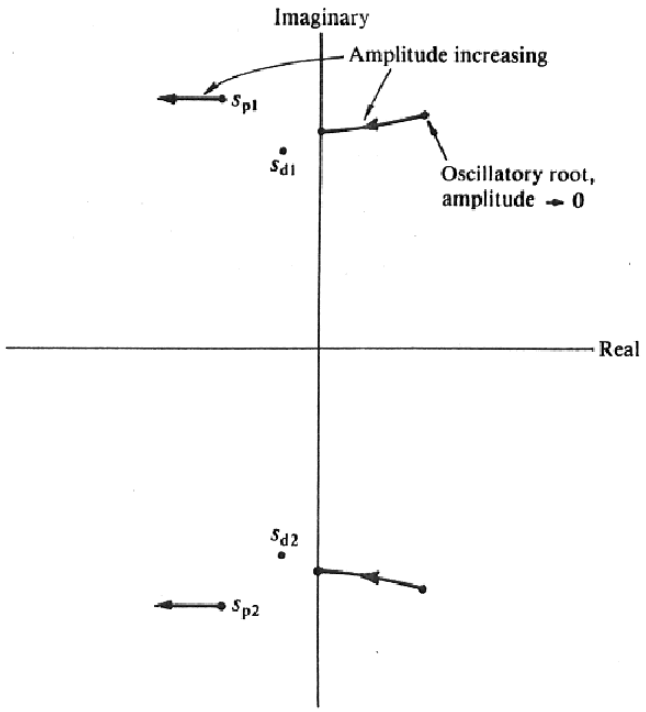

Figure 19 Root locus for Q_p decreasing with increasing amplitude [27].

Equation for stroke ratio and power

At equilibrium, on solving we obtain the complex form of piston and displacer motion as shown below.

$$x_{d1}(t) = X_{d1}e^{iw_c t}$$

$$\text{And } x_p(t) = X_p e^{iw_c t}$$

And on simplifying we get

$$\frac{X_{d1}}{X_p} = \frac{-\alpha_p}{T_{d1}(i\omega_c)}$$

[Equation set 3.30]

Where $X_{d1}$and X_p are complex amplitudes by considering only the real parts.

Hence, we now get stroke ratio and piston/displacer phase angle by:

$$\left|\frac{X_{d1}}{X_p}\right| = \frac{(\alpha_p)}{K_{d1}}\left\{\left[1-\left(\frac{\omega_c}{\omega_{d1}}\right)^2\right]^2 + \left(\frac{\omega_c}{\omega_{d1}}\frac{1}{2\pi}\left(\frac{1}{Q_{d1}}+\frac{\delta_1}{Q_{s1}}\right)\right)^2\right\}^{-\frac{1}{2}}$$

[Equation 3.31]

We now get, $$\phi = \tan^{-1}\left[\frac{\left(\frac{\omega_c}{\omega_{d1}}\frac{1}{2\pi}\left(\frac{1}{Q_{d1}}+\frac{\delta_1}{Q_{s1}}\right)\right)}{\left(\frac{\omega_c^2}{\omega_{d1}^2}-1\right)}\right]$$ [Equation 3.32]

For practical engines, we generally have $40^o < \varphi < 90^o$

And also for $\omega_c \approx \omega_p = \omega_{d1}$, we have $\varphi = \frac{\pi}{2}$

And $$\left|\frac{X_{d1}}{X_p}\right| = \frac{(\alpha_p)}{\omega}\sqrt{\frac{1}{2\pi}}\left(\frac{2\pi Q_{s1}}{2\pi Q_{s1} D_{d1}+\delta_1 \omega m_{d1}}\right)$$ [Equation 3.33]

And also we get, $$P = \frac{\omega|\alpha_T|}{2}|X_{d1}|\left|X_p\right|\sin\phi$$ [Equation 3.34]

And we observe that $P = P_{max}$ @ $\phi = 90^o$ such that $\omega_p = \omega_{d1}$.

The accuracy of the above equation in determining power is limited by extrapolation of linear solutions to large values of amplitude and the accuracy in determining α_p and α_T [27]. These two values can be reasonably approximated using simple isothermal analysis of the system.

3.2 Adiabatic analysis of Stirling engine [50]

Adiabatic analysis of the Stirling cycle

The engine is divided into 5 control volumes for this analysis, and it is assumed that the expansion and compression processes follow the adiabatic law.

$$PV^{\gamma} = \text{constant} \qquad \text{[Equation 3.35]}$$

Where, γ= ratio of specific heat of working fluid = 1.67 for Helium

Assumptions:

a) The expansion and compression process is adiabatic.
b) The temperature of hot end heat exchanger, cold end heat exchanger and regenerator is constant.
c) The working fluid obeys ideal gas law.
d) The specific heats for the working fluid (Helium) are constant.
e) The pressure is uniform throughout the engine at all instants.
f) The volume inside the engine varies in a sinusoidal manner.
g) There is no leakage of working fluid from the engine.
h) Perfect regeneration occurs in the regenerator volume.
i) The heat transfer in the hot end heat exchanger and cold end heat exchanger occurs at constant temperature.
j) The initial pressure is known.
k) 0^{o} crank angle corresponds to topmost position of displacer.

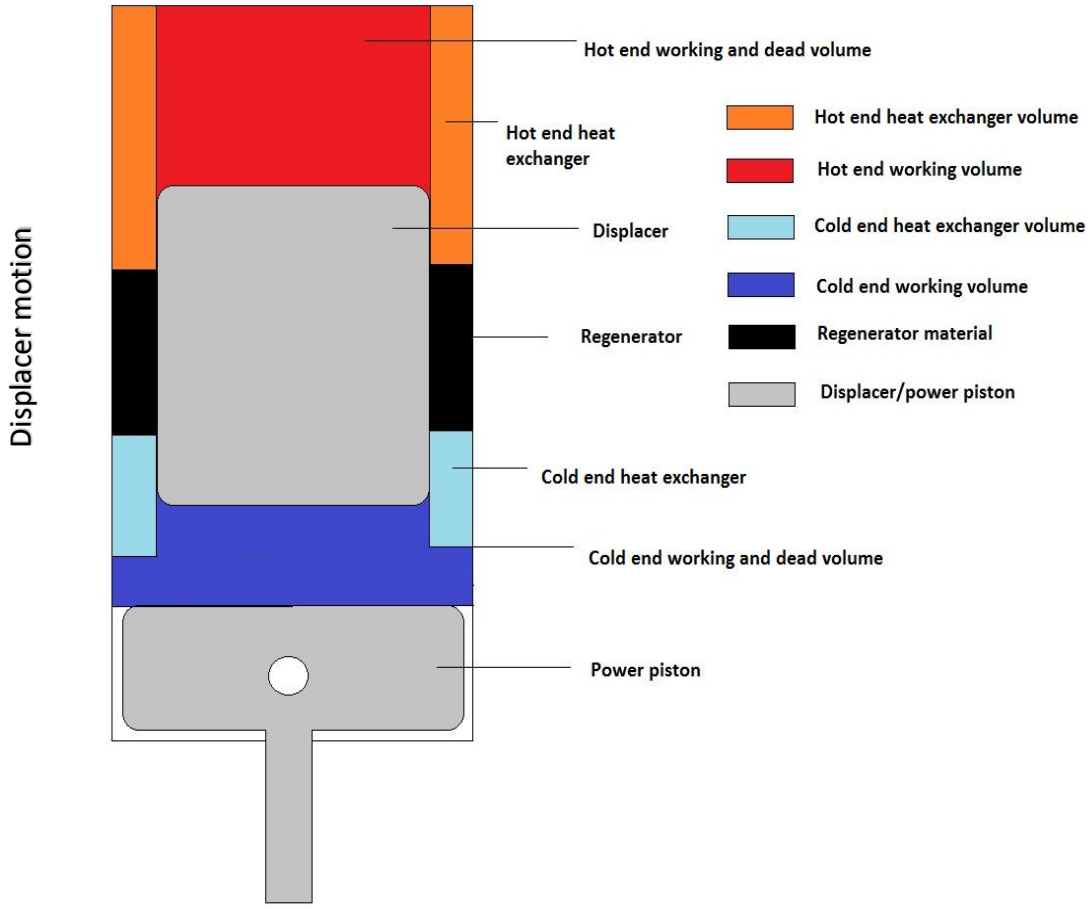

Figure 20 Schematic of control volumes in the Stirling engine for adiabatic analysis [50]

Dead volume is accounted for in the working volume, in adiabatic analysis. The engine is divided into 5 control volumes. Energy balance equation is applied to each control volume. Instantaneous volume is known, as sinusoidal volume variation is assumed. Total moles of gas is constant as there is no leakage. The variables are pressure (in the engine) and temperature (in the expansion and compression spaces).

The temperatures in the hot end heat exchanger, cold end heat exchanger and the regenerator are constant. The temperature in the expansion and compression

spaces can be predicted as they follow the adiabatic expansion/compression law. We write temperature in terms of pressure variable and use conservation of mass to get an implicit equation for the unknown pressure. The implicit equation of pressure is solved here using the 'Direct approximate analytical solution' given by Urieli and Berchowitz, and presented in the thesis work by Jose Martinez, [52]. The exact solution can be obtained by performing a few iterations. Owing to complex nature of the analysis, every data point is recorded for better understanding, resulting in an extensive nomenclature which includes two dimensional arrays.

Energy balance and other equations

Energy balance is performed on each of the five volumes inside the engine. The energy balance for all the volumes is shown in the diagram below. The big box represents the engine, which is the larger control volume. The smaller boxes represent the individual volumes inside the engine. These five boxes are the individual control volumes. Heat and mass flow across these individual smaller control volumes, while only heat can flow across the outer, bigger control volume representing the engine.

In the figure given below, gAck*Cp*Tck and other similar terms are the heat energy given by the equation $m*C_p*dT$. Pressure losses in the individual control volumes are ignored and heat transfer in the heat exchanger is assumed at constant temperature. Work and efficiency are calculated using the above energy balance.

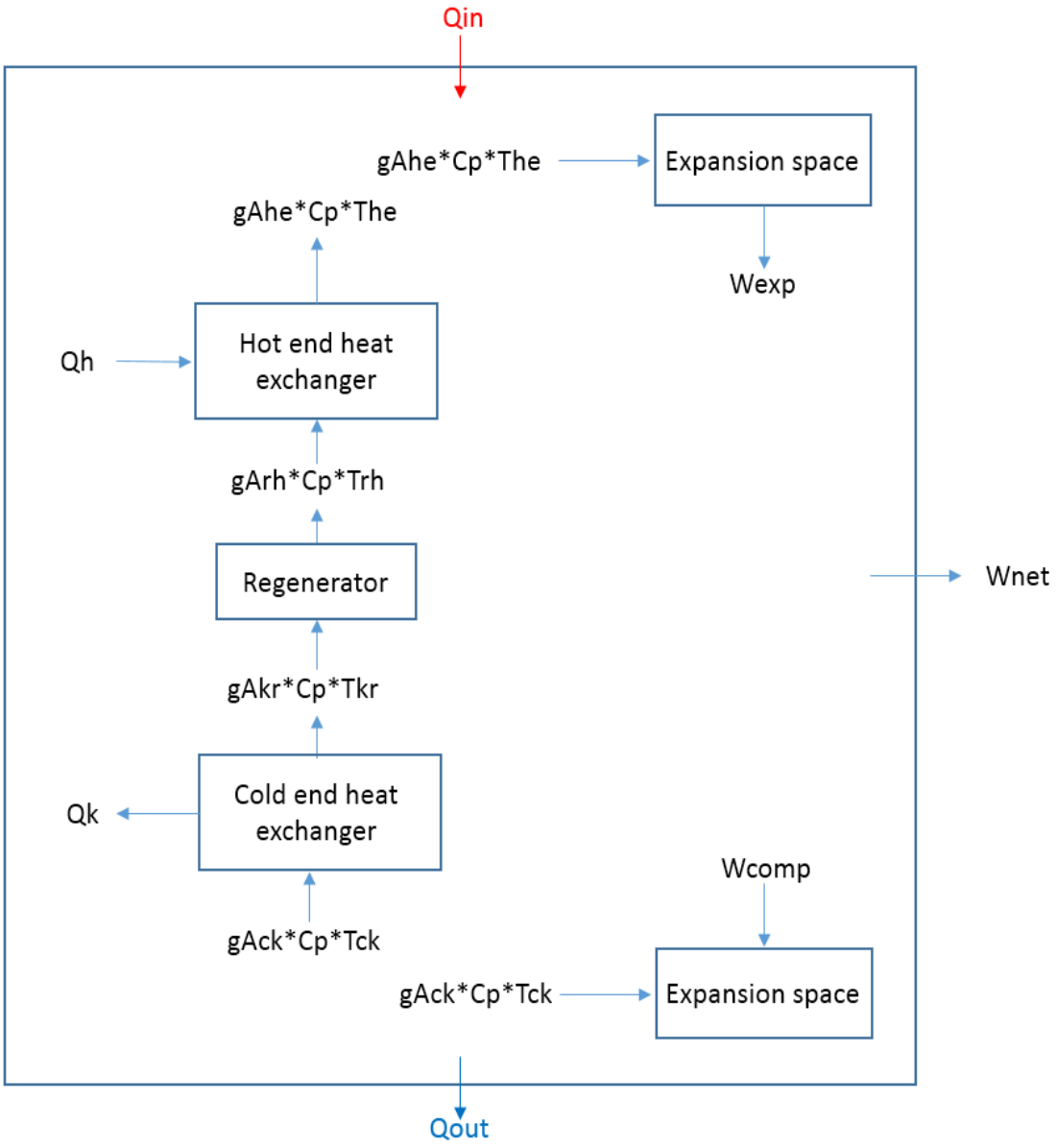

Figure 21 Energy balance diagram of control volumes in Stirling engine [50]

Formulae Used [50]: [Equation set 3.36]

1) Regenerator temperature

$$\mathrm{Tr} = \frac{\mathrm{TH} - \mathrm{TC}}{\ln(\frac{\mathrm{TH}}{\mathrm{TC}})}$$

2) Moles of working gas inside engine

$$M = \frac{P(1)(VA)\ln\left(\frac{TH}{TC}\right)}{R(TH - TC)}$$

3) Maximum hot end live volume

$$Vem = \frac{\pi}{4}(2)(RC)(DB)^2$$

4) The hot end dead volume is given by

$$Ved = 2(h)[(DB)^2 - (DD)^2](\frac{\pi}{4})$$

5) The instantaneous hot end live volume is given by

$$Ve = \frac{Vem}{2}[1 - \cos(F)] + Ved$$

6) Maximum cold end live volume associated with displacer

$$Vcm = 2(RC)[(DB)^2 - (DD)^2](\frac{\pi}{4})$$

7) The cold end dead volume is given by

$$Vcd = 2(h)[(DB)^2 - (DD)^2](\frac{\pi}{4})$$

8) The cold end live volume at any instant N is given by

$$Vc = \frac{Vcm}{2}[1 + \cos(F)] + Vcd + \frac{Vp}{2}[1 - \cos(F - AL)]$$

9) Regenerator volume

$$Vr = 2(LR)[(DB)^2 - (DD)^2](\frac{\pi}{4})$$

10) The hot end heat exchanger volume is given by

$$\mathrm{Vhe} = 2(\mathrm{LH})[(\mathrm{DB})^2 - (\mathrm{DD})^2](\frac{\pi}{4})$$

11) The cold end heat exchanger volume at any instant is given by

$$\mathrm{Vce} = 2(\mathrm{LC})[(\mathrm{DB})^2 - (\mathrm{DD})^2](\frac{\pi}{4})$$

12) The total volume at any instant N is then given by

$$\mathrm{V(N)} = \mathrm{Vc} + \mathrm{Vcd} + \mathrm{Ve} + \mathrm{Ved} + \mathrm{Vhe} + \mathrm{Vce} + \mathrm{Vr}$$

13) The analytical formula for change in pressure is given as

$$\mathrm{Dp} = -\frac{\gamma \mathrm{p}\left(\left(\frac{\mathrm{DVc}}{\mathrm{Tck}}\right) + \left(\frac{\mathrm{DVe}}{\mathrm{The}}\right)\right)}{\left(\frac{\mathrm{Vc}}{\mathrm{Tck}}\right) + \gamma\left(\frac{\mathrm{Vce}}{\mathrm{Tce}} + \frac{\mathrm{Vr}}{\mathrm{Tr}} + \frac{\mathrm{Vhe}}{\mathrm{Th}}\right) + \frac{\mathrm{Ve}}{\mathrm{The}}}$$

14) The change in mass in compression space is given as

$$\mathrm{Dmc} = \frac{\mathrm{pDVc} + \frac{\mathrm{VcDp}}{\gamma}}{\frac{\mathrm{R}}{\mathrm{Tck}}}$$

15) The mass content in the cold end heat exchanger, regenerator, hot end heat exchanger and expansion spaces is respectively given as

$$\mathrm{mce} = \frac{(\mathrm{p})(\mathrm{Vce})}{(\mathrm{R})(\mathrm{Tk})};\quad \mathrm{mr} = \frac{(\mathrm{p})(\mathrm{Vr})}{(\mathrm{R})(\mathrm{Tr})};\quad \mathrm{mhe} = \frac{\mathrm{pVhe}}{\mathrm{RTh}};$$

$$\mathrm{me} = \mathrm{M} - (\mathrm{mc} + \mathrm{mce} + \mathrm{mr} + \mathrm{mhe})$$

16) The temperatures in the expansion and compression spaces are then given by

$$\mathrm{Te} = \frac{(\mathrm{p})(\mathrm{Ve})}{(\mathrm{R})(\mathrm{me})};\quad \mathrm{Tc} = \frac{(\mathrm{p})(\mathrm{Vc})}{(\mathrm{R})(\mathrm{mc})}$$

17) The change in mass in the cold end heat exchanger, regenerator and hot end heat exchanger is given by

$$\mathrm{Dmce} = \frac{(\mathrm{mce})(\mathrm{Dp})}{\mathrm{p}};\quad \mathrm{Dmr} = \frac{(\mathrm{mr})(\mathrm{Dp})}{\mathrm{p}};\quad \mathrm{Dmhe} = \frac{(\mathrm{mhe})(\mathrm{Dp})}{\mathrm{p}}$$

18) The mass exchanges between the control volumes are given by

$$\mathrm{gAck} = -\mathrm{Dmc};\quad \mathrm{gAkr} = \mathrm{gAck} - \mathrm{Dmce};\quad \mathrm{gArh} = \mathrm{gAkr} - \mathrm{Dmr};\quad \mathrm{gAhe} = \mathrm{gArh} - \mathrm{Dmhe}$$

19) Now the conditional temperatures 'Tck' and 'The' are assigned values as below. Note that before the first iteration, 'Tck 'and 'The' may be assigned the values 'Tc' and 'Th' respectively.

$$\text{If } \mathrm{gAck} > 0 \quad \text{then, } \mathrm{Tck} = \mathrm{Tc} \quad \text{else, } \mathrm{Tck} = \mathrm{Tk}$$

$$\text{If } \mathrm{gAhe} > 0 \quad \text{then, } \mathrm{The} = \mathrm{Th} \quad \text{else, } \mathrm{Tck} = \mathrm{Te}$$

20) Finally the differential work, heat input at hot end heat exchanger, regenerator heat and heat given out at cold end heat exchanger are given respectively as

$$\mathrm{DW} = \mathrm{p}(\mathrm{DVc} + \mathrm{DVe})$$

$$\mathrm{DQk} = \frac{(\mathrm{Vce})(\mathrm{Dp})(\mathrm{Cv})}{\mathrm{R}} - \mathrm{Cp}((\mathrm{Tck})(\mathrm{gAck}) - (\mathrm{Tkr})(\mathrm{gAkr}))$$

$$\mathrm{DQr} = \frac{(\mathrm{Vr})(\mathrm{Dp})(\mathrm{Cv})}{\mathrm{R}} - \mathrm{Cp}((\mathrm{Tkr})(\mathrm{gAkr}) - (\mathrm{Trh})(\mathrm{gArh}))$$

$$\mathrm{DQh} = \frac{(\mathrm{Vhe})(\mathrm{Dp})(\mathrm{Cv})}{\mathrm{R}} - \mathrm{Cp}((\mathrm{Tkr})(\mathrm{gAkr}) - (\mathrm{The})(\mathrm{gAhe}))$$

The differential work and heat transfers are added cumulatively to get the total work and heat exchanges of the engine per cycle. The entire process is repeated until a stable solution is obtained, that is, the variation in pressure over the entire cycle stabilizes.

Program and validation: The program and validation is presented in Appendix B. Adiabatic analysis results can be presented as a parametric study to understand the effect of each variable and eventually optimize the work and efficiency.

3.3 Software aided simulation results

MATLAB software is used to simulate the dynamic and thermodynamic mathematical model created. The code integrates both the approaches and optimizes the engine. The dynamic analysis draws parametric values of pressure, temperature etc. and changes in them from the adiabatic analysis to start with. Further, it optimizes the results predicted by the adiabatic analysis and accounts for damping, viscous forces, spring stiffness, mechanical losses etc. The MATLAB code for this integrated approach is given in APPENDIX B.

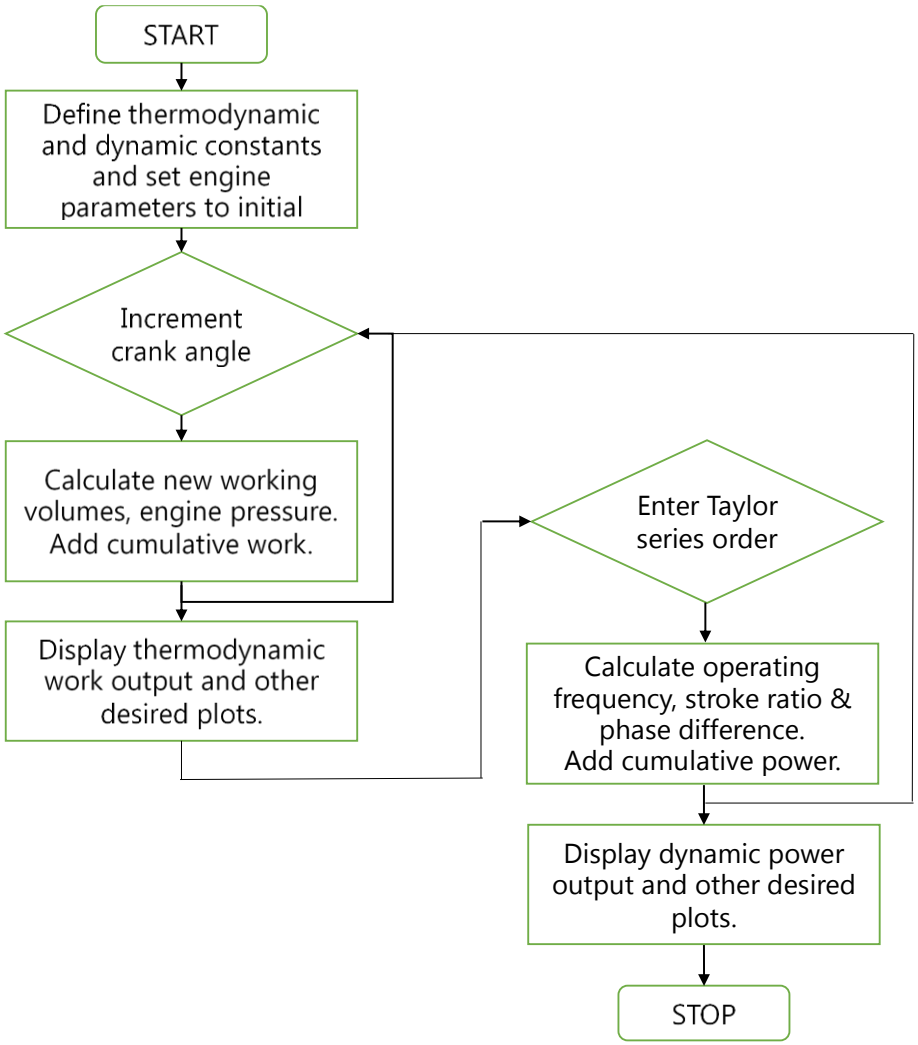

Figure 22 Flow diagram to demonstrate the MATLAB code

Features of the code:

- Generalized for alpha, beta, gamma and free piston Stirling engines
- Dynamic part of code is optimized for spring based Stirling engines but all systems can be analyzed
- Flywheel systems are evaluated by analyzing an equivalent spring system. Energy balance on flywheel yields equivalent spring system values.

Using the code (Input parameters):

Thermodynamic inputs →

Volumes	– hot end heat exchanger, cold end heat exchanger, regenerator, expansion end working volume, compression end working volume
Temperatures	– hot end heat exchanger, cold end heat exchanger
Pressure	– initial charging pressure

Dynamic inputs →

Masses	– casing, power piston, displacer/hot end piston,
Choose between flywheel or spring design	
Strokes	– power piston, displacer/hot end piston
Clearances	– power piston (compression space), displacer/hot end piston (expansion space)
Damping coefficients	– hot end viscous damping, cold end viscous damping, power piston spring, displacer/hot end piston spring
Spring stiffness, number of springs and spring orientation if spring design is chosen	

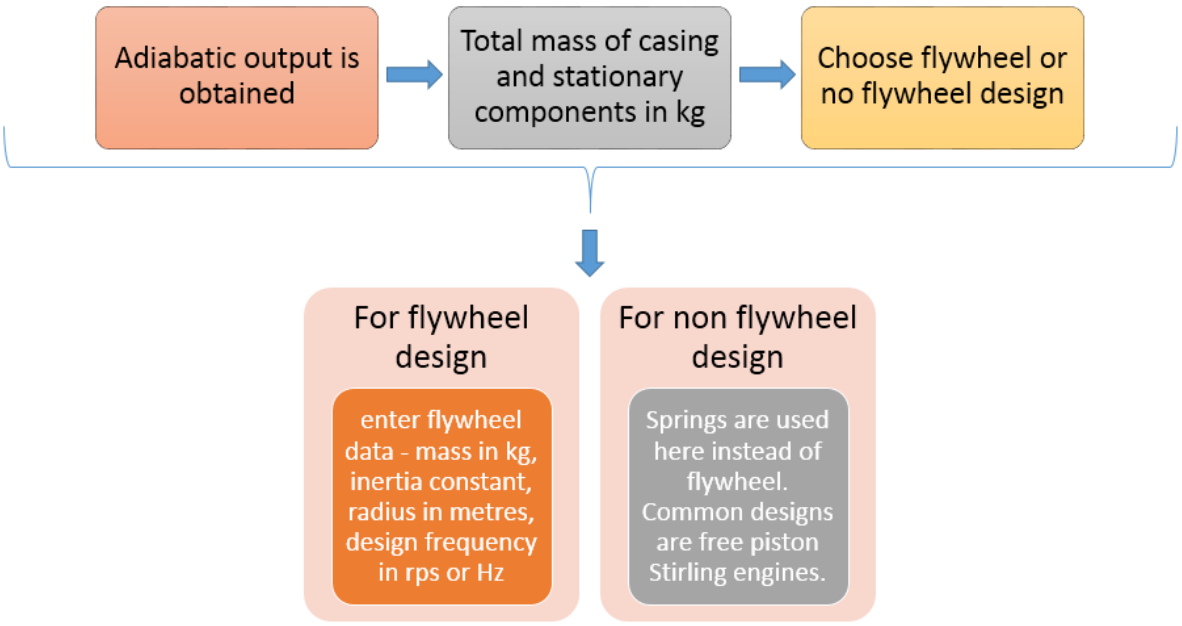

Flywheel design

Hot end piston – mass in kg, stroke in mm, clearance in mm, viscous damping coefficient, flywheel damping coefficient, diameter in mm

Cold end piston – mass in kg, stroke in mm, clearance in mm, viscous damping coefficient, flywheel damping coefficient, diameter in mm

Expected/design phase difference in degrees (starting point for iteration)

Taylor series order for higher accuracy and precision (generally an order of 6 will suffice)

Non-flywheel design

Displacer– mass in kg, stroke in mm, clearance in mm, viscous damping coefficient, flywheel damping coefficient, diameter in mm

Spring at displacer – number of springs, spring damping coefficient, orientation (angle in radians), spring stiffness in N/m

Power piston – mass in kg, stroke in mm, clearance in mm, viscous damping coefficient, flywheel damping coefficient, diameter in mm

Spring at power piston – number of springs, spring damping coefficient, orientation (angle in radians), spring stiffness in N/m

Expected/design phase difference in degrees (starting point for iteration)

Taylor series order for higher accuracy and precision (generally an order of 6 will suffice)

3.4 Analysis of the GPU-3 Stirling engine with integrated model

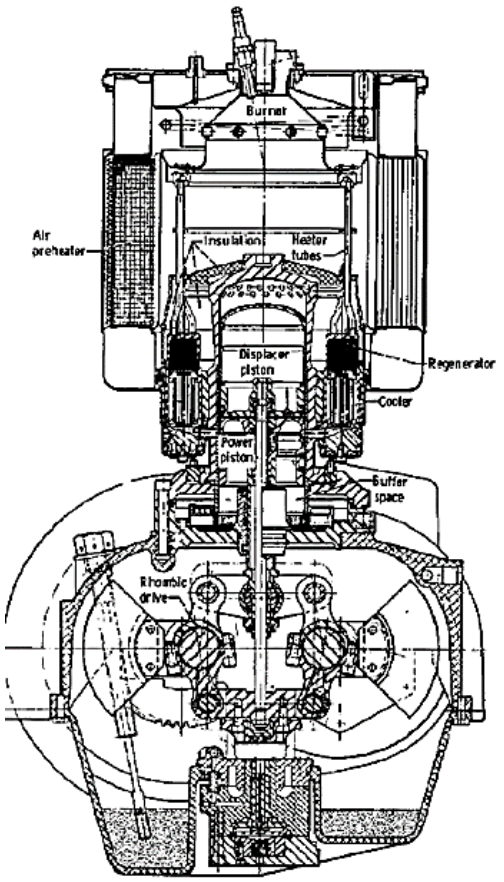

Cylinder bore at liner, cm (in)	6.99 (2.751)
Cylinder bore above liner†, cm (in)	7.01 (2.76)
Cooler	
Tube length, cm (in)	4.61 (1.813)
Heat transfer length, cm (in)	3.55 (1.399)
Tube inside diameter, cm (in)	0.108 (0.0425)
Tube outside diameter, cm (in)	0.159 (0.0625)
Number of tubes per cylinder (or number of tubes per regenerator)	312 (39)
Heater	
Mean tube length, cm (in)	24.53 (9.658)
Heat transfer length, cm (in)	15.54 (6.12)
Cylinder tube, cm (in)	11.64 (4.583)
Regenerator tube, cm (in)	12.89 (5.075)
Tube inside diameter, cm (in)	0.302 (0.119)
Tube outside diameter, cm (in)	0.483 (0.19)
Number of tubes per cylinder (or number of tubes per regenerator)	40 (5)
Cold end connecting ducts	
Length, cm (in)	1.59 (0.625)
Duct inside diameter, cm (in)	0.597 (0.235)
Number of ducts per cylinder	8
Cooler end cap, cm^3 (in^3)	0.279 (0.0170)
Regenerators	
Length (inside), cm (in)	2.26 (0.89)
Diameter (inside), cm (in)	2.26 (0.89)
Number per cylinder	8
Material	Stainless steel wire cloth
Number of wires, per cm (per in)	79 × 79 (200 × 200)
Wire diameter, cm (in)	0.004 (0.0016)
Number of layers	308
Filler factor, percent	30.3
Angle of rotation between adjacent screens, deg	5
Drive	
Connecting rod length, cm (in)	4.60 (1.810)
Crank radius, cm (in)	1.38 (0.543)
Eccentricity, cm (in)	2.08 (0.820)
Miscellaneous	
Displacer rod diameter, cm (in)	0.952 (0.375)
Piston rod diameter, cm (in)	2.22(0.875)
Displacer diameter, cm (in)	6.96 (2.740)
Displacer wall thickness, cm (in)	0.159 (0.0625)
Displacer stroke, cm (in)	3.12 (1.23)
Expansion space clearance, cm (in)	0.163 (0.064)
Compression space clearance, cm (in)	0.030 (0.012)
Buffer space maximum volume, cm^3 (in^3)	521 (31.78)
Total working space minimum volume, cm (in)	233.5 (14.25)

† Top of displacer seal is at top of liner at displacer TDC.

Figure 23 GPU-3 Stirling engine schematic and important engine dimensions (built originally by General Motors Research Laboratory)

The GPU-3 Stirling engine is chosen in order to test and validate the integrated adiabatic and dynamic model developed here. This engine is one of the most popular and widely tested Stirling engines. Extensive experimental results and theoretical modeling explain the working of this system. It therefore, serves as a good reference point to compare and validate our approach.

MATLAB code output for GPU-3 Stirling engine (Mean pressure of 4.14 MPa):

```
Adiabatic Analysis
------------------

Compression ratio for the engine =
   1.459
Heat given per cycle in J =
     2.413e+02

Heat rejected per cycle in J =
    -1.111e+02

Regenerator net heat per cycle in J =
    -1.259e-06

Work output per cycle in J =
     1.302e+02

Efficiency of the engine in percentage =
  53.967

Power output for a 41.67 Hz operating
frequency in W =
     5.426e+03
```

```
Dynamic Analysis
----------------

Power output per cycle from engine in Watts
=
    5.127e+03

Average operating frequency of engine in
Hertz=
  41.662

Stroke-ratio of engine =
  19.227

Optimal Phase difference between displacer
and power piston in degrees =
  89.99
```

Plots for GPU-3 Stirling engine (mean pressure = 4.14 Mpa):

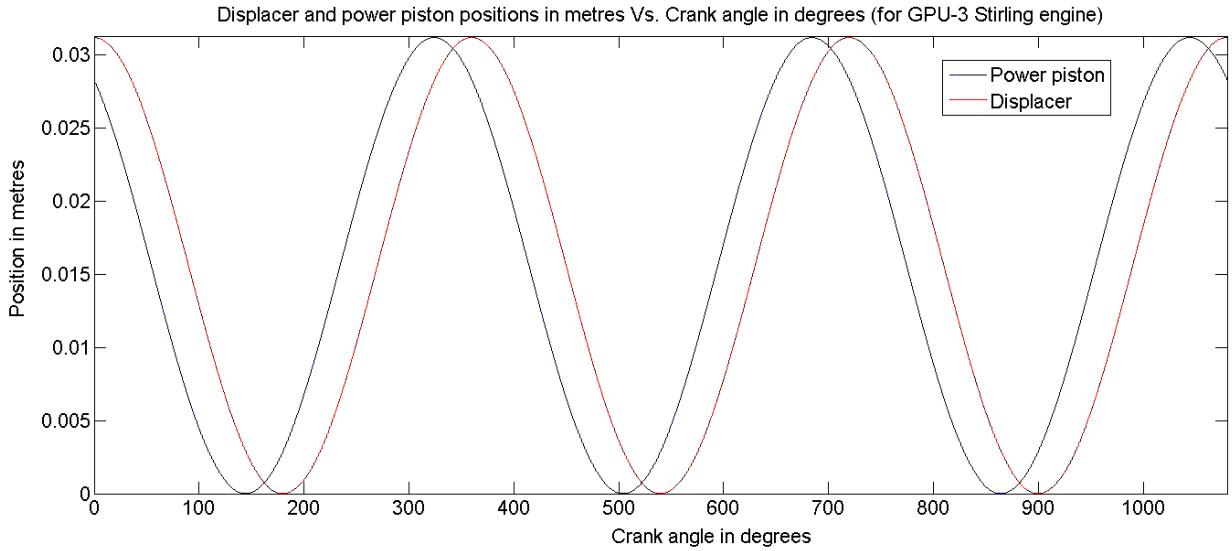

Figure 24 Displacer and power piston position vs. crank angle over 3 cycles in GPU-3 Stirling engine

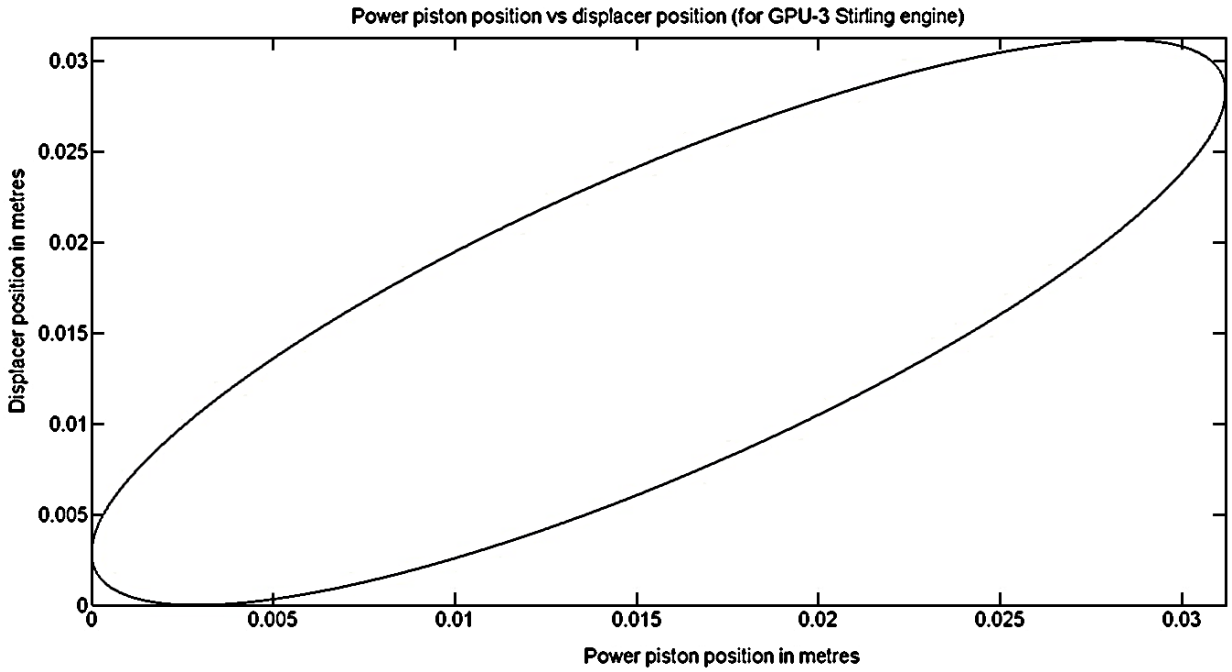

Figure 25 Displacer vs. power piston position in GPU-3 Stirling engine

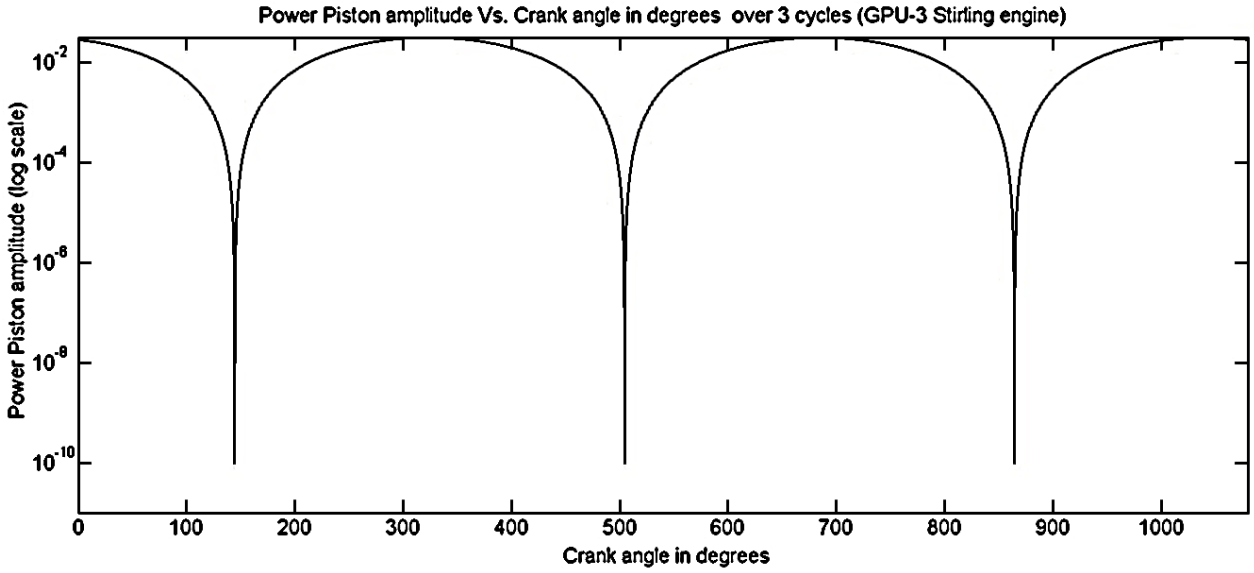

Figure 26 Power piston position (log scale) vs. crank angle for GPU-3 Stirling engine (over 3 cycles)

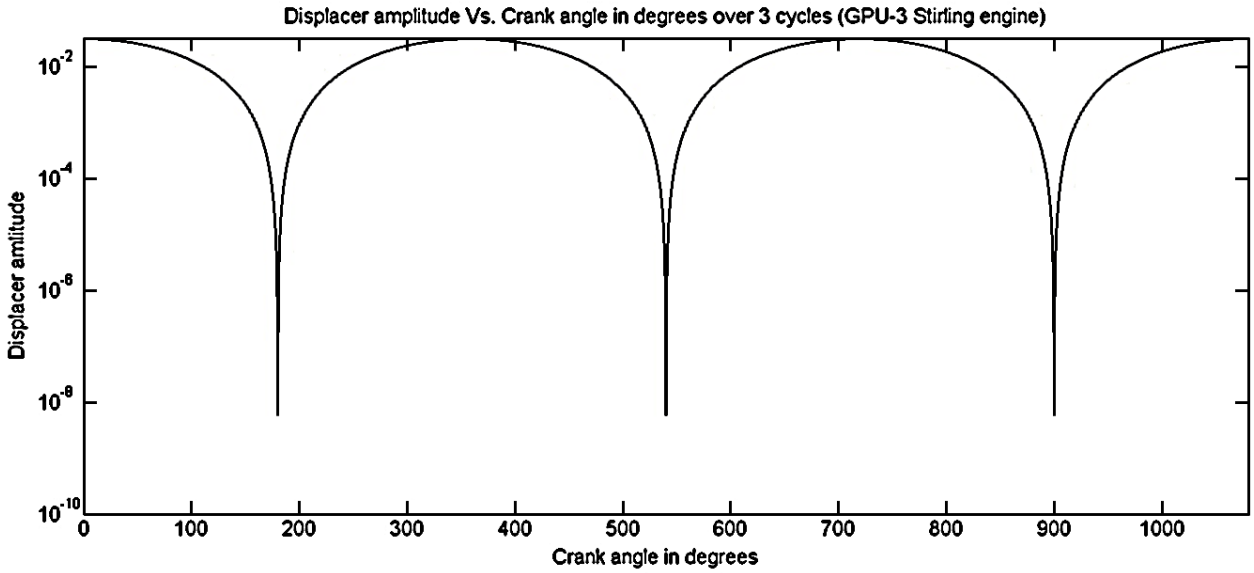

Figure 27 Displacer position (log scale) vs. crank angle for GPU-3 Stirling engine (over 3 cycles)

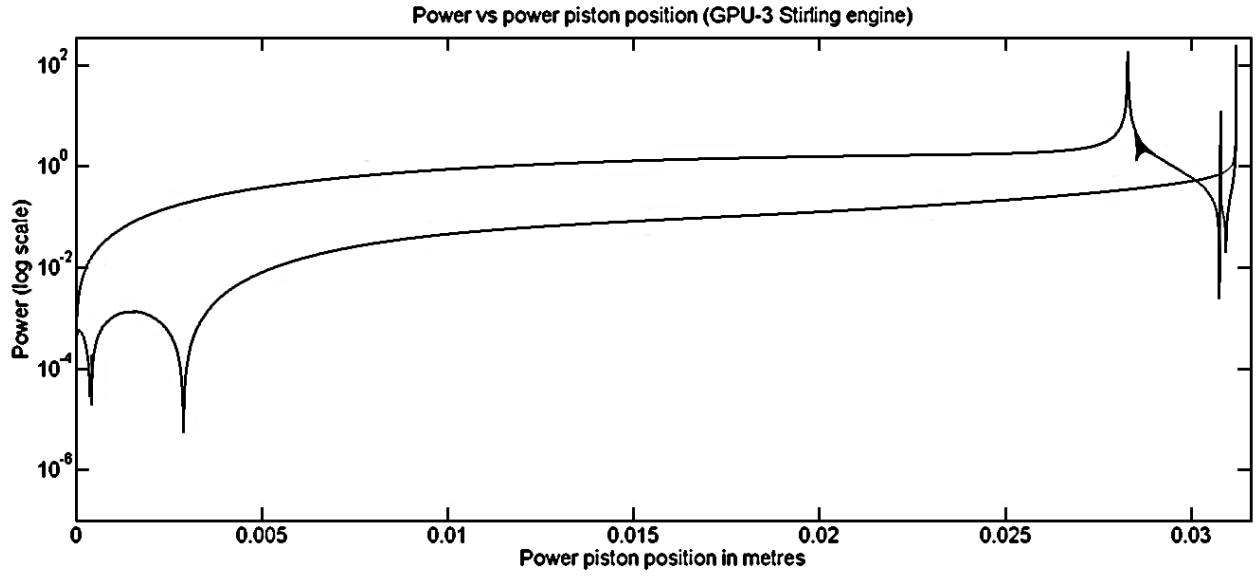

Figure 28 Power output (log scale) vs. power piston position for GPU-3 Stirling engine (over 3 cycles)

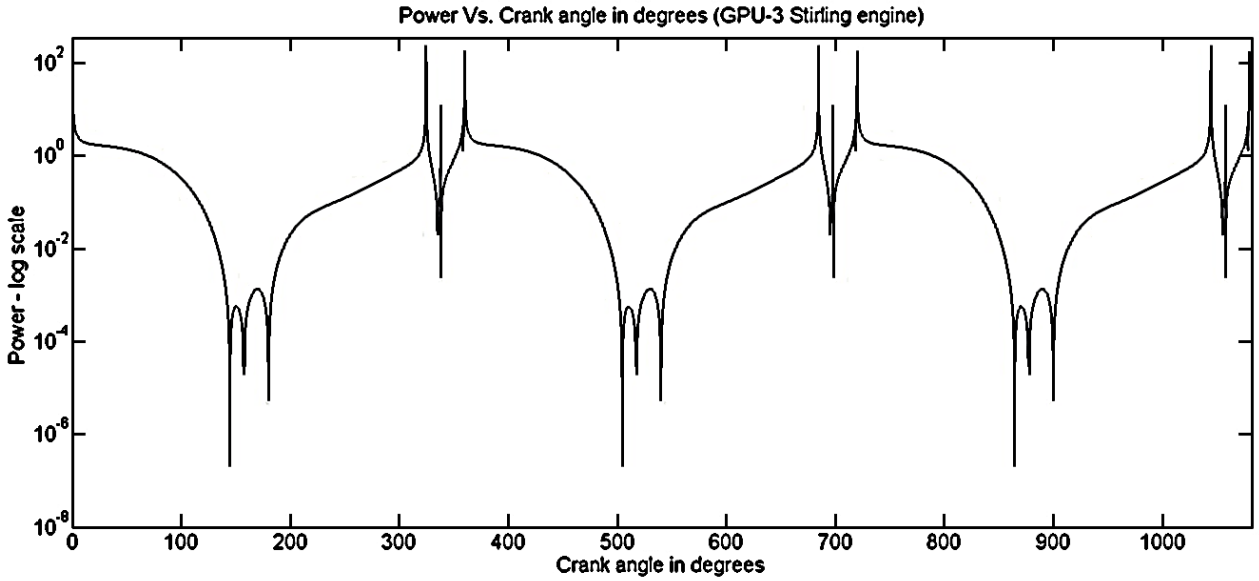

Figure 29 Power output (log scale) vs. crank angle for GPU-3 Stirling engine (over 3 cycles)

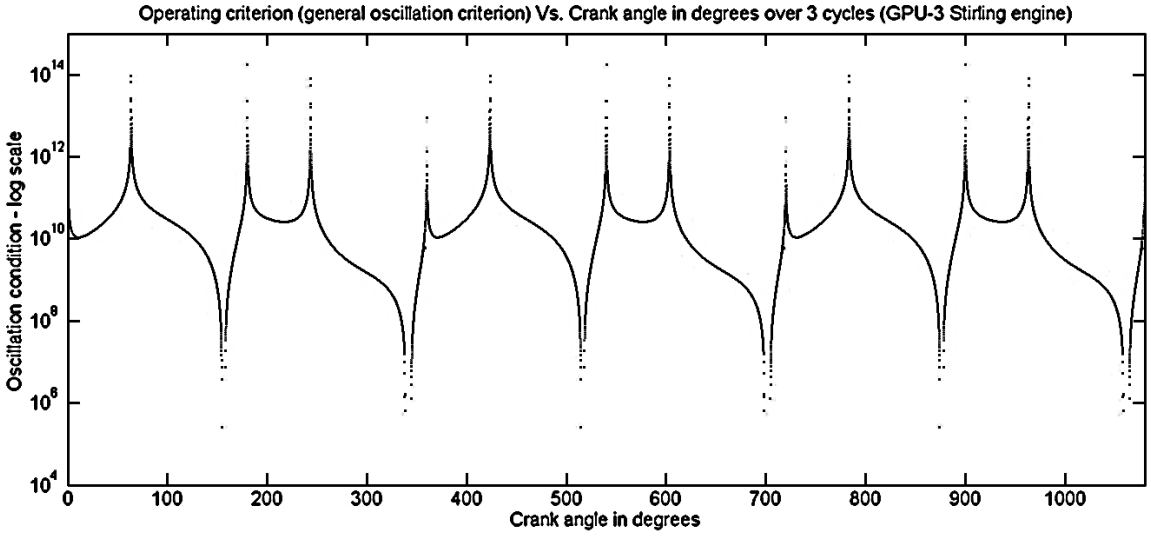

Figure 30 General oscillation criterion vs. crank angle for GPU-3 Stirling engine (over 3 cycles)

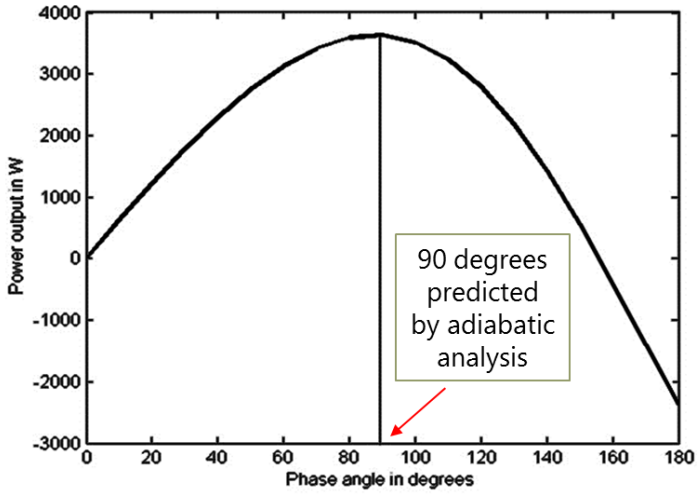

Figure 31 Optimal phase angle from dynamic and adiabatic analysis (subject to operating parameters)

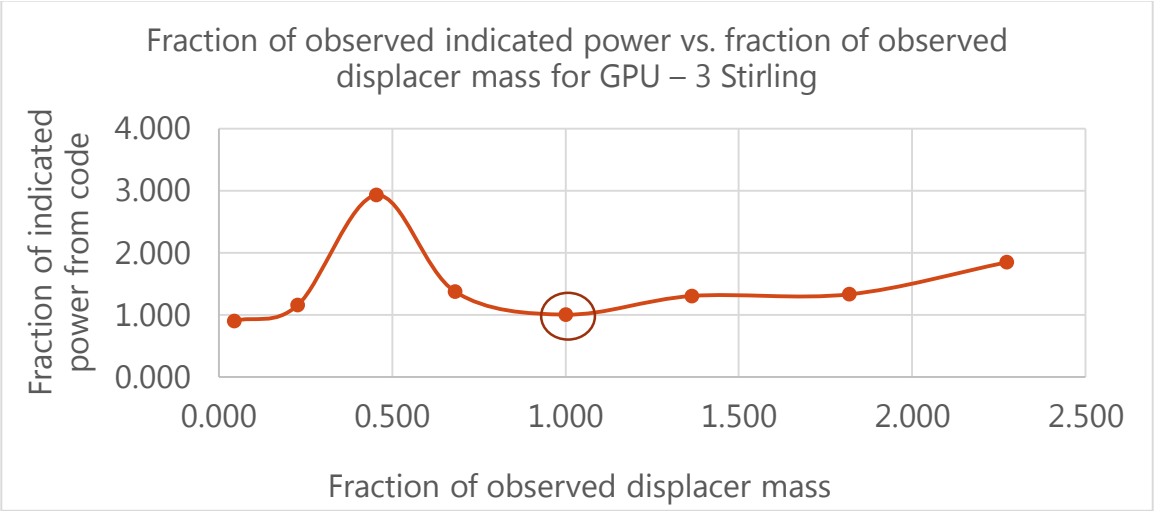

Figure 32 Fraction of indicated power vs. fraction of displacer mass for GPU-3 Stirling engine

The above graph clearly shows the variation of indicated power of the GPU-3 Stirling engine with respect to change in displacer mass. We notice that peak power is obtained for approximately 45% of actual displacer mass. This is consistent with theoretical predictions of increased power density at lower displacer masses. The power output in reality depends on a host of other factors apart from displacer and power piston mass. The choice of higher values in the GPU-3 Stirling engine is better explained in the following excerpt:

"Maximizing operating frequency while minimizing piston and displacer masses is key to increasing the power density. However, down-scaling these devices has proven problematic given that losses such as viscous friction in the piston seals and leakage (blow-by) dominate at small scales." - Riofrio et al, 'Control-Based Design of Free-Piston Stirling Engines', 2008, American Control Conference.

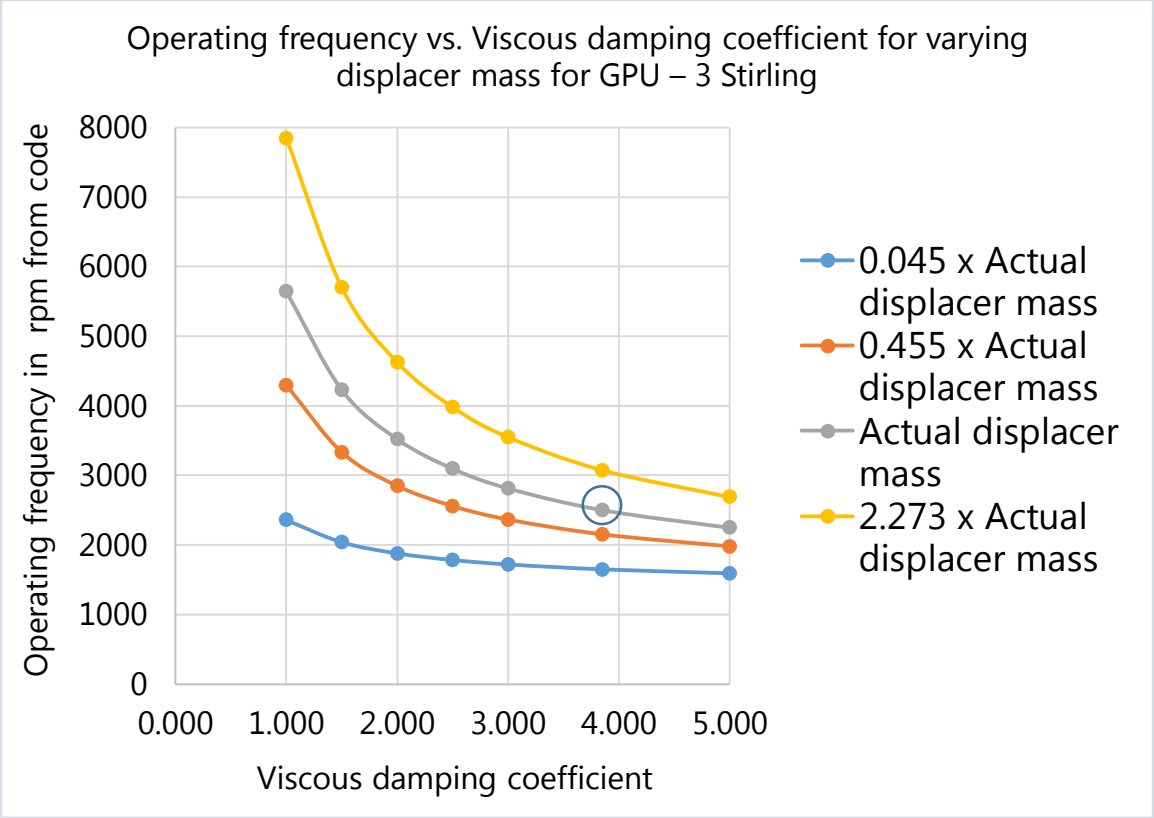

Figure 33 Operating frequency (rpm) vs. viscous damping coefficient at displacer for varying displacer masses in GPU-3 Stirling engine

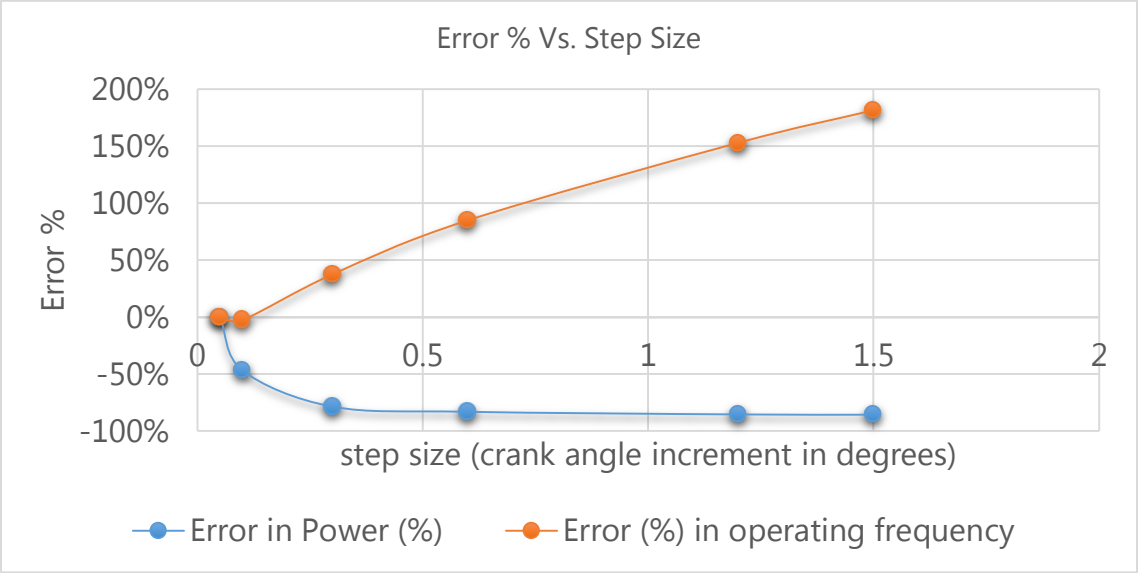

Figure 34 Error % vs. step size (crank angle increment) in dynamic analysis of GPU-3 Stirling engine

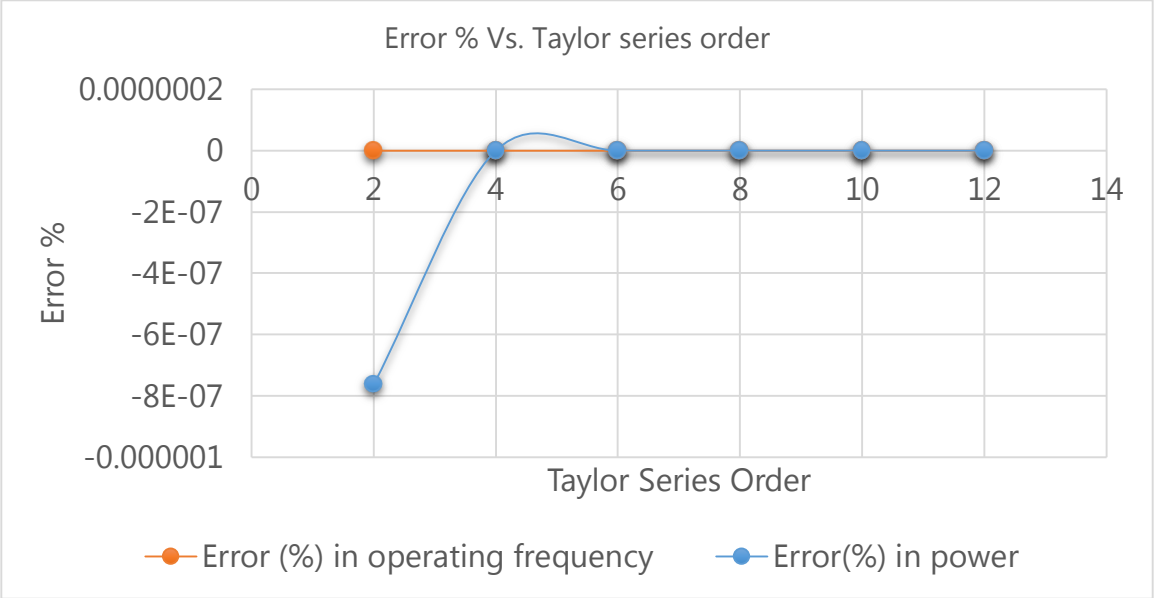

Figure 35 Error % vs. Taylor series order in dynamic analysis of GPU-3 Stirling

3.5 Validation of results obtained for GPU-3 Stirling engine with the MATLAB code (integrated adiabatic & dynamic model)

Validation of integrated code - part 1:

The analytical results are validated after comparing them with results obtained from previous research and mathematical models. Timoumi et al [56] presented a tabulated comparison of the performance predictions of GPU-3 Stirling engine obtained from various theoretical models in his research titled, 'Design and performance optimization of GPU-3 Stirling engines'. Our findings are presented in the same table for better comparison and understanding of the predicted results. This helps us understand some of the parameters considered or neglected by each of the approaches listed in the table.

Comparison of various model results

Numerical model	Heat (J/cycle)	Indicated power output	
		(W)	(J/cycle)
Adiabatic model	327	8286.7	198.62
Urielli and Berchowitz adiabatic model		*8300*	
Dynamic model without losses	314	7109.3	170.4
Urielli and Berchowitz quasi-steady flow		*7400*	
Dynamic model with loss dissipation = (M1)	291	6372.4	152.47
Urielli and Berchowitz quasi-steady flow (pressure drop included)		*6700*	
(M1) + Internal conduction loss = (M2)	294	6355.2	152.32
M2 + External conduction loss = (M3)	314	6061	145.27
M3 + Shuttle loss = (M4)	352	5886.1	141
Adiabatic analysis by Hirve N.	**241.27**	**5425.74**	**130.21**
Integrated dynamic analysis	**241.27**	**5127.38**	**123.07**
M4 + losses by gas spring hysteresis = dynamic model with losses	262	4273	99.5
Experiment	–	*3958*	–

Urieli and Berchowitz model and experimental results are shown in italics.

Y. Timoumi et al. / Energy 33 (2008) 1100–1114

Table 4 Comparison of various model results for GPU-3 Stirling engine [56]

It is clear from the above table that the integrated model predicts engine performance better than other mathematical models. The thermodynamic and dynamic model used in the integrated approach does not account for shuttle losses and conduction losses. This augurs well for the integrated model as consideration for these losses would yield much more accurate results. We also note that heat input per cycle in the integrated model is lower. This is because the other models do not account for dead volume or they consider the dead volume to be a part of the regenerator volume. The integrated model however considers the dead volume to be a part of the working volume and its contribution to the work done. This improves the accuracy of the model. Improvement of engine power prediction is observed when the dynamic and adiabatic models are clubbed together as against just adiabatic analysis of the system. This is consistent with the fact that adiabatic analysis does not take into account frictional losses, damping losses and vibrational losses.

Validation of integrated code - part 2:

Results obtained here are compared with the results of GPU-3 Stirling engine published in 'Stirling engine design manual' by William R. Martini in January, 1983 [51]. Extensive tests were carried out under different operating conditions and results were documented in detail in the report by William R. Martini. Given below are some of the tabulated test results published in this report. Subsequently data obtained from the integrated model is compared with the experimental findings from the Martini report to understand the accuracy and limitations of the integrated model.

Measurements of GPU-3 Engine Performance
by NASA-Lewis - Part V (79a)
Helium Gas, 649C (1200F) Nominal Heater Gas Temperature,
13C (56F) Cooling Water Inlet Temperature

Pt	Mean Pressure MPa	Mean Pressure PSIa	Engine Speed HZ	Engine Speed RPM	Brake Power KW	Brake Power HP	Heat Input* KW	Heat Input* HP	Brake Eff.* %
1	2.76	400	16.67	1000	0.82	1.10	3.95	5.3	20.5
2	2.76	400	25	1500	1.12	1.50	5.41	7.25	20.7
3	2.76	400	33.33	2000	1.21	1.62	6.64	8.9	18.0
4	2.76	400	41.67	2500	1.21	1.62	7.64	10.25	15.2
5	2.76	400	50	3000	1.04	1.40	8.95	12.00	11.8
6	2.76	400	58.33	3500	0.56	0.75	9.88	13.25	5.4
7	4.14	600	25	1500	1.79	2.40	7.23	9.70	24.8
8	4.14	600	33.33	2000	2.20	2.95	9.17	12.30	23.9
9	4.14	600	41.67	2500	2.42	3.25	11.33	15.20	21.3
10	4.14	600	50	3000	2.35	3.15	12.83	17.20	18.2
11	4.14	600	58.33	3500	1.73	2.32	14.32	19.20	12.0
12	5.52	800	41.67	2500	3.28	4.40	14.69	19.70	22.5
13	5.52	800	50	3000	3.28	4.40	17.45	23.40	18.8
14	5.52	800	58.33	3500	2.76	3.70	19.18	25.72	14.2
15	6.9	1000	50	3000	3.93	5.27	20.88	28.0	18.7
16	6.9	1000	58.33	3500	3.37	4.52	23.15	31.05	14.2

*Based upon energy balance at cold end.

Table 5 GPU-3 Stirling test data for Helium gas [51]

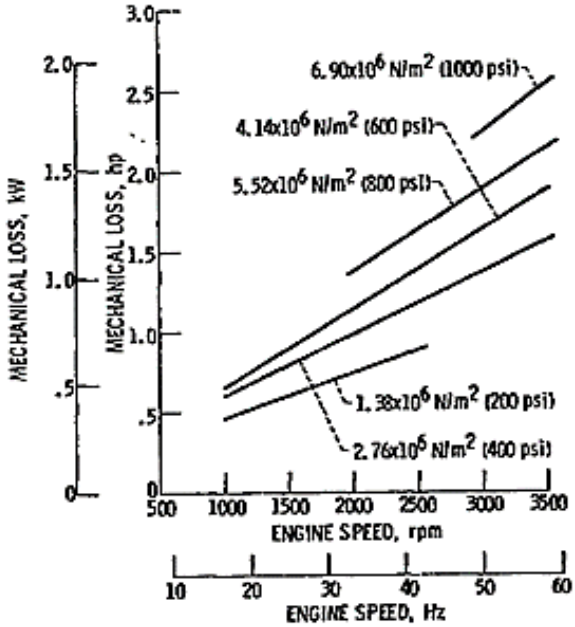

Mechanical Loss As a Function
of Engine Speed for Helium Working Gas
(Determined from experimental heat balance.)

Figure 36 Mechanical loss as a function of engine working speed for helium [51]

The above graph helps estimate the mechanical losses at various engine pressures for different operating speeds in GPU-3 Stirling engine. This data is based on extensive testing of GPU-3 Stirling engine in varying operating conditions. Integrated model results are compared with these results in the table shown below.

S.No	Mean pressure	Frequency	Analysis output	Heat transfer losses	Indicated power by analysis	Mechanical loss (NASA)	Brake power by analysis results	Experimental Measured brake power	Input power by analysis	Experimental Input power	Brake efficiency by analysis	Experimental Measured efficiency
	MPa	Hz	kW	kW	kW	kW	kW	kW	kW	kW	%	%
1	2.76	33.33	2.75	0.63	2.13	0.8	1.33	1.21	5.4	6.64	24.59	18.22
2	4.14	41.67	5.13	0.78	4.34	1.4	2.94	2.42	10.15	11.33	29.02	21.30
3	5.52	50	7.23	0.94	6.29	1.9	4.39	3.28	15.58	17.45	28.20	22.50

Table 6 GPU-3 Stirling engine test results (experimental vs. analytical)

The GPU-3 Stirling engine is analyzed at three mean pressure values (2.76 MPa, 4.14 MPa, 5.52 MPa) using the integrated code. Heat transfer loss values [56] are applied to the analysis results and indicated power is obtained. Application of mechanical loss values (from the graph above, [51]) to the indicated power, yields brake power. The calculated brake efficiency and the experimentally measured brake efficiency are in good agreement. As the mean pressure is increased, difference between calculated brake efficiency and experimentally measured brake efficiency decreases. The integrated model performs better at higher mean pressures. The following graph explains this better.

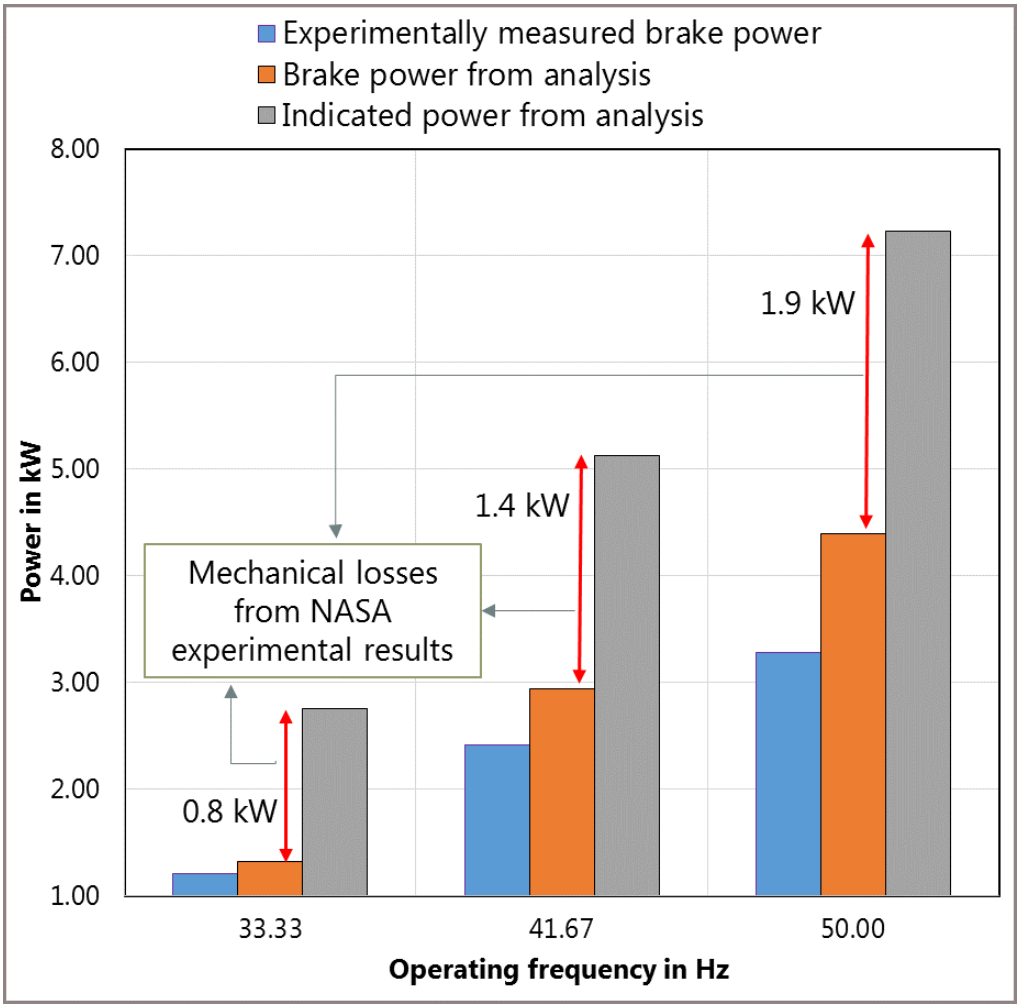

Figure 37 Comparison of power output of GPU-3 Stirling engine

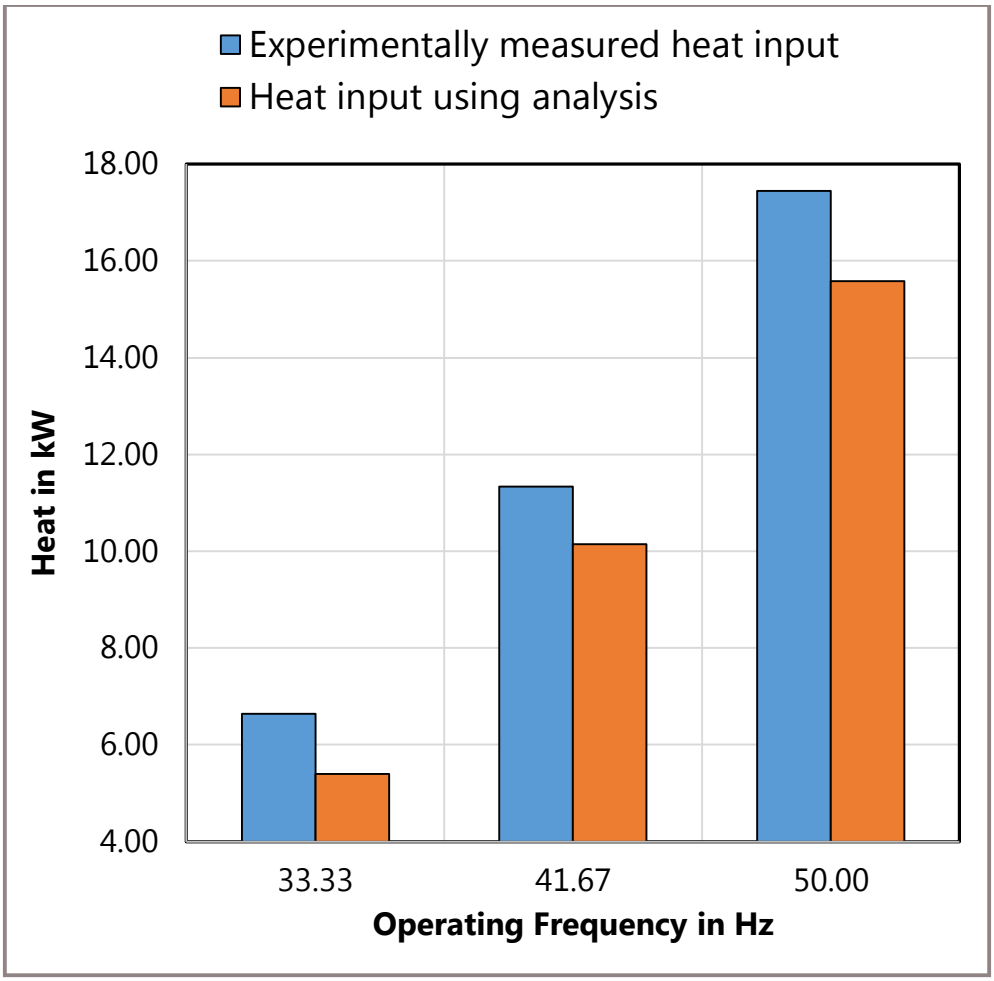

Figure 38 Heat input (analytical vs. experimental) for the GPU-3 Stirling engine

We observe from the above graphical data that the input power (in the form of heat) for the GPU-3 Stirling engine is higher in the experimentally measured data than what is predicted analytically by our integrated code. This is justified by the slightly higher brake efficiency predicted by our integrated code than what is observed experimentally.

Validation of integrated code - part 3:

The integrated is validated by comparing its results with those obtained from the research (based on experimental data) by Johannes Matthias Strauss [57] with

respect to the GPU-3 Stirling engine. Greater understanding is achieved by comparing the force acting at power piston of GPU-3 Stirling engine with displacement for different mass to power ratios.

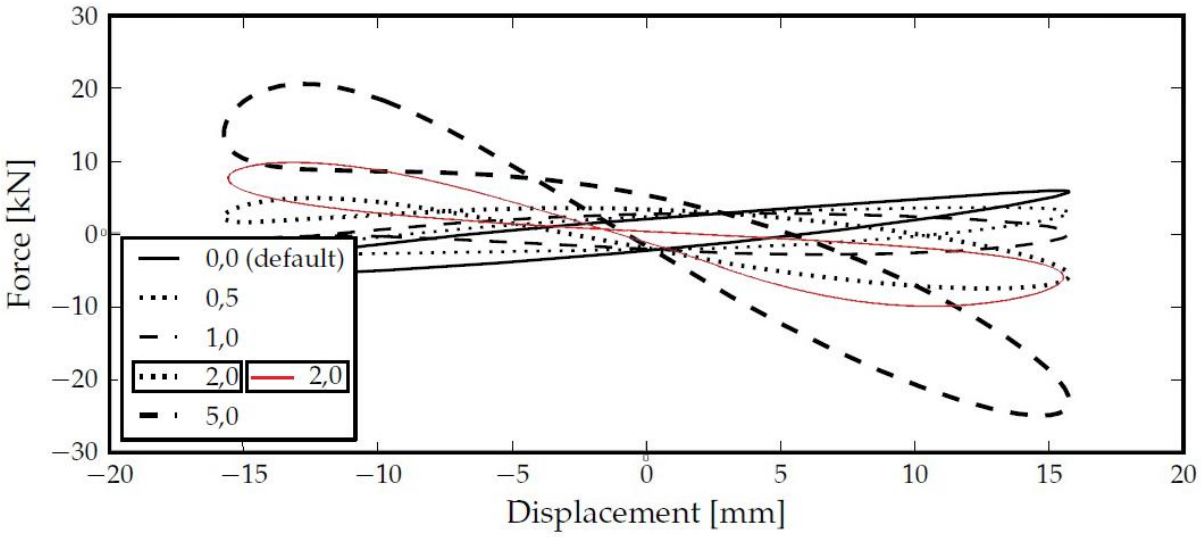

Power piston linear machine force against displacement for various mass to power ratios.

Figure 39 Power piston force vs. displacement for various mass to power ratios in the GPU-3 Stirling engine (mean pressure 4.14 MPa) [57]

The power piston force is calculated by the integrated code and plotted (mass to power ratio of 2 g/W). The analytically calculated values (shown in the red curve in the above graph) are in close agreement with the experimental values (black dotted curve for 2 g/W). The slightly higher force values evident from the locus of the red curve in the graph are justified by higher power output predicted by integrated code. Higher power output & efficiency correspond to higher power piston force. Clearly, the close agreement of the results from the integrated code with three different accepted research findings (as discussed above) is sufficient validation of the efficacy of the integrated model developed here.

CHAPTER FOUR

4. Design and optimization of a simple free piston Stirling engine

4.1 Preliminary design and analysis of free piston Stirling engine (FPSE)

An analysis is now carried out to design a sample free piston Stirling engine using the theoretical model (integrated code) developed earlier. The approximate equation for power output of a Stirling engine is given in the book on Stirling engines by Walker [53]. It was developed by William Beale, using statistical data of numerous Stirling engines manufactured over the years, and is given as

$$P = 0.015\, f\, V\, p \qquad \text{[Equation 4.1]}$$

Where,

P= Power output, in W

f= Frequency of operation of engine, in Hz

V= total working volume of the engine, in cm^3

p= mean pressure inside engine, in bar

Helium gas is the working fluid. The targeted power output for the test case will be 500 Watts. Using the above equation and assuming an engine frequency of 15 Hz (900 rpm), and mean pressure of 3 bar, the required working volume equals 740 cm^3 to produce a work output of 500 W. This equation does not depend on the working fluid or the engine hot end and cold end temperatures. But output accuracy is definitely constrained by operating temperatures and working fluid. This equation works best for medium temperature differential (which is our case). The actual power output will change subject to manufacturing precision and

engine design. The above equation gives a broad view of the power output to be expected, and provides a start point. Hot end and cold end temperatures are assumed to be 600^{o}C (873K) and 50^{o}C (323K) respectively. The design process is iterative to optimize performance and parameters.

Results from integrated MATLAB code:

Parameters used are:

• Helium initial pressure = 7 bar. • Cold end working volume = 740/3 = 246.67cm^3. • Displacer hot end and cold end volume = 120 cm^3. • Hot end temperature = 800K. • Cold end temperature = 300K. • Regenerator effectiveness = 1.

Viscous damping coefficients from 2.5 to 4 are considered for working piston and displacer with the higher value being assigned to the displacer. Spring damping values from 1 to 1.8 are considered with lower value being assigned to displacer. Mass of stationary engine components in direct contact with the oscillating surfaces is considered to be 4.2 kg. The mass of displacer is 50 grams and that of working piston is 110 grams. Spring stiffness values of 550 N/m and 1000 N/m are respectively considered for displacer and the working power piston. We assume one spring each connected to displacer and power piston.

Code output for given set of parameters:

```
Adiabatic Analysis
--------------------
Enter the crank angle increment in degrees: 0.1
Enter number of iterations: 6
```

```
Compression ratio = 1.4246

Work output per cycle in Joules = 129.3130

Heat input per cycle at hot end in Joules = 252.9031
Heat rejected per cycle at cold end in Joules = -130.7632
Heat absorbed/rejected by regenerator per cycle in Joules =
-3.9033e-07

Cycle efficiency in % ge = 51.1314

Dynamic Analysis
-------------------

Enter the required Taylor series order: 8

Power output per cycle from engine in Watts =
2.639161696720816e+02

Average operating frequency of engine in Hertz=
12.972132636936044

Optimal Phase difference between displacer and working piston
in degrees = 89.9
```

A significant efficiency drop is observed in the dynamic analysis results because of the high value of various damping coefficients considered here. Phase difference predicted is very close to the optimal theoretical value of 90^{o}. The dynamic analysis predicts the power output to be about 264 watts and an operating frequency of

approximately 13 Hz. Each cycle is 360 degrees of crank angle for simplicity in nomenclature. Graphs are plotted with respect to crank angle in degrees.

Plots for various engine parameters are shown below:

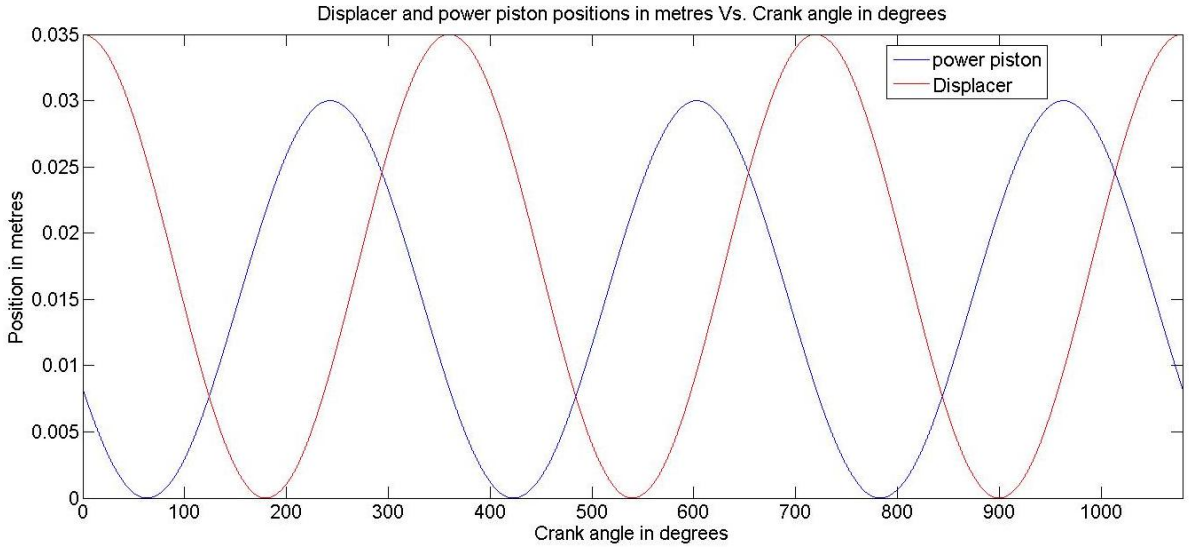

Figure 40 Piston positions vs. Crank angle - (Phase difference)

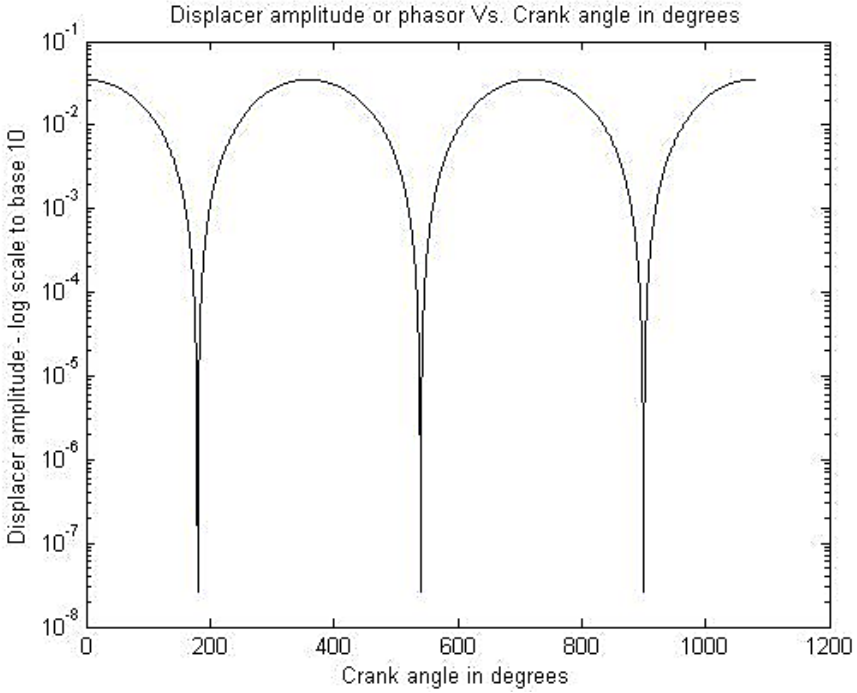

Figure 41 Displacer amplitude vs. Crank angle in degrees

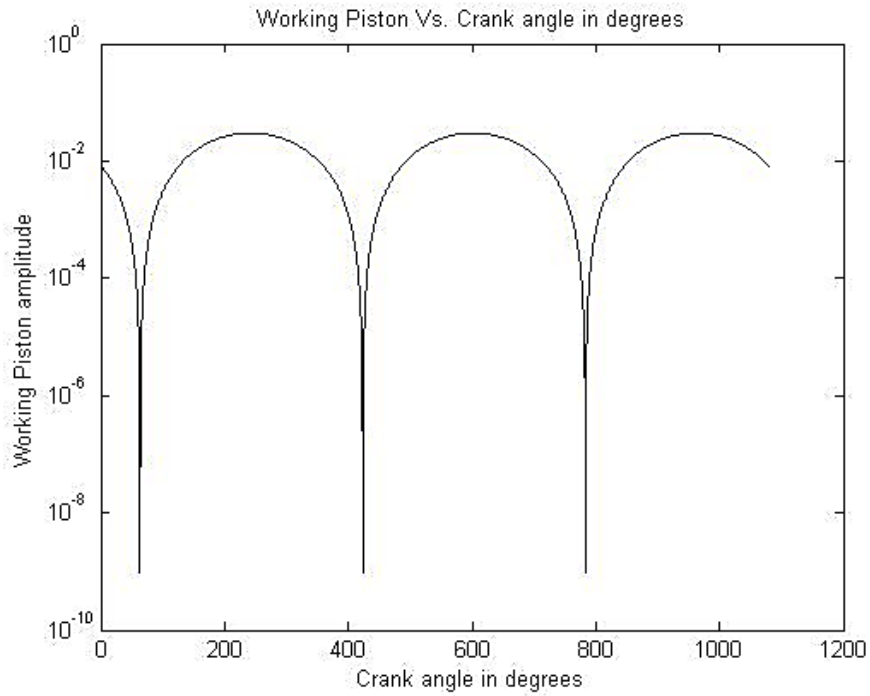

Figure 42 Working piston amplitude vs. Crank angle

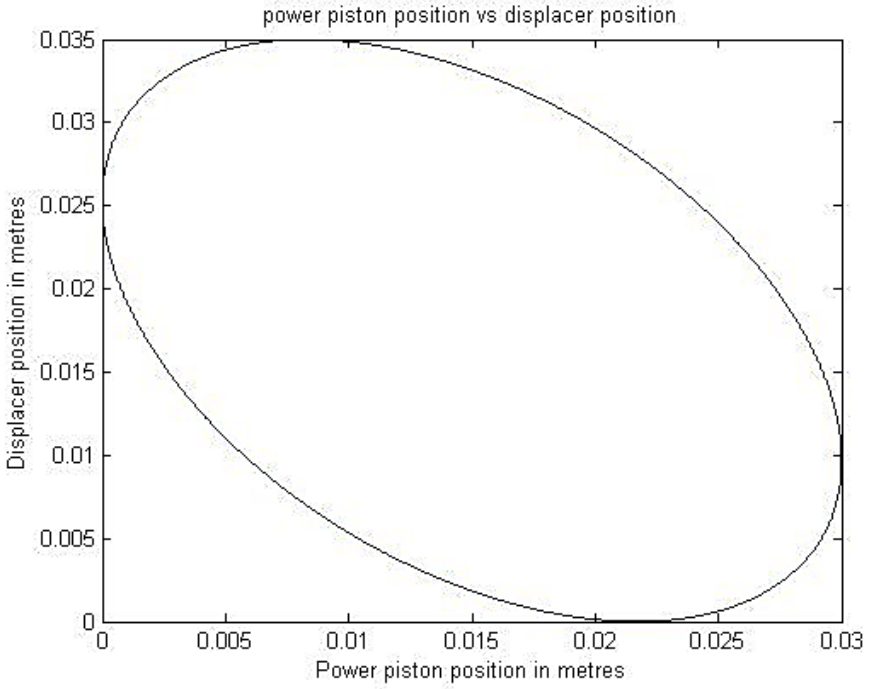

Figure 43 Power piston position vs. displacer position

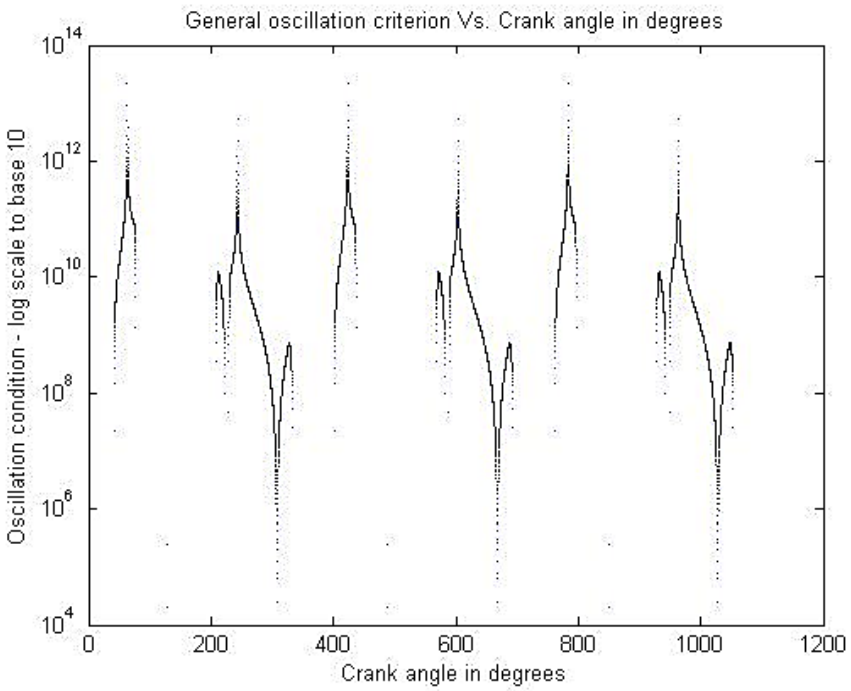

Figure 44 General Oscillation Criterion vs. Crank Angle

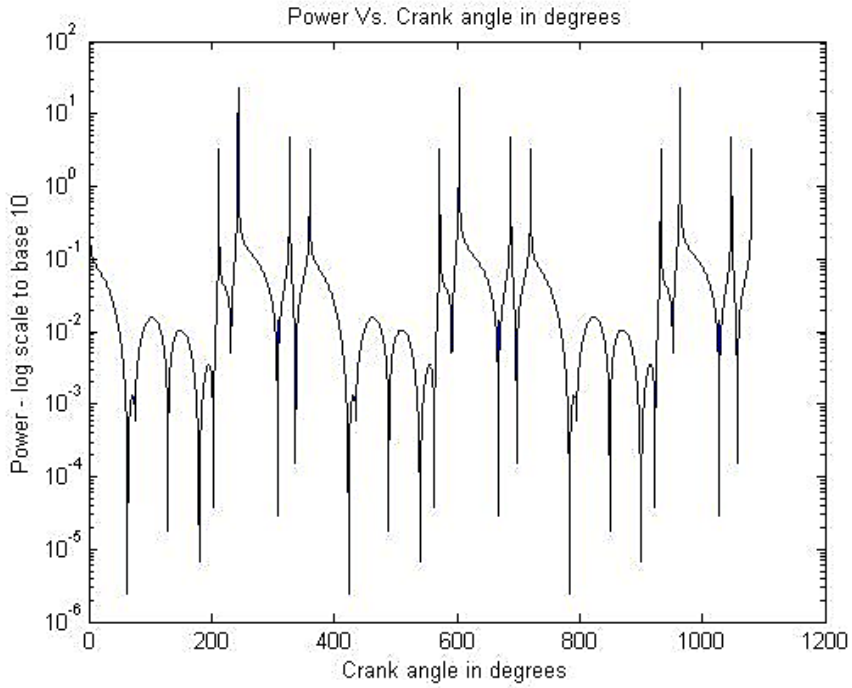

Figure 45 Power vs. Crank angle

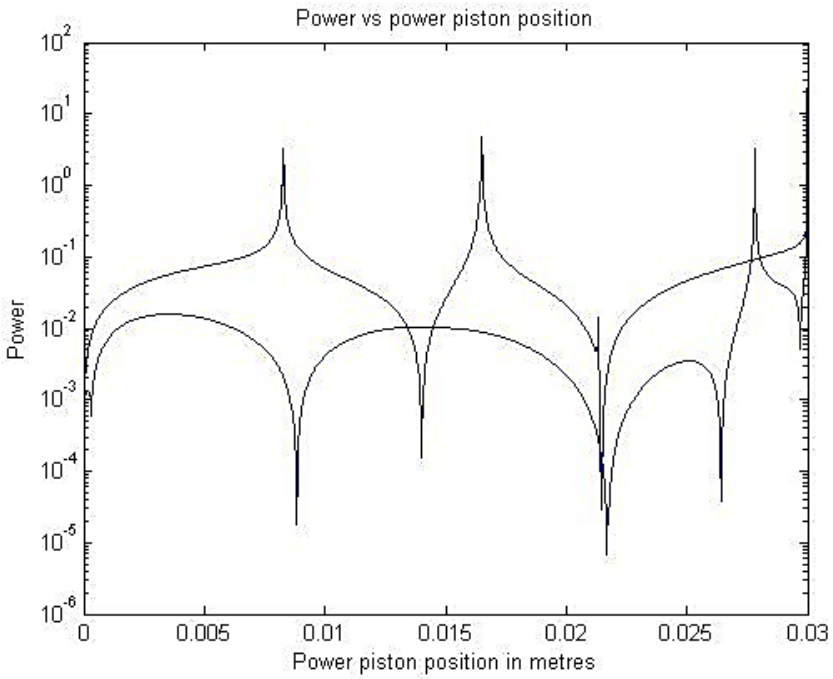

Figure 46 Power output vs. Power piston position over 3 cycles of engine run

4.2 Free piston Stirling engine schematic diagram and transient thermal analysis of the structure in ANSYS

The results obtained above were used to create the geometric design of the free piston Stirling engine. The engine design progressively underwent changes. The following figures illustrate this design evolution process. Subsequent manufacturing also underwent numerous changes. Theoretical results were used to fine tune the engine further. A maximum tolerance study was carried out to decide the tolerances and clearances at various points in the free piston Stirling engine.

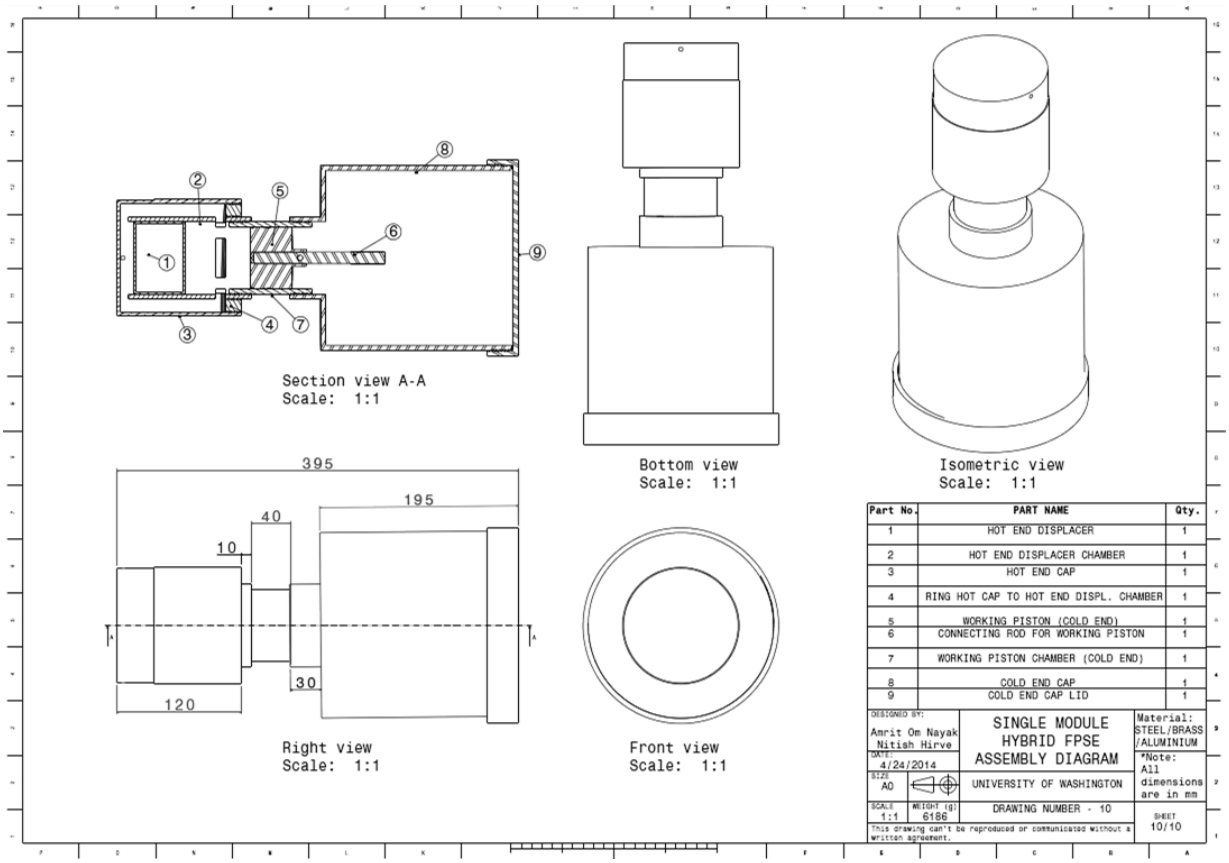

Figure 47 Drafting of free piston Stirling engine design

Results from transient analysis in ANSYS:

The following are some of the parameters used for transient analysis in ANSYS.

Parameters	**Properties of Helium used for transient analysis**
Constants	
Density (kg/mm^-3)	1.63E-10
Specific heat (mJ kg^-1 C^-1)	5.19E+06
Thermal conductivity (W mm^-1 C^-1)	1.51E-05
Viscosity (MPa s)	1.99E-11
Molecular weight (kg mol^-1)	4.00E-03
Formation enthalpy (MPa mm^3 mol^-1)	-3.12E+06
Reference temperature (degree C)	25

Formation entropy (mJ C^-1)	1.26E+08
Critical pressure (MPa)	0.229
Critical temperature (degree C)	-267.85
Critical volume (mm^3)	1.44E+07
Ideal Gas EOS	
Adiabatic exponent (ϒ)	1.66
Adiabatic constant	22.15
Pressure shift (Mpa)	100
Reference temperature (degree C)	30
Specific internal energy (mJ kg^-1)	1.00E-02
	Copper constants used for transient analysis
Thermal conductivity (W mm^-1 C^-1)	0.4
Density (kg mm^-3)	8.93E-06
Specific heat (mJ kg^-1 C^-1)	3.85E+05

Table 7 (Table set) Parameters for transient analysis in ANSYS

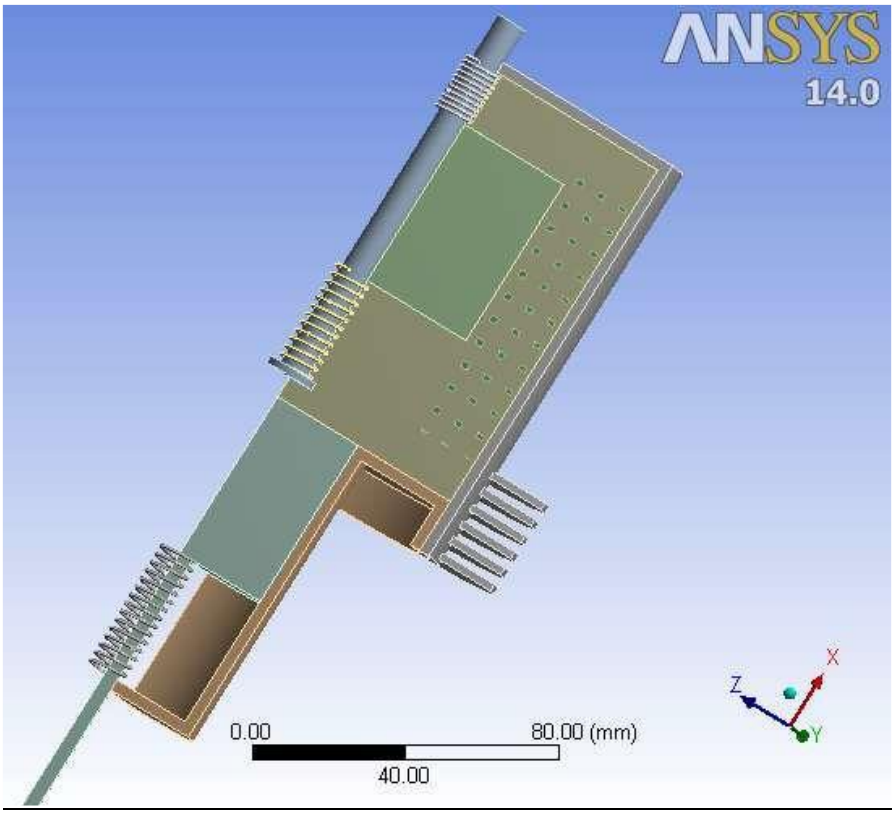

Figure 48 Sectional view of free piston engine used for transient analysis

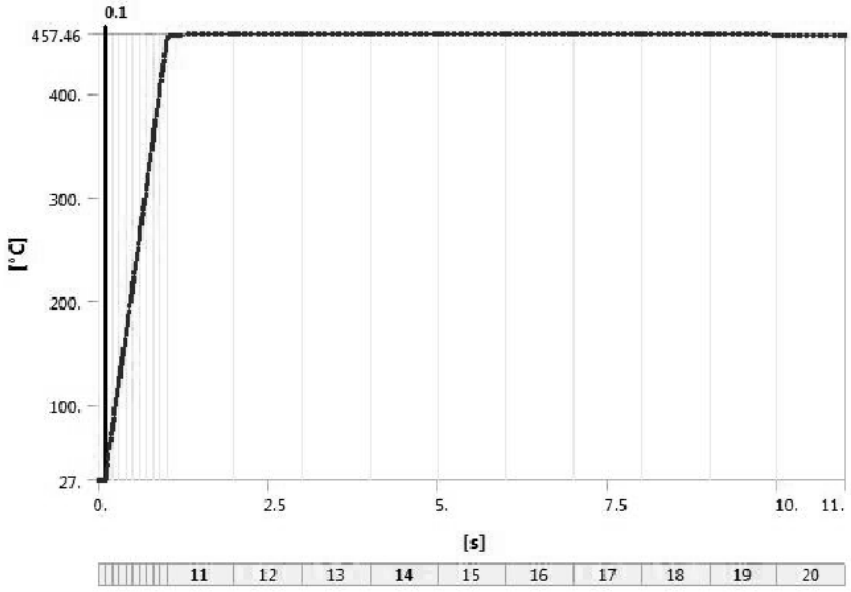

Figure 49 ANSYS transient analysis - temperature of hot end brass cap after 11 seconds of heating with a propane burner

Steps	Time [s]	Temperature [°C]
1	0.	27.
	0.1	
2	0.2	= 74.
3	0.3	= 121.
4	0.4	= 168.
5	0.5	= 215.
6	0.6	= 262.
7	0.7	= 309.
8	0.8	= 356.
9	0.9	= 403.
10	1.	450.
11	2.	= 450.
12	3.	
13	4.	
14	5.	
15	6.	
16	7.	
17	8.	
18	9.	
19	10.	
20	11.	

Table 8 Temperature values of hot end cap with time in transient ANSYS analysis

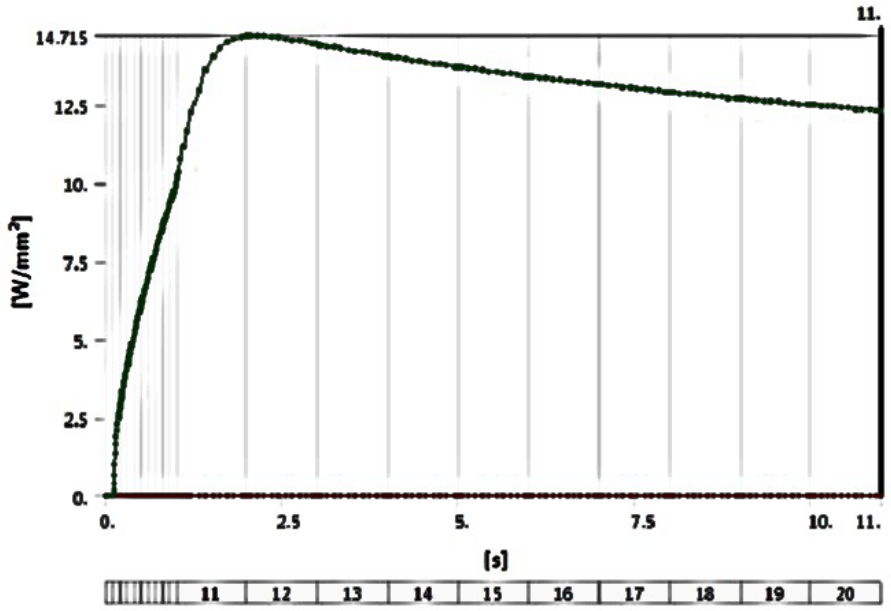

Figure 50 Total heat flux in transient ANSYS analysis

4.3 Maximum tolerance study and manufacturing of FPSE

Volumetric expansion study to decide tolerances

Hot end cylinder:

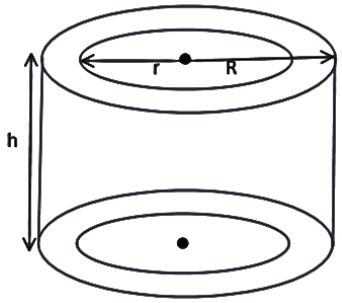

Figure 51 Hot end cylinder schematic - thermal expansion based tolerance study

For the cylinder shown above, let initial volume $(V_i) = \pi h(R^2 - r^2)$ [Equation 4.2]

Final Volume of cylinder after heating,

$(V_f) = V_i + \Delta V = \pi(h + \Delta h)[(R + \Delta R)^2 - (r - \Delta r)^2]$

$$= V_i + \Delta V + 2\pi\{R(\Delta R) - (r\Delta r)\}(h + \Delta h) + \pi h(\Delta R^2 - \Delta r^2) + \pi(\Delta h)(R^2 - r^2)$$

[Equation 4.3]

In practice, the hot end cap is at a maximum temperature and displacer cylinder is at a lower temperature. Further, the displacer cylinder top is close to the hot end and its bottom is close to the cold end. Hence, we take an average of the two temperatures. We now take $T_{H,max}$ = 800 K and T_C = 315 K. Further, we consider for heating expansion, a value of 'R/2', a heating factor value of 0.8 for the actual heat reaching the hot end displacer cylinder and 'h' to be constrained. This is a preliminary estimate. We now apply the coefficient of linear expansion formula to each of the dimensions 'R', 'r', and 'h' so as to obtain the maximum possible expansion in them in the case of the entire heat being applied to them individually. Let 'α' be the coefficient of linear expansion of the material used here. If the material used is steel, then $\alpha = 13 \times 10^{-6}\ K^{-1}$ or $^oC^{-1}$

ΔR_{max} (when r & h are constrained) $= 0.8\alpha R(\Delta T) = 0.8 \times 13 \times 10^{-6} \times (0.5R) \times (800\text{-}315)$

$= 0.002522R$ metres [Equation 4.4]

Similarly, Δr_{max} ('R' & 'h' are constrained) $= 0.8\alpha r(\Delta T) = 0.8 \times 13 \times 10^{-6} \times (0.5r) \times (800\text{-}315) = 0.002522r$ metres [Equation 4.5]

And $\Delta h_{max} = 0 \rightarrow h_{final,\ max} = h_i$ [Equation 4.6]

Hence, $V_{f,\ max} = 1.005050360484V_i + \Delta V_{max}$ [Equation 4.7]

But if β (coefficient for volumetric expansion ≈ 3α) for steel is $39 \times 10^{-6}\ K^{-1}$ or $^oC^{-1}$, then we get,

$\Delta V_{max} = \beta V_i(\Delta T) = 39 \times 10^{-6} \times 0.5V_i \times (800 - 315) = 0.0094575V_i$ [Equation 4.8]

$V_{f,\ max} = 1.01450786V_i$ [Equation 4.9]

Where $R_{f,\,max} = 1.002522R$; $r_{f,\,max} = 1.002522r$; $h_{f,\,max} = h$ [Equation 4.10]

Hot end displacer (subscript 'd' is used to indicate displacer dimensions):

Let 'V_{da}' represent the actual volume of the displacer shell and let 'V_d' represent the total of the displacer (calculated by using 'R_d' as the radius).

$V_{da} = \pi h_d(R_d^2 - r_d^2)$ [Equation 4.11]

$V_d = \pi h_d R_d^2$ [Equation 4.12]

In this case we constrain r_d and $h_d \rightarrow \Delta r_{max,d} = \Delta h_{max,d} = 0$

And we get, $\Delta R_{max,d} = 0.002522R_d$ [Equation 4.13]

$V_{f,\,max,d} = V_{da} + \Delta V_d + 2\pi\{R_d(0.002522R_d)\}h_d + \pi h_d(0.002522R_d)^2$

$= V_{da} + \Delta V_d + \pi h_d\{0.005050360484R_d^2\}$ [Equation 4.14]

& $\Delta V_d = 0.8\ \beta V_{da}(\Delta T) = 39 \times 10^{-6} \times V_{da} \times (800 - 315) \times 0.5 = 0.0094575V_{da}$

[Equation 4.15]

$V_{f,\,max,d} = 1.0094575V_{da} + 0.00505036V_d$ [Equation 4.16]

Where $R_{f,\,max,\,d} = 1.002522R_d$; $r_{f,\,max,\,d} = r_d$; $h_{f,\,max,\,d} = h_d$ [Equation 4.17]

The table below shows a sample analysis using the mathematical relations derived above (refer to Appendix C for materials used).

	r (in cm)	R(in cm)	h(in cm)	V(in cm^3)	r.f(max) (in cm)	R.f(max) (in cm)	h.f(max) (in cm)	ΔV(max) (in cm^3)	V.f(max) (in cm^3)	% INCREASE
cylinder	5.5	6.5	6.6	248.81	5.51	6.52	6.6	2.35	252.42	1.45
displacer	5.1	5.5	3	39.96	5.1	5.51	3	0.76	41.78	4.55

Table 9 Volumetric expansion (thermal) sample analysis

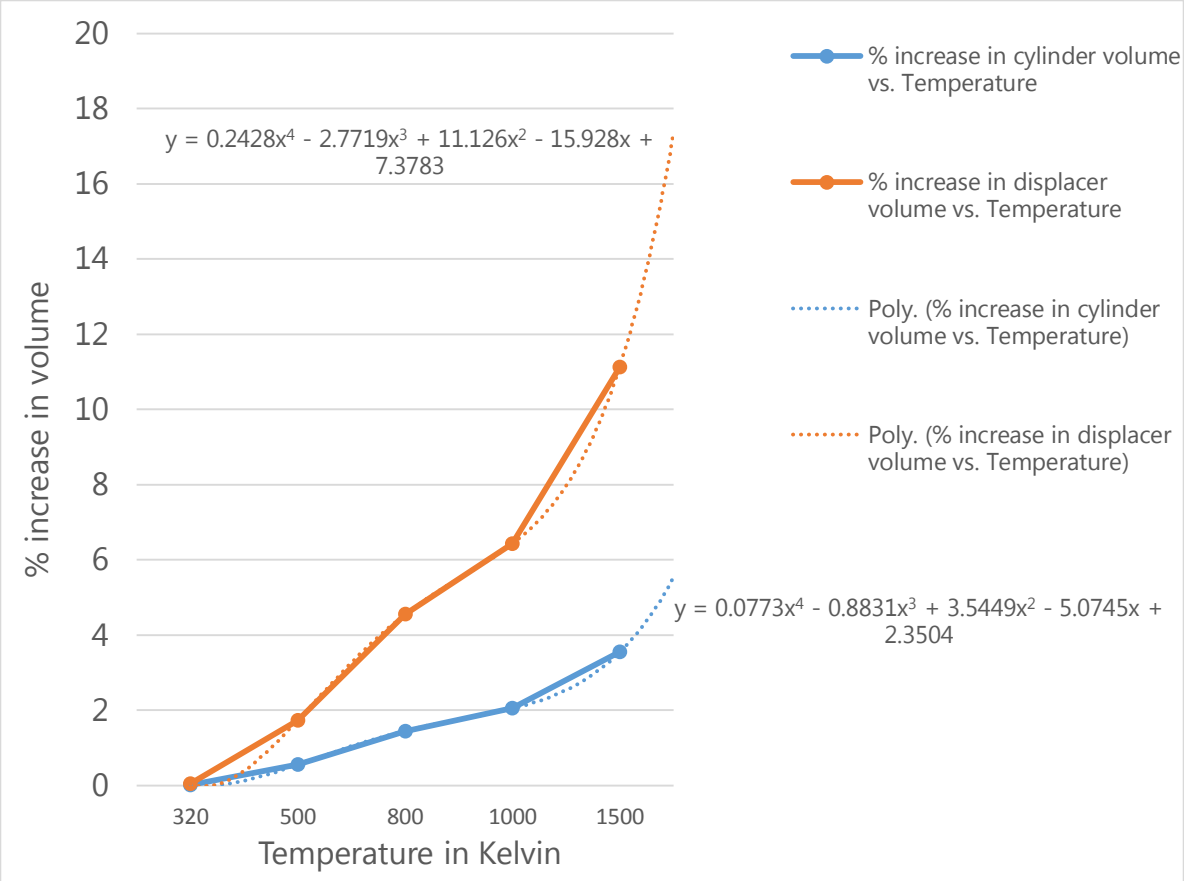

Figure 52 Percentage increase in volume of hot end cylinder and displacer with rise in temperature

The first stage of manufacturing was followed by design optimization after preliminary testing. The aluminum power piston at the cold end was replaced with a piston made of Acetal (or Delrin) plastic polymer. A thorough analysis yielded favorable results in support of this move. This greatly improved machinability and surface finish while reducing machining time. It was also observed that steel body of the cold end cylinder would wear out the new piston made of Acetal. Hence, a thin cylinder lining made out of Acetal was fabricated for the cold end cylinder. This helped reduce component mass, friction and eliminated the need for special operations at the cold end. Piston rings made out of Acetal were fabricated for the

new cold end piston so as to obtain better suction and reduce leakages. Software aided optimization was also carried out using the MATLAB code developed previously.

Figure 53 First set of engine components manufactured

4.4 Software simulation of manufactured free piston Stirling engine

Engine dimensions remain the same as mentioned in previous chapter. Mass of steel displacer is 264 grams. Power piston made of Acetal weighs 110 grams. Mass of stationary engine components directly affecting oscillation is 5.8 kg.

MATLAB output:

```
Adiabatic Analysis
------------------
Enter the crank angle increment in degrees: 0.01
Enter number of iterations: 9
Compression ratio = 1.3859
Work output per cycle in Joules = 16.6654
Heat input per cycle at hot end in Joules = 29.6967
Heat rejected per cycle at cold end in Joules = -15.5192
Heat absorbed/rejected by regenerator per cycle in Joules =
-2.1517e-04
Cycle efficiency in %ge = 56.1189

Dynamic Analysis
----------------

Enter the crank angle increment in degrees: 0.1
Enter number of iterations: 6
Enter the required taylor series order: 8
Average Power from engine in Watts = 57.320961565215846
Average operating frequency of engine = 13.148354491987975
Stroke-ratio of engine =    1.093457321442433

Optimal Phase difference between displacer and working piston
in degrees = 82.212576286029801
```

Graphical results:

The following graphical results are for a crank angle increment of 0.1 degree and Taylor series order of 8.

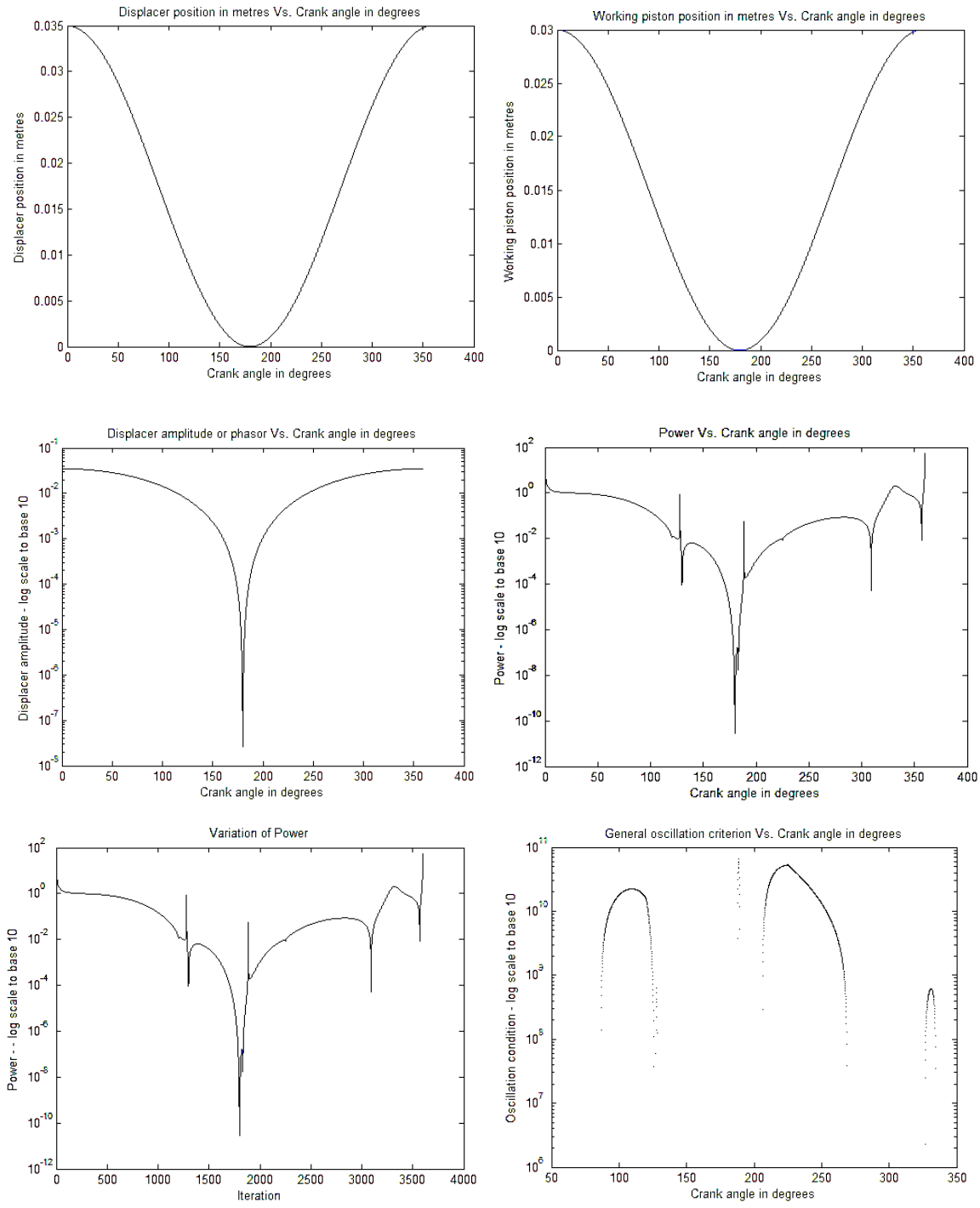

Figure 54 Dynamic analysis of fabricated free piston Stirling engine (first design)

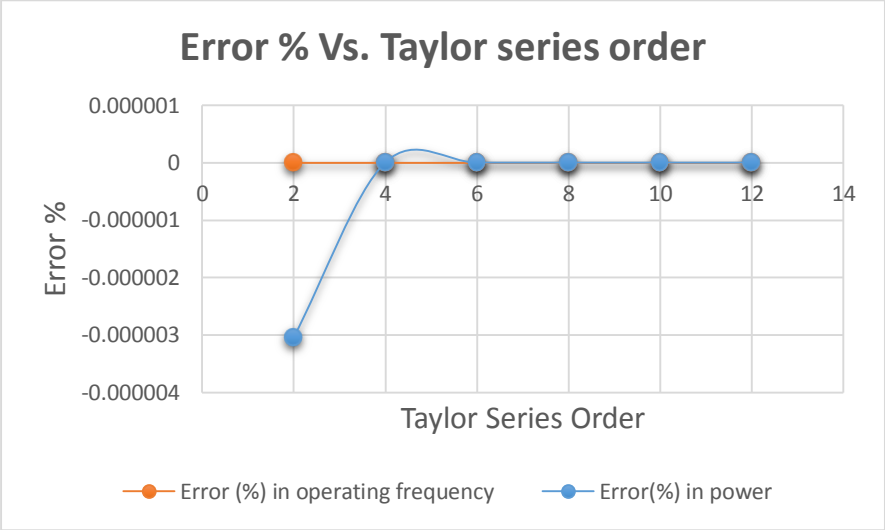

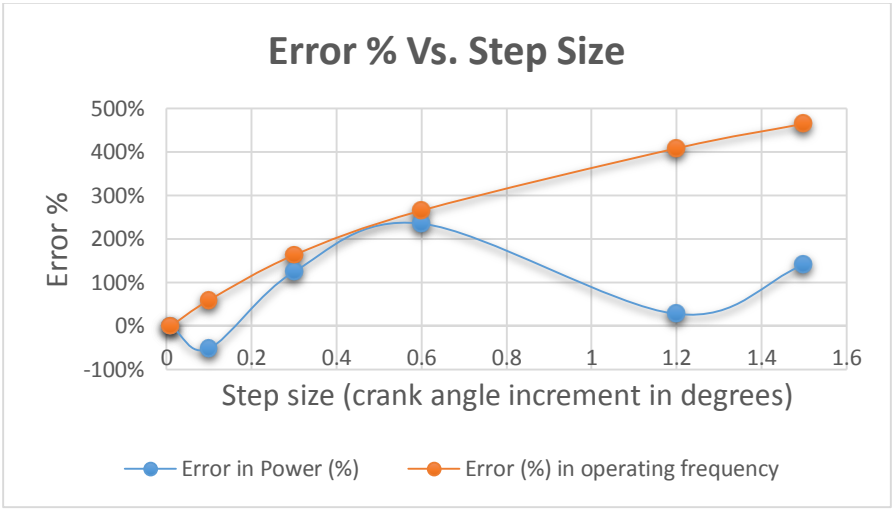

Figure 55 Error % in dynamic analysis

Inferences

→ Power output of engine predicted by adiabatic analysis is 249.98 Watts. However, dynamic analysis shows predicts just 57.321 Watts. This means that remaining power is lost in damping, viscous forces etc. consistent with observed extreme difficulty in starting of the free piston Stirling engine in question.

→ The operating frequency is predicted by the dynamic analysis to be about 13.15 Hz which is close to the design operating frequency of 15 Hz. However, for higher

iterations and smaller step size (smaller crank angle increments), we obtain lower values consistent with loss in power due to damping, viscous forces etc.

→ The general oscillation criterion graph shows the regions where the criterion is violated. These are 130 degrees to 200 degrees and 270 degrees to 325 degrees of displacer positions, also reflected in the power output graphs where sudden is observed. We infer no net power is generated in these regions and damping occurs. The system tries to continue using momentum and energy stored in springs. This is consistent with the flattened regions in the power graph.

→ Viscous damping, spring damping and spring stiffness needs to be reduced. It is also necessary to reduce friction along sliding surfaces. Displacer is too heavy for the system resulting in greater inertia while starting and overall damping.

→ At very small step size (say 0.01 crank angle increment or lower), the power (118 Watts) and operating frequency (8 Hz) values undergo appreciable changes and are more realistic. This suggests that the dynamic model requires a very large number iterations (>50000) to obtain stable solutions due to the complexity of the mathematical model. However, such low step sizes require more than 2000 seconds to process and the time required increases drastically with reduction in step size. Therefore, the process is expensive and more powerful computing resources are required to evaluate the model more accurately.

→ Phase difference value of about 82.215 degrees obtained here is almost similar the adiabatic analysis prediction of about 81 degrees.

4.5 Design optimization and improvements in free piston Stirling engine

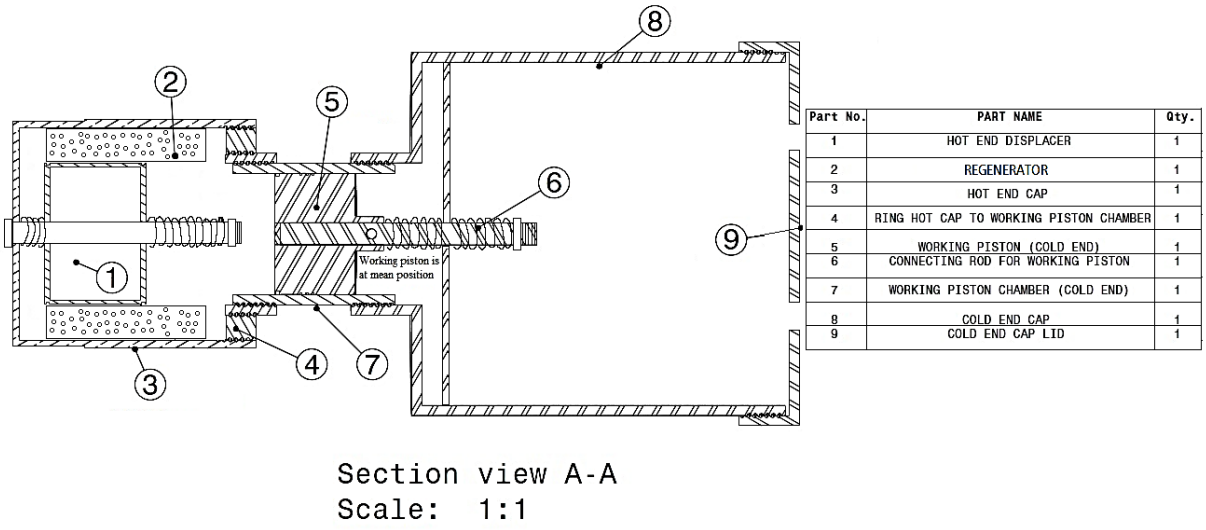

Part No.	PART NAME	Qty.
1	HOT END DISPLACER	1
2	REGENERATOR	1
3	HOT END CAP	1
4	RING HOT CAP TO WORKING PISTON CHAMBER	1
5	WORKING PISTON (COLD END)	1
6	CONNECTING ROD FOR WORKING PISTON	1
7	WORKING PISTON CHAMBER (COLD END)	1
8	COLD END CAP	1
9	COLD END CAP LID	1

Figure 56 Schematic of improved design of free piston Stirling engine

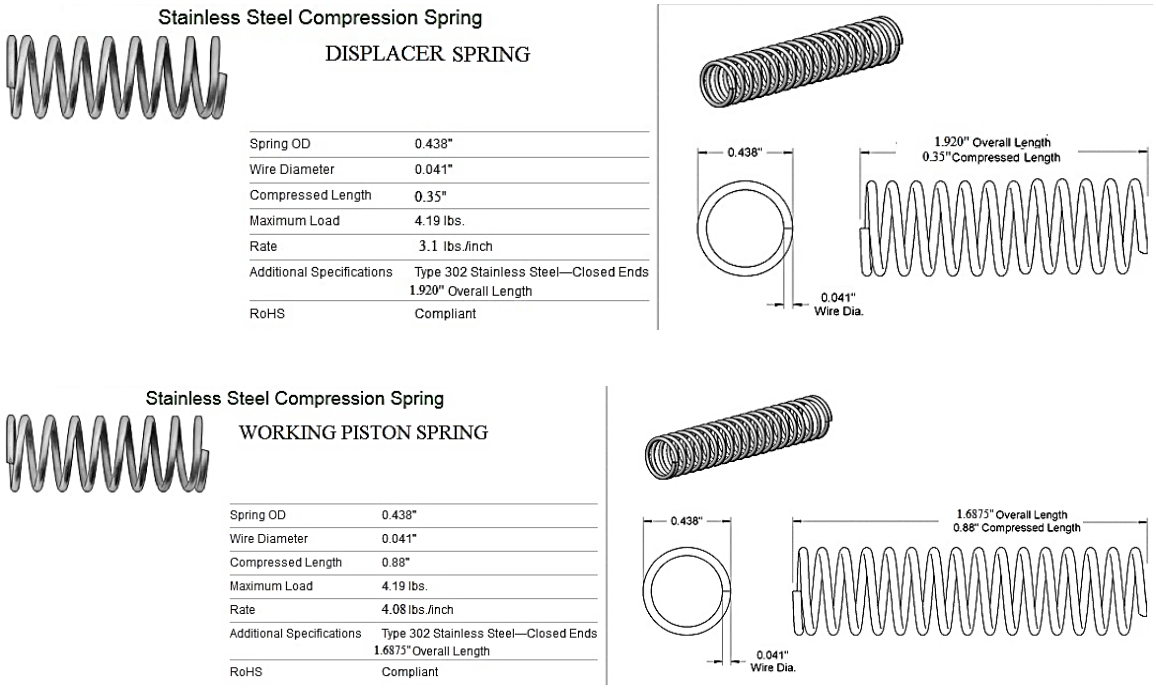

Figure 57 Springs used for displacer and power piston in modified engine design

The modified free piston Stirling engine design photographs are shown in Appendix C of the report.

CHAPTER FIVE

5. Auxiliary systems

5.1 Schematic of proposed biomass combustion system for CHP

Fluidized bed combustion technology is proposed for biomass combustion in the free piston Stirling engine based CHP system.

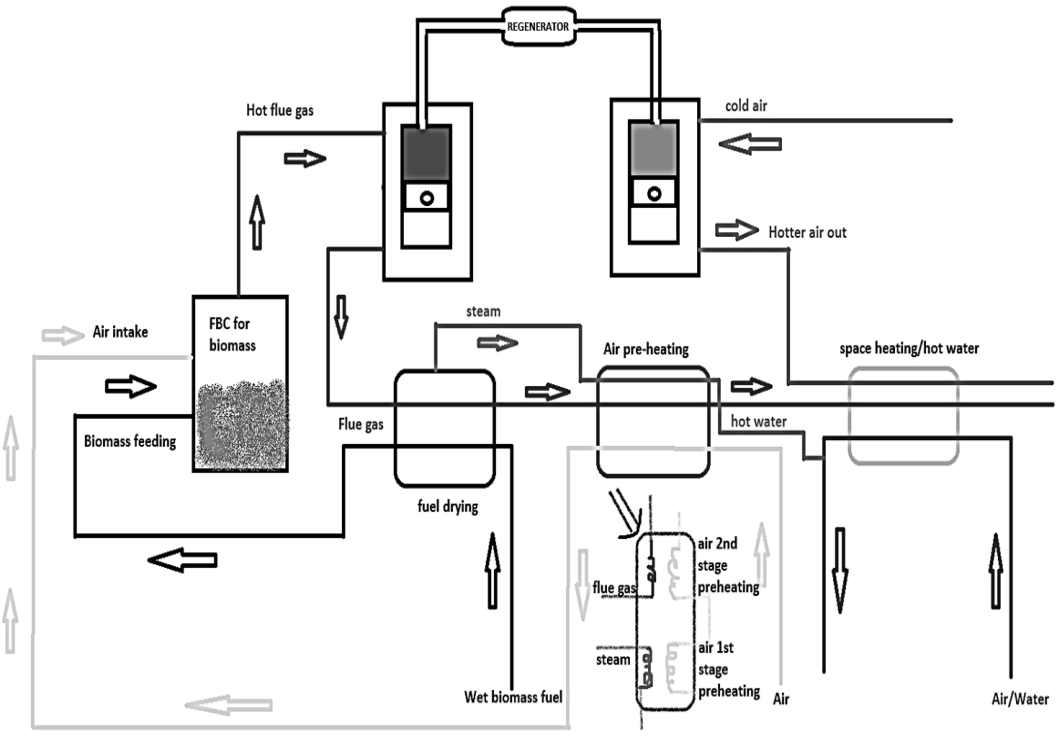

Figure 58 Schematic of biomass unit of the CHP Stirling system.

The CHP system will be flexible enough to work in tandem with existing space heating systems. Waste heat from these systems can run the Stirling power generation systems. Alternately, heat obtained by combusting biomass can be used to generate power in the Stirling power generation set up while remaining heat can be used for heating applications.

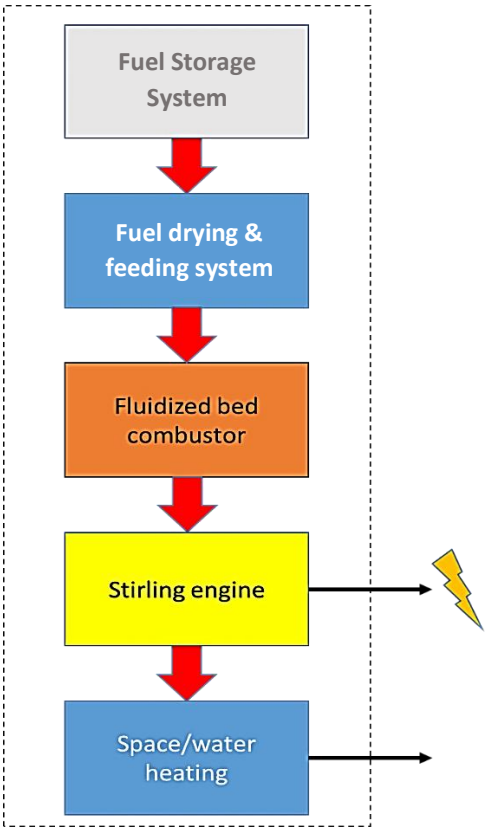

Figure 59 Schematic of co-generation system [50]

5.2 Biomass moisture removal system (BMRS) design, analysis and optimization using heat storage fluids for use in the CHP Stirling system

The fuel drying unit in the biomass section of CHP system as indicated in above figure can acquire multiple grades of naturally occurring biomass. This includes wood chips, organic waste, dead organic matter, agro-waste etc. Majority of these contain varying degrees of moisture. The calorific value of a fuel is affected greatly by presence of moisture content. High moisture content in the fuel has a negative impact on the combustion that takes place in the combustor or gasifier. Fuel with high moisture content leads rust oxide formation, heat loss and irreversibility due to vapor formation, explosive steam pockets during combustion, incomplete

combustion resulting in emission of carbon monoxide and particulate matter. A cost effective moisture removal system is designed such that heat trapped from exhaust flue gas can be reused for useful work. Available work potential of exhaust flue gas is analyzed for effective heat reuse in the CHP system. A fluid pocket containing viscous fluid with relatively high specific heat capacity and high thermal conductivity is placed in the path of exhaust flue gas for this express purpose.

Methodology

The moisture removal system was modeled in COMSOL for feasibility and verification of predicted output. The drying unit was provided with conical fins containing heat storing fluid for enhanced heat transfer. Heat from flue gas at 430 K can be captured with a warm bed filled with heat storing fluid. Waste heat from flue gas is absorbed by the dryer bed for optimum drying of biomass. The selection of material for the warm bed is studied using simulation results of COMSOL. Heat transfer between the flue gas and heat storing fluid and biomass is studied. Further, available work potential of exhaust flue gas after passing through the biomass drying unit is also evaluated using a combination of thermodynamic analytical method and COMSOL simulation results.

Software used: COMSOL

Preliminary simulation efforts highlighted the need for creating two separate flow domain models.

● Analysis to find optimal heat storage fluid for the BMRS is done on a flow domain which is in 1:160 scale of the original unit size. Choice of such a small scale was influenced mainly by the limitations imposed by computational resources

● Work potential of exhaust flue gas was evaluated by analyzing a flow domain of 1:10 scale because of unrealistic results for a scale smaller.

Selection of heat storing fluid for rapid moisture removal from biomass

Selection of a suitable heat storing fluid depends on the amount of heat captured by it from exhaust flue gas and the time taken by it to transfer the same to biomass. This can be done by comparing and combining the analytical solutions with the numerically obtained values. Analytical solution can be obtained by using the following equation.

$$Q = m \times C_p \times \Delta T \qquad \text{[Equation 5.1]}$$

Where, Q = energy absorbed by heat storing fluid from exhaust flue gas in kJ

m = mass in kg

C_p = specific heat capacity at constant pressure in J/kg.K

ΔT = temperature difference in K (obtained from simulation results)

The heat storing fluid which absorbs the maximum amount of energy, 'Q', in the least amount of time is the most effective fluid for the system. Reynolds number is also calculated in all the cases. It is given by the equation:

$$Re = (\rho \times v \times D_H)/\mu \qquad \text{[Equation 5.2]}$$

Where, 'D_H' is diameter of cylinder for flow past cylinder analysis (in metres).

'v' is the mean velocity of the fluid (in m/s).

'μ' the dynamic viscosity of the fluid (Pa·s or N·s/m^2 or kg/(m·s)).

'ρ' is the density of the fluid (kg/m^3).

The three heat storing fluids used as test cases are listed below along with their properties.

i) 20W50 Motor Oil

	Property	Name	Value	Unit
✓	Density	rho	884	kg/m³
✓	Dynamic viscosity	mu	0.146896	Pa·s
✓	Thermal conductivity	k	0.167	W/(m…
✓	Heat capacity at constant pres…	Cp	22473.45	J/(kg·K)
✓	Ratio of specific heats	gamma	1.1	1

Table 10 Properties of 20W50 motor oil

ii) Monoethylen glycol (20% mix)

	Property	Name	Value	Unit
✓	Density	rho	1030	kg/m^3
✓	Dynamic viscosity	mu	0.00165	Pa*s
✓	Thermal conductivity	k	0.521	W/(m*K)
✓	Heat capacity at constant pr…	Cp	3900	J/(kg*K)
✓	Ratio of specific heats	gam…	1.1	1

Table 11 Properties of monoethylen glycol (20% mix)

iii) Ammonia gas

	Property	Name	Value	Unit
✓	Density	rho	0.717	kg/m³
✓	Dynamic viscosity	mu	0.000138	Pa·s
✓	Thermal conductivity	k	0.022	W/(m…
✓	Heat capacity at constant pres…	Cp	2190	J/(kg·K)
✓	Ratio of specific heats	gamma	1.32	1

Table 12 Properties of ammonia

Property	Flue Gas	Biomass
Density (ρ)(in kg/m^3)	0.748	1250
Dynamic Viscosity (μ) (in Pa.s)	24.5	13.82
Thermal Conductivity (k) (in W/m.K)	0.0384	0.105
Heat Capacity at constant pressure (C_p) (in J/kg.K)	1097	1545
Ratio of specific heats (γ)	1.3767	1.1

Table 13 Properties of flue gas and biomass

Evaluating work potential of exhaust flue gas

The maximum available work potential of exhaust flue gas is termed as 'W_{max}'. Energy given by flue gas to biomass, Q_{fb}, is found using COMSOL which plots streamlines that helps figure out flue gas penetration into the viscous fluid pocket. Hydrostatic force acting at the interface between flue gas and viscous fluid in the pocket is calculated using pressure graph. The flow penetration of flue gas is given by the recirculation zone length observed from the streamline plot. The product of this length and the hydrostatic force gives hydrostatic energy of exhaust flue gas, Q_h. The internal energy change in flue gas, ΔQ_{ie}, is evaluated in COMSOL. The line integral of the domain outlet gives the viscous drag force value in the domain. The product of viscous drag force and the flow penetration length gives the energy lost by flue gas due to viscous forces, Q_v. Irreversible work lost (Q_i) is neglected. Actual available work potential of flue gas in the system (before heat transfer to biomass)

is termed as W_{a1}. Actual available work potential of flue gas in the system after heat transfer to biomass is termed as W_{a2}. Ideally, $W_{a1} = Q_{fb} + Q_h$ and $W_{a2} = Q_h$

[Equation set 5.3]

We observe that $W_{a1} < W_{max}$. This is due to the work potential lost by the system due to irreversibility (Q_i). But since irreversibility is neglected, $W_{a1} \approx W_{max}$.

$\Delta Q_{ie} = W_{max} + Q_v - (Q_{fb} + Q_h)$

Hence, $W_{max} = (\Delta Q_{ie} + Q_{fb} + Q_h) - Q_v$ [Equation set 5.4]

W_{max} is calculated using exergy analysis approach [47]. The theoretical maximum

can be calculated by using the classic exergy equation (W_{max}, physical exergy):

$W_{max} = \dot{m} \times (e - e_o) = \dot{m} \times (h - h_o - T_o \times (s - s_o)$ [Equation 5.5]

Where '$\dot{m}$' is the mass flow, 'e' the initial exergy of a stream of substance, 'e_o' the exergy of a stream of substance in the state of the surroundings, h the initial enthalpy, s the initial entropy, 'T_o' is temperature [K] of the surroundings. Flue gas is assumed to follow the equation of state for a perfect gas. Hence, for flue gas physical exergy is calculated using:

$W_{max} = \dot{m} \times [C_p \times (T - T_o) - T_o \times \{(Cp \times \ln (T/T_o)) - ((R/M) \times (\ln (p/p_o))\}]$

[Equation 5.6]

Where 'T' is the temperature [K] of the excess heat, 'C_p' the average specific heat capacity between the temperatures 'T' and 'T_o', 'R' the molar gas constant, 'M' the molar mass of the gas, 'p' the pressure of the stream and 'p_o' the pressure of the surroundings. Analytical thermodynamic results are combined with the numerical COMSOL results to test the stability of the solution. Larger flow domain and only

one fluid, 20W50 motor oil, is used to do this (since available work potential of flue gas will remain the same irrespective of any heat storing fluid used for).

Problem Sketch

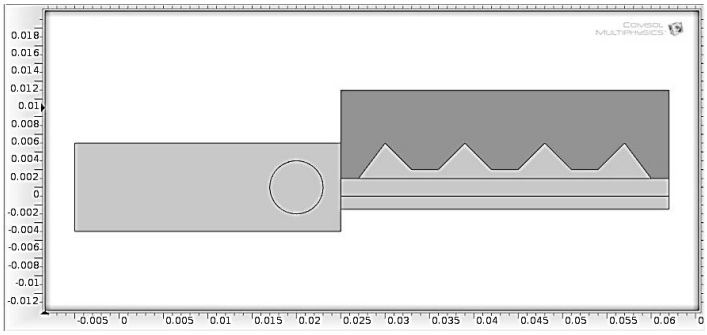

Figure 60 Section highlighted in dark grey represents biomass

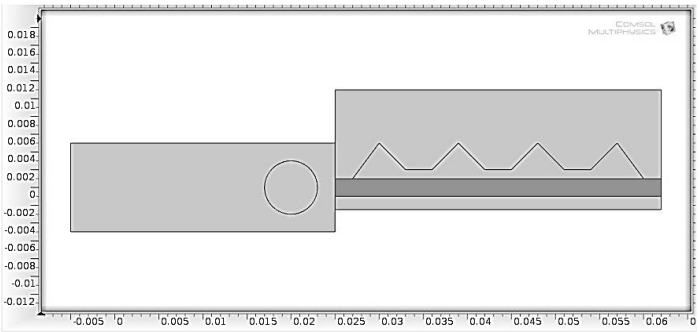

Figure 61 Section highlighted in dark grey represents flue gas

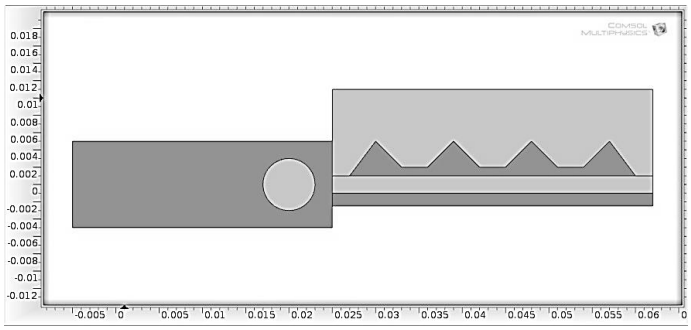

Figure 62 High viscosity, high thermal conductivity heat storage fluid in dark grey

The circle in the first rectangle in the above diagrams is the static cylinder used to evaluate the work potential of flue gas by regularizing the flow.

Analytical Calculations

Reynolds number calculation: [Refer equation 5.2]

Reynolds number of flow in the flue gas domain is given by:

$Re_{fg} = (0.748 \times 0.0167 \times 0.002)/24.5 = 1.019722449E\text{-}6$

Reynolds number of flow passing over static cylinder is given by:

$*Re_{fp} = (0.748 \times 0.0167 \times 0.006)/24.5 = 3.059167347E\text{-}6$

Inference:

This theoretical value of Reynolds number for flue gas flow over the static cylinder is obtained by assuming zero resistance flow path for flue gas inside fluid pocket domain. In reality, Reynolds number changes continuously from the inlet of fluid pocket up to its outlet due to continual flow resistance (as high viscous medium exists in fluid pocket) resulting in changing flow velocities. However, small values of ideal Reynolds number, inlet flow velocity and flow domain dimensions indicate fairly low Reynolds number throughout simulation, suggestive of laminar flow.

Energy absorbed by biomass [Refer equation 5.1]

$Q_{fb} = m \times C_p \times \Delta T = m \times 1545 \times \Delta T$ (in Joules) [Equation 5.7]

We now, calculate mass of biomass in the system.

Area of biomass domain = (Area of rectangle) – (Area of prismatic domain)

[Referring to figures 2(d) & 2(f)]

$= (0.037 \times 0.01) - \{(4\times0.5\times0.0065\times0.004) + (3\times0.5\times0.003\times0.001)\} = 3.135E\text{-}4\ m^2$

It is assumed that the test domain in all cases has a unit width (for simplicity).

Hence, volume of biomass domain, V = (3.135E-4 × 1) m^3 = 3.135E-4 m^3

Hence, mass of biomass in domain = ρ × V = (1250 × 3.135E-4) kg = 0.391875 kg

Hence equation 5.7 can be rewritten as,

Q_{fb} = 0.391875 × 1545 × ΔT (in Joules) = (605.446875 × ΔT) in Joules

[Equation 5.8]

Available work potential in exhaust flue gas (1:10 scale)

Reynolds number calculation: [Refer equation 5.2]

Reynolds number of flow in the flue gas domain is given by:

Re_{fg} = (0.748 × 1.67 × 0.02)/24.5 = 1.019722449E-3

Reynolds number of flow while passing over static cylinder is given by:

**Re_{fp} = (0.748 × 1.67 × 0.06)/24.5 = 3.059167347E-3

Inference:

Reynolds number remains fairly low throughout the simulation and the flow is therefore laminar for all practical purposes.

Maximum theoretical available work (W_{max}) calculation: [Refer equation 5.6]

This calculation is performed the inlet boundary of the entire test domain to obtain maximum available work potential of flue gas. p = p_o here. A unit width of 1 m is considered throughout the flow domain for simplicity.

W_{max} = 4,700,000 J approximately = 4,700 kJ [Equation 5.9]

Calculation of hydrostatic energy of flue gas (Q_h)

Hydrostatic energy (Q_h) = Hydrostatic force (F_h) × Flow penetration length (d_{pl}) (in joules)

= Fluid pressure at flue gas-fluid pocket interface (p_i) × Area of interface (A_i) × d_{pl}

$Q_h = p_i \times A_i \times d_{pl} = p_i \times 0.02 \times d_{pl}$ (in Joules) [Equation 5.10]

Calculation of viscous energy in fluid pocket (Q_v):

The line integral of the entire domain's outlet using COMSOL provides the viscous drag force per unit length value.

Viscous energy (Q_v) = Drag per unit length (F_d) × Cross-sectional area of fluid pocket (A_{fp})

$Q_v = F_d \times (0.3 \times 0.1) = 0.03F_d$ (in Joules) [Equation 5.11]

Energy absorbed by biomass [Refer equation 5.1]

$Q_{fb} = m \times C_p \times \Delta T = m \times 1545 \times \Delta T$ (in Joules) [Equation 5.12]

Mass of biomass in the system is now calculated.

Area of biomass domain = (Area of rectangle) – (Area of prismatic domain)

[Referring to figures 36 & 38)]

$= (0.37 \times 0.1) - \{(4 \times 0.5 \times 0.065 \times 0.04) + (3 \times 0.5 \times 0.03 \times 0.01)\}$

$= 3.135E\text{-}2\ m^2$

Volume of biomass domain, $V = (3.135E\text{-}2 \times 1)\ m^3 = 3.135E\text{-}2\ m^3$

Hence, mass of biomass in domain = $\rho \times V = (1250 \times 3.135E\text{-}2)$ kg = 39.1875 kg

Hence equation 5.12 can be rewritten as,

$Q_{fb} = 39.1875 \times 1545 \times \Delta T$ (in Joules) = $(60544.6875 \times \Delta T)$ in Joules

[Equation 5.13]

Numerical results & calculations from COMSOL simulation

Selection of heat storing fluid

Uniform inlet mass flow rate value of 0.00000005 kg/s is considered for exhaust flue gas. Analysis is carried out for 540 seconds

Analysis for 20W50 motor oil as the heat storing fluid

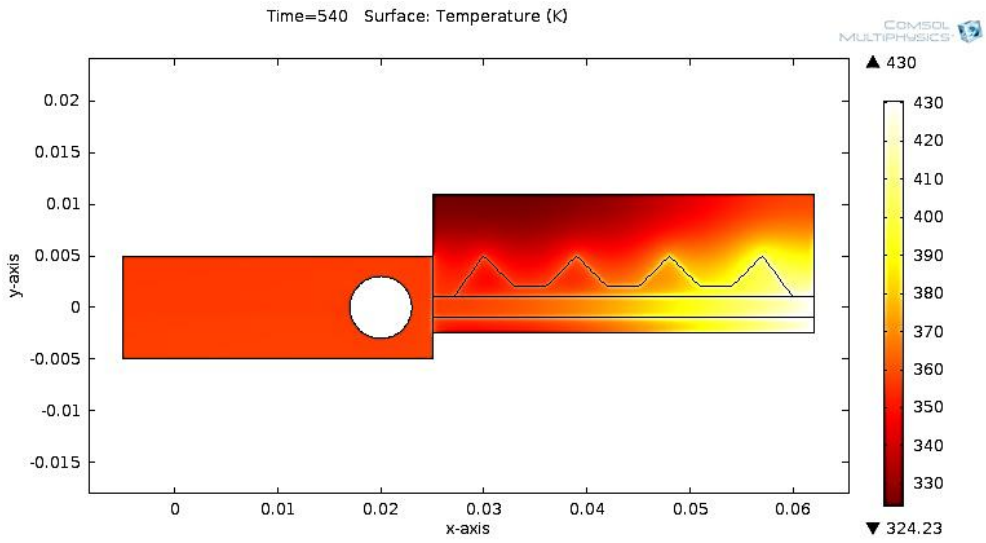

Figure 63 Temperature profile (at 540 seconds) of 20W50 motor oil

Inference:

After 540 seconds, Average temperature of biomass domain = 370 K

Q_{fb} = 605.446875 × (370 – 303) = 40564.94063 J [Refer Equation 5.8]

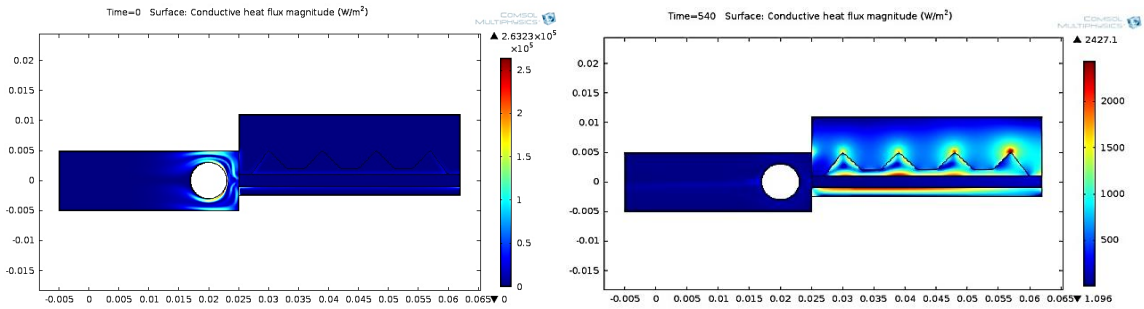

Figure 64 Change in conductive heat flux with time of 20W50 motor oil

Analysis for monoethylen glycol (20% mix) as the heat storing fluid

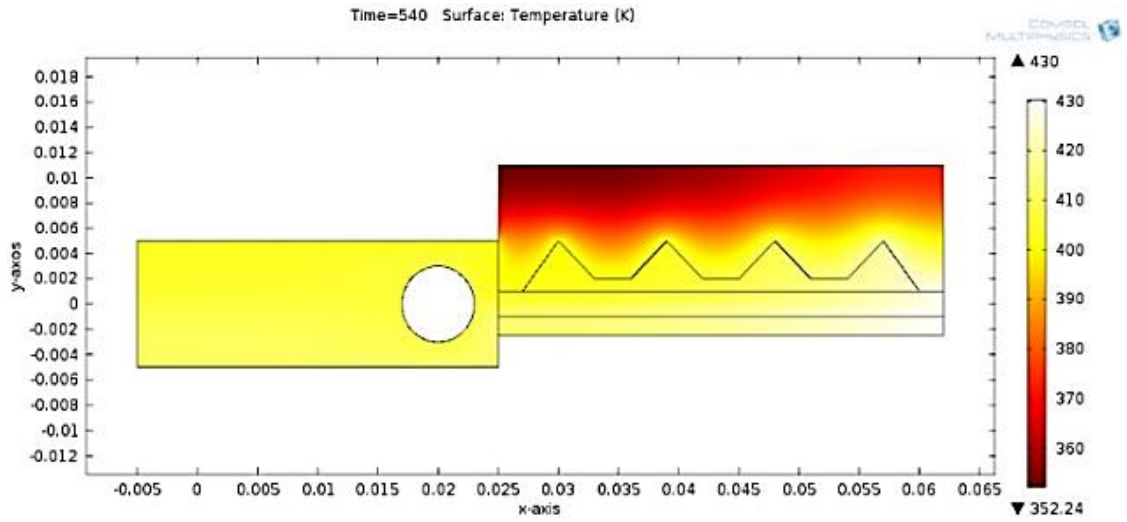

Figure 65 Temperature profile (at 540 seconds) of monoethylen glycol (20% mix)

Inference:

After 540 seconds, Average temperature of biomass domain = 390 K

Q_{fb} = 605.446875 × (390 – 303) = 52,673.87813 J [Refer Equation 5.8]

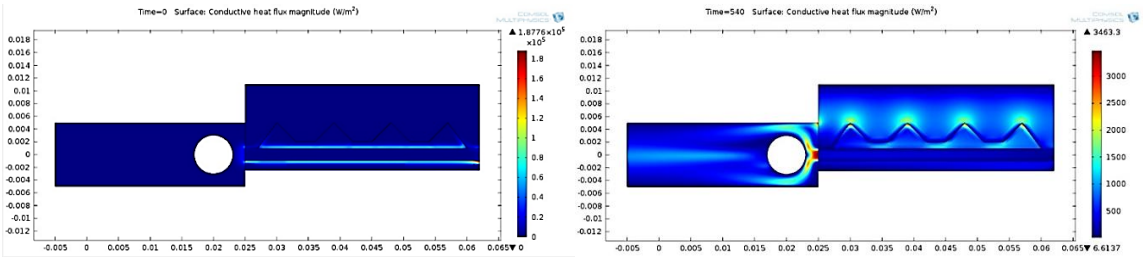

Figure 66 Change in conductive heat flux with time: monoethylen glycol (20%)

Analysis for ammonia as the heat storing fluid

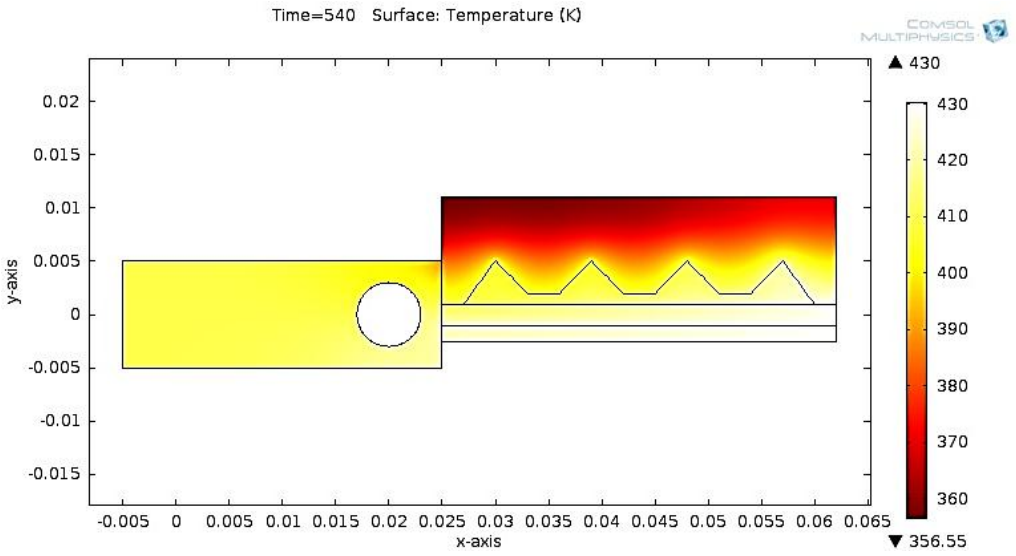

Figure 67 Temperature profiles (at 540 seconds) of ammonia

Inference:

After 540 seconds, Average temperature of biomass domain = 385 K

Q_{fb} = 605.446875 × (385 – 303) = 49,646.64375 J [Refer Equation 5.8]

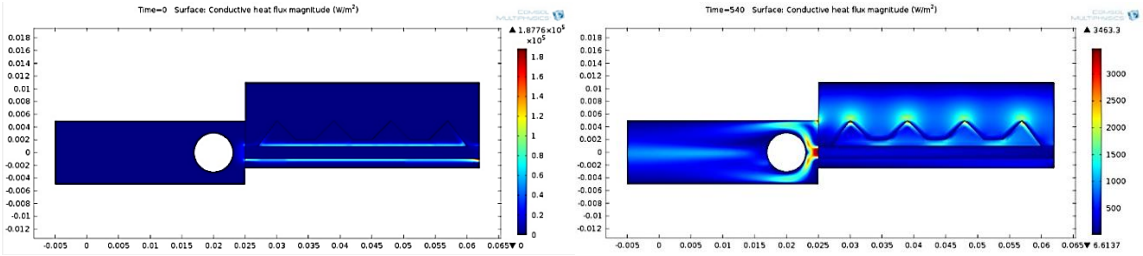

Figure 68 Graphs showing change in conductive heat flux with time

Available work potential in exhaust flue gas (fluid domain is larger: 1:10 scale)

All simulations have been carried out for a uniform inlet mass flow rate of 0.0005 kg/s for exhaust flue gas. The time dependent analysis was carried out for 1080 seconds for each of the test cases.

Analysis of 20W50 motor oil in larger domain (scale 1:10)

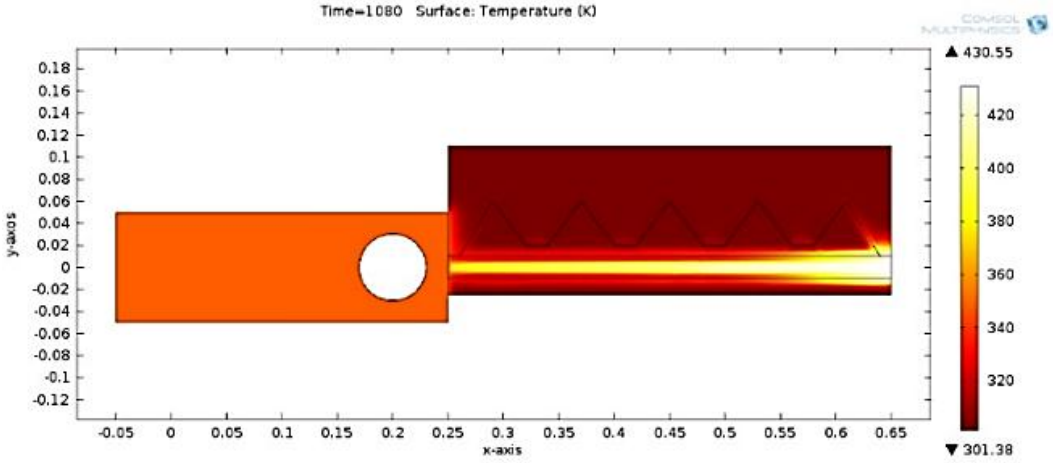

Figure 69 Temperature profile (at 1080 seconds) of 20W50 motor oil

Inference:

After 1080 seconds, Average temperature of biomass domain = 385 K

[Refer Equation 5.13]

Q_{fb} = 60544.6875 × (330 – 303) = 1,634,706.563 J [Equation 5.14]

Velocity profile and Cell Reynolds number (scale 1:10) for 20W50 motor oil

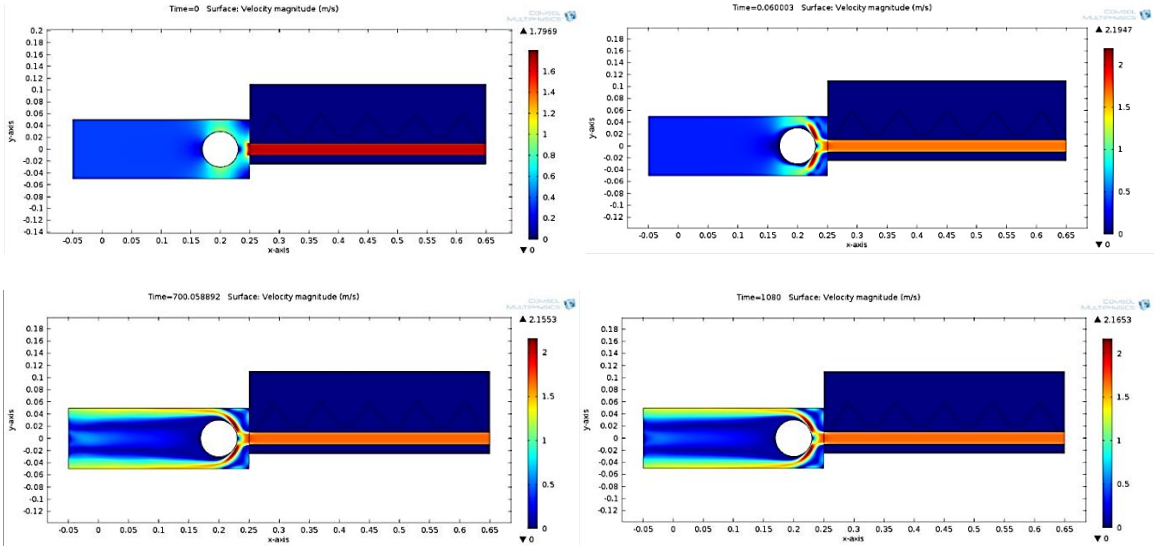

Figure 70 Graphs showing change in flow velocity with time for 20W50 motor oil

Inference:

In 1080 seconds, maximum velocity of 2.1947 m/s is reached at 0.06 seconds. Hence, Reynolds number is given by:

Re = (0.748 × 2.1947 × 0.06)/24.5 = 4.02033E-3 **(laminar flow)**

Pressure profile

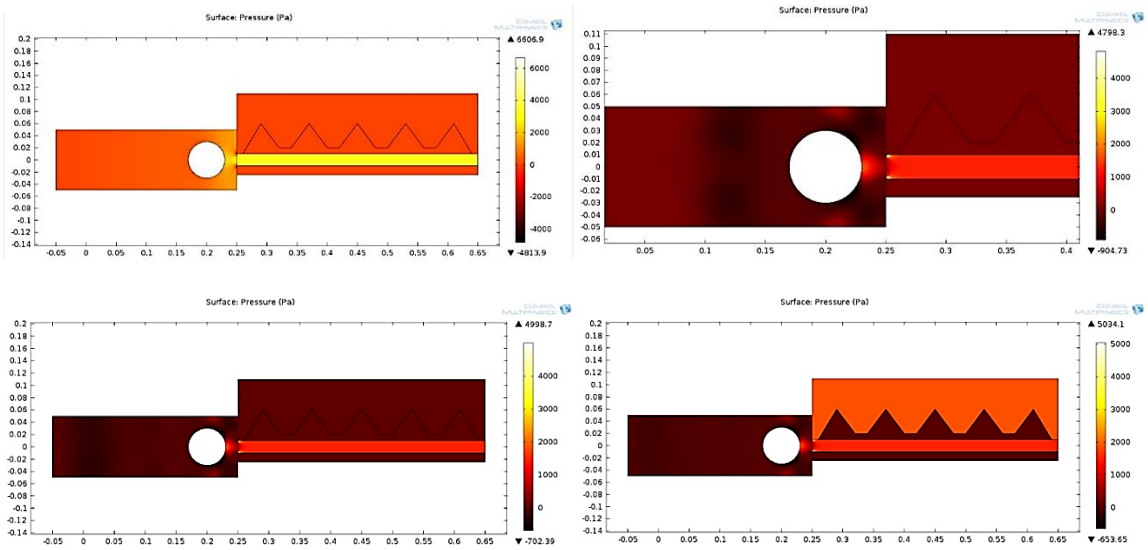

Figure 71 Change in pressure with time (scale 1:10) for 20W50 Motor oil

Inference

Inlet pressure of flue gas = 3000 Pascal = 0.03 bar

Max pressure = 6606.9 Pascal = 0.06069 bar

Streamline profile

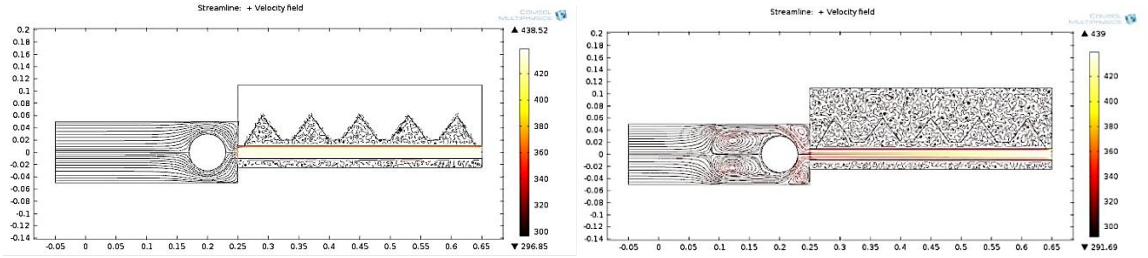

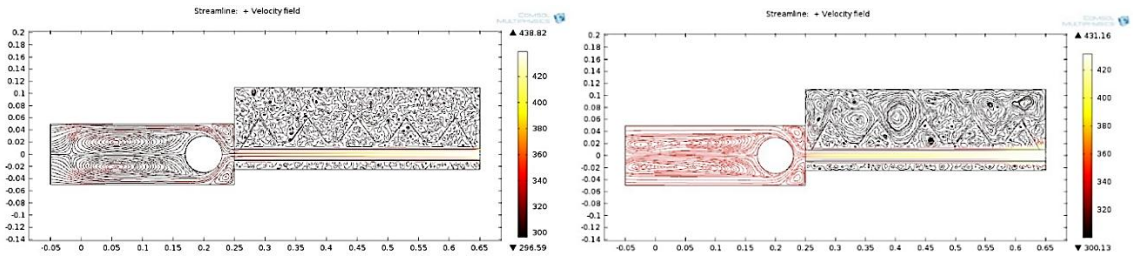

Figure 72 Streamline variation with time (20W50 Motor oil - scale 1:10 domain)

Inference
Recirculation zone develops in the flow as time passes. The direction of recirculation is anti-clockwise. Velocity is very less in recirculation zone as evident from velocity and streamline profile graphs.

Shear rate

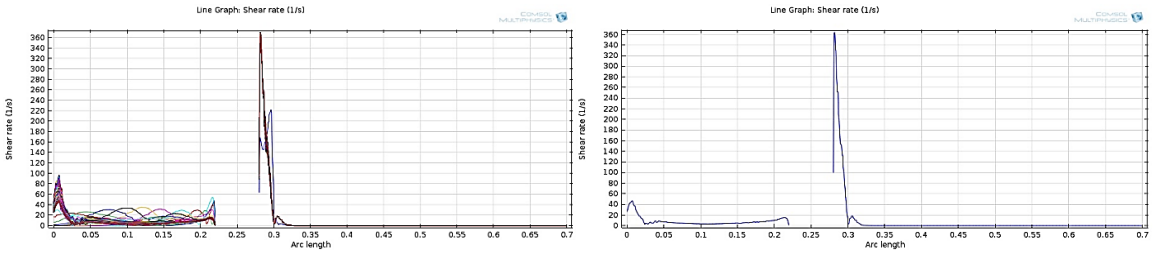

(a) shear rate vs arc length (all time steps) (b) shear rate vs arc length (time=1080s)

Figure 73 Shear rate graphs for 1:10 scale domain for 20W50 motor oil

Inference
Flow recirculation zone length = 0.22 m (at 1080 seconds)
Flow penetration length, d_{pl} = 0.22 m

Drag per unit length

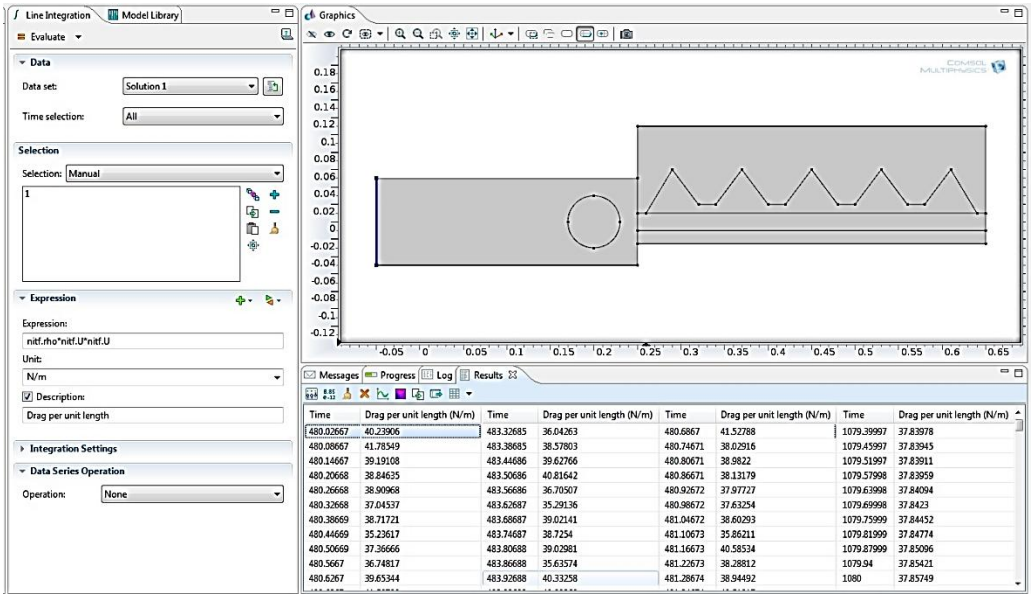

Figure 74 Drag per unit length (N/m) (scale 1:10 domain) for 20W50 Motor oil

INFERENCE
Average drag per unit length from above figure, F_d = 40 N/m
[Equation 5.17]

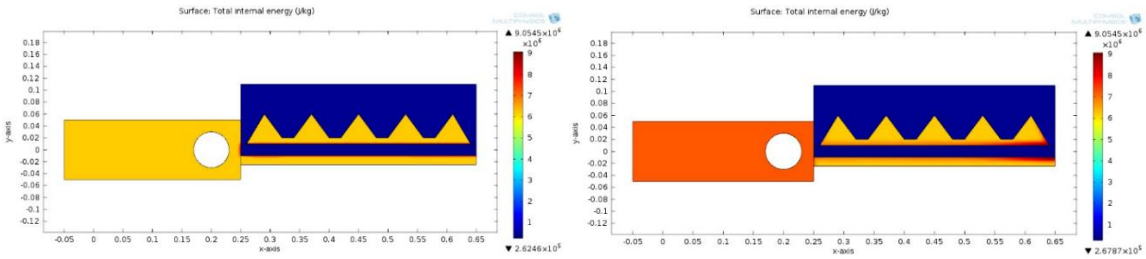

Figure 75 Change in internal energy with time (scale 1:10) for 20W50 motor oil

Inference
Change in internal energy of the system, ΔQ_{ie} = (9E6 – 6E6) J/kg = 3E6 J/kg
[Equation 5.18]

Calculations for evaluating work potential of flue gas

Calculation of Q_h: [Refer equations 5.10, 5.15 & 5.16]

$Q_h = 6606.9 \times 0.02 \times 0.22 = 29$ J [Equation 5.19]

Calculation of viscous energy in fluid pocket (Q_v): [Refer equations 5.11 & 5.17]

$Q_v = 0.03 \times 40 = 1.2$ J [Equation 5.20]

Available work potential of flue gas (before heat transfer to biomass) (W_{a1}): [Refer equations 5.3, 5.14 & 5.19]

$W_{a1} = (1{,}634{,}706.563 + 29)$ J = 1,634,735.563 J = 1,634.706563 kJ [Equation 5.21]

Work potential of flue gas (after heat transfer to biomass) (W_{a2}): [Refer equations 5.3 & 5.19]

$W_{a2} = Q_h = 29$ J [Equation 5.22]

Result Validation for work potential of flue gas

Analytical vs. Numerical (from simulation) value of W_{max}: [Refer equation set 5.4]

$W_{max,numerical} = 4{,}634{,}734.363$ J = 4,634.7344 kJ < $W_{max,analytical}$ (= 4700 kJ) [Equation 5.23]

Error % = 1.38863% [Equation 5.24]

Inferences for BMRS based on above analysis

Best heat storing fluid for the given system (for domain with 1:160 scale)

	20W50 motor oil	**Monoethylen glycol (20% mix)**	**Ammonia**
Energy absorbed by biomass (in J) when heat storing fluids are used	40,564.94063	52,673.87813	49,646.64375

Table 14 Best heat storing fluid comparison for BRMS

Clearly, in 540 seconds, maximum heat of 52.673 kJ is transferred to biomass when Monoethylen glycol (20% mix) is used as the heat storing fluid. Monoethylen glycol (20%) mix is chosen as the suitable fluid for the biomass moisture removal system.

Flue gas work potential evaluation: [Refer equation 5.23]

$W_{max,numerical}$ = 4,634,734.363 J = 4,634.7344 kJ < $W_{max,analytical}$ (= 4700 kJ)

W_{a1} is slightly lower than W_{max}. Since, irreversibility is neglected, the minor discrepancy can be attributed to computational errors during iteration.

Error % = 1.38863% [Refer equation 5.24]

Clearly, this error is within acceptable limits.

5.3 Solar energy capture set up using Fresnel lens and Fresnel reflectors

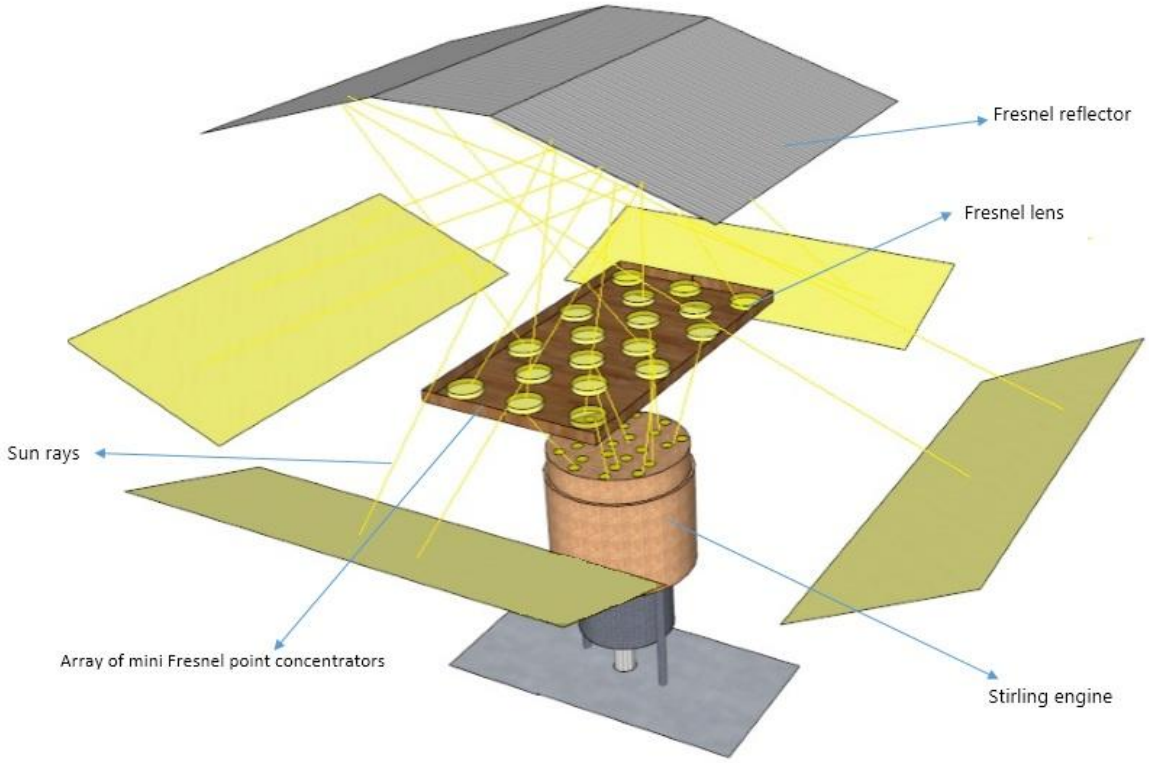

Figure 76 Solar concentrator set up for optimized heating of Stirling engine

Above figure shows a concept design of a solar energy concentrating set up where point Fresnel concentrator lenses and Fresnel linear mirrors are used. This type of arrangement is relatively low cost and offers flexibility. The reason for choosing an array of small Fresnel concentrators is to ensure more uniform heating on the hot head. This ensures a well distributed heat flux and eliminates concentration of heat at a point. A combination of point and line Fresnel concentrators can also be used as shown below. In the figure below, a fluid can be heated up using solar energy and in turn be used to heat the hot end of the Stirling engine thereby, allowing greater flexibility in engine placement and minimizing solar tracking requirements.

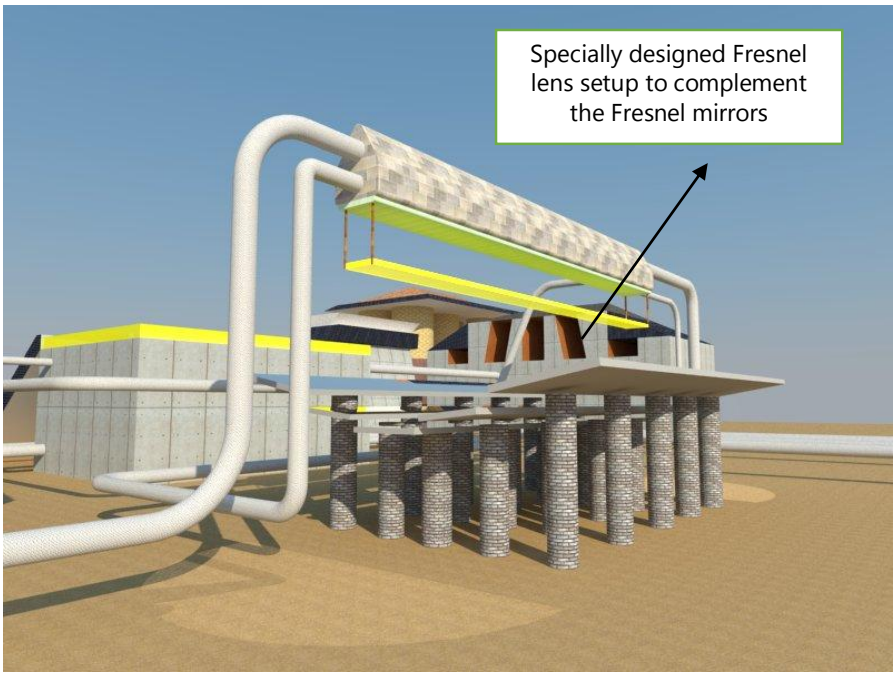

Figure 77 Special Fresnel linear concentrators for indirect use of solar energy using heating fluids

5.4 Thermal energy storage system design concept for storing solar energy

Sample design of TESS for CHP system for 6 hours backup

The Stirling system designed here has 5.97 x 10^{-5} kg (mass denoted by 'm') Helium (working fluid @ 10 bar, 360^{o}C, heating volume of 78.5 cc and Helium density of 0.7604 kg /m3). For simplicity, it is considered that one requires 30 joules of heat per cycle (input heat denoted by 'Q') for running the engine. Now, specific heat capacity of helium at constant volume (C_v) is 3120 J/kg.K. Hence, change in temperature of Helium per cycle is given by,

$dT = Q/m.C_v = 161.06$ Kelvin [Equation 5.25]

If ambient starting temperature of Helium is considered to be 300 Kelvin, hence increased temperature of helium after the first cycle will be approximately 461.06

Kelvin. For simplicity, we ignore conduction, convection and radiation losses here. The system is operated at a suitable lower temperature of 633 Kelvin when the TESS is used. This results in a lower power output but is economically beneficial as it allows for use of common materials for construction. Now, amount of heat required to raise the temperature of Helium to 633 Kelvin is given by,

Q_{total} = 62 Joules [Equation 5.26]

The Stirling engine is designed to operate at 13 Hertz as seen from the dynamic analysis results. Output energy of the engine is 16 joules/cycle (from thermal analysis). Considering losses (from dynamic analysis), output of present system will be approximately 5 joules/cycle. System loses close to 25 joules of heat per cycle because of friction, conductive losses, convective losses, radiation losses and viscous forces. The regenerator effectiveness is considered to estimate the amount of thermal energy stored in the system per cycle (i.e. energy not lost due to the various losses). This energy is available to the gas as the gas passes from cold end to hot end. Hence, effective heating required at the hot end decreases in subsequent cycles. Given below is a small discussion on regenerator performance.

Materials with porosity of 90%				
Proprieties	Stainless steel 304L	Copper	Aluminum	Monel 400
Density ($kg.m^{-3}$)	7.850	8.920	2.700	8.800
Thermal capacity ($J.kg^{-1}.K^{-1}$)	477	385	902	430
Thermal conductivity ($W.m^{-1}.K^{-1}$)	26	390	237	22

Table 15 Common regenerator materials and their properties [48]

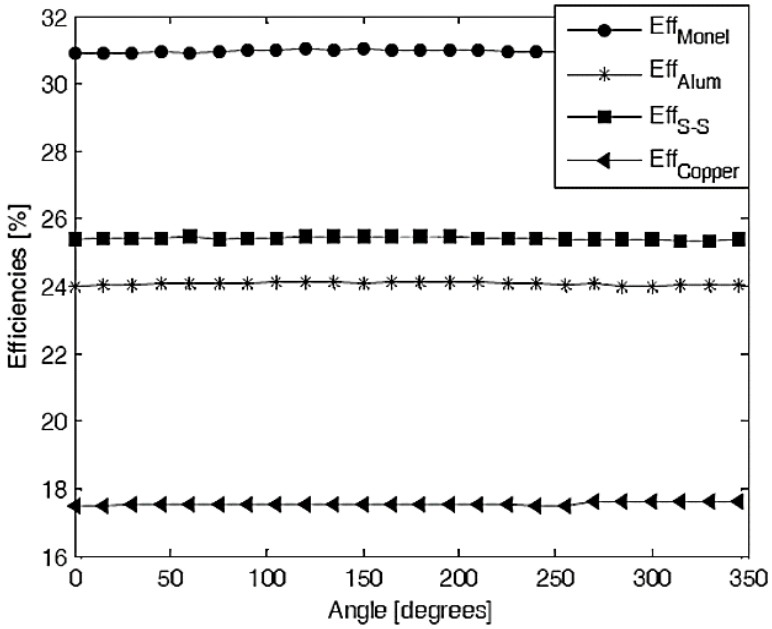

Figure 78 Regenerator's efficiencies vs. Acquisition time [48]

Dr. James Klett, developed a highly thermally conductive graphite foam material at ORNL. These foams of varying porosity and density provide thermal conductivity equivalent to aluminum alloys at substantially lower weight. The invention has an open porous structure with more than 100 times greater surface area than typical heat exchangers (>20 m2/g). The cell walls are made of highly oriented graphite planes, similar to high performance carbon fibers, which have been estimated to exhibit a thermal conductivity greater than 1700 W/m·K (copper is 400 W/m·K). The foam also exhibits excellent RF shielding and acoustic management properties [49].

Comparing with previous results on regenerator working effectiveness, an effectiveness value of 0.75 is assigned to graphite foam. This means that graphite foam stores 25% of the heat per cycle. This value amounts to about 7.5 joules per cycle and this heat is available to the gas in subsequent cycles. This extra heat reduces the work load at the heating end.

Now, @ 30 joules per cycle and 13 cycles/second, the system requires 390 joules/second to operate. The extra 7.5 joules/cycle is neglected as the system is designed for low efficiency. Hence, 8,424,000 joules of heat needs to be supplied over 6 hours to the system. TESS needs to supply this heat to the system over a period of 6 hours in the absence of any other external heating source.

Heat storage fluid analysis carried out previously suggests use of monoethylen glycol (20% water mix) as the fluid in the TESS. TESS is designed to have a maximum fluid temperature of 875 K. The boiling point of monoethylen glycol is 400.15 Kelvin. Energy stored in fluid in TESS is

$$Q_{TESS} = m_{fluid} \times C_{p,\,fluid} \times dT_{(300\ K\text{-}400.15\ K)} + m_{fluid} \times L_{fluid} + m_{fluid} \times C_{p,\,fluid} \times dT_{(400.15\ K\text{-}875\ K)}$$

Where $C_{p,\,fluid}$ = specific heat capacity of monoethylen glycol (20% mix)

= 2790.5022 J/(kg.K)

L_{fluid} = latent heat of vaporization of monoethylen glycol (20% mix)

= 860620.108 J/kg

Hence, m_{fluid} = mass of monoethylen glycol (20% mix) in the TESS ≈ 3.5 kg

ρ_{fluid} = density of monoethylen glycol (20% mix) = 1112.5 kg/m^3

Hence, V_{fluid} = volume of monoethylen glycol (20% mix) in TESS = 3146.1 cc

[Equation set 5.27]

Therefore, a specially designed thermally insulated system is needed to store TESS fluid for 6 hours backup. Temperature of TESS drops gradually as it loses heat while the temperature of hot end of CHP system is maintained at 633 K. This helps in effective functioning of TESS system up to a temperature of 633 Kelvin (since, delta T reduces over time in absence of solar energy). When temperature of TESS drops

below 633 K, heat doesn't flow from it and the temperature of TESS and CHP system decreases together. In reality, a TESS with at least 1.5 times greater capacity needs to be built to account for losses. This gives us the actual required volume of the TESS to be about 6300 cc.

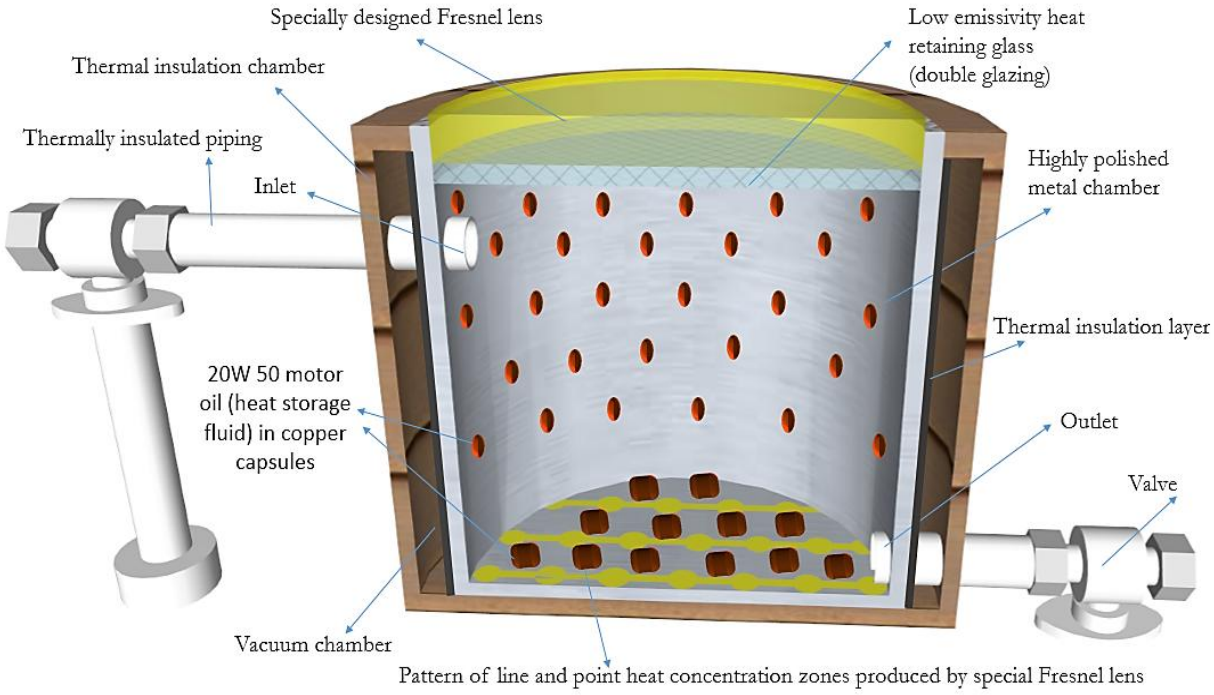

Figure 79 Schematic of TESS (concept design)

The above figure represents a novel concept design. The innermost chamber is a highly polished metal surface to reflect as much heat as possible into the system. This metal chamber is surrounded by a thermal insulation layer. This arrangement exists in a slightly larger chamber (made of poor heat conducting material). There is a vacuum between the two chambers to minimize heat loses. The metal chamber is covered on the top with a low–e glass. The "e" in low-e stands for emissivity - the ability to emit radiant energy. Low-e coating emits almost no radiant energy. Low-e glass has a special coating which is a poor radiator of heat and does not

allow heat to be transferred to the outside. Instead, the low-e coating actually reflects the heat back. The coating is an invisible metal or metallic oxide film that's deposited on the surface of the glass during or after the manufacturing process. This microscopic layer allows light (short-wave energy) to penetrate the glass, but blocks most ultraviolet (UV) long-wave energy, which we feel as heat. The TESS fluid warms up as it absorbs this solar energy. Warm fluid re-radiates the energy (long wave radiation). The low-e glass does not let the longer wavelength radiation pass through the coated low-e surface and is an effective reflector. The energy entering TESS and heat energy present are reflected back from the low-e glass.

The TESS has a specially designed Fresnel lens just above the low-e glass lid. This Fresnel lens is a combination of line and point solar concentrators. This type of concentration pattern of solar energy helps maintain a more uniform heat distribution within the TESS and prevents large temperature gradients inside the TESS. Copper capsules containing 20W50 motor oil are placed along the walls of the metal chamber. Fluid analysis earlier in the report shed light on the high thermal retention capacity of 20W50 motor oil. Motor oil has low thermal conductivity and retains heat for longer time. These copper capsules store solar energy and release it over a long period of time thereby aiding the TESS fluid in energy storage. The TESS is provided with thermally insulated piping for inlet at the top and outlet at the bottom. Monoethylen glycol (20% mix) (TESS fluid), has low boiling point of 400.15 K and TESS is at a higher temperature than that. The fluid is therefore in its gaseous state, which is desirable.

Heat exchanger* calculations using NTU method for heat transfer between TESS fluid and helium (working fluid of engine)

[*This process is the source of heat throughout the period when direct solar energy isn't available]

For each heat transfer process:

$c_{p,\ TESS\ fluid}$ = specific heat capacity of monoethylen glycol (20% mix) = 2790.5022 J/(kg.K) $\rho_{TESS\ fluid}$ = density of monoethylen glycol (20% mix) = 1112.5 kg/m^3

$\dot{V}_{TESS\ fluid}$ = Volumetric flow rate of TESS fluid in system = 0.00025 m^3/s (Value set for optimal heat transfer)

$\dot{m}_{TESS\ fluid}$ = Mass flow rate of TESS fluid in system = 0.278125 kg/s

$C_{TESS\ fluid} = \dot{m}_{TESS\ fluid} \times c_{p,\ TESS\ fluid}$ = 776.1084244 J/K.s [Equation set 5.28]

Now, engine completes 13 cycles per second which implies that helium inside the engine makes 13 effective passes for heat transfer at hot end per second. The effective heating mass of helium therefore is given by:

$\dot{m}_{He}$ = 13 x 5.97 x 10^{-5} = 7.761 x 10^{-4} kg/s

And $c_{v,\ He}$ = Specific heat capacity at constant volume for Helium = 3120 J/kg.K

Hence, we get, C_{He} = 2.421432 J/K.s

$C_{max} = C_{TESS\ fluid}$ = 776.1084244 J/K.s

$C_{min} = C_{He}$ = 2.421432 J/K.s

$C = \frac{Cmin}{Cmax}$ = 3.11996613 x 10^{-3} [Equation set 5.29]

We use a heat exchanger with a total available surface area of 0.043501429 m^2. We now estimate the overall heat transfer coefficient value for the process. of 500 $W/m^2.K$;

This is given by $\frac{1}{U_o A} = \frac{1}{h_{He} A_{He}} + \frac{dx_w}{k_{brass} A} + \frac{1}{h_{TESS\ fluid} A_{TESS\ fluid}}$

Where,

U_o = the overall heat transfer coefficient (W/m^2K)

A = the contact area for each fluid side (m^2) = $A_{He} = A_{TESS\ fluid}$ (in our approach)

k = the thermal conductivity of the material (W/m.K) (brass in this case) = 109 W/m.K

h = the individual convection heat transfer coefficient for each fluid (W/m^2K)

We take h_{He} = 500 $W/m^2.K$ and $h_{TESS\ fluid}$ = 600 $W/m^2.K$. and k_{brass} = 109 W/m.K

dx_w = the wall thickness (m) = 0.0002 m

Hence, on solving $U_o \approx 272.6$ W/m^2K

NTU = $\frac{Uo \times Ao}{Cmin}$ = 4.897304382

$\dot{Q}_{max} = C_{min}(T_{h,i} - T_{c,i})$ = 2.421432 x (633 - 300) = 806.336856 Watts

$\varepsilon = \frac{1 - e^{(-NTU(1-C))}}{1 - Ce^{(-NTU(1-C))}}$ = 0.992441829

$\dot{Q} = \dot{Q}_{max} \times \varepsilon$ = 800.24242248 Watts [Equation set 5.30]

The above quantity tells us the amount of heat transfer taking place in the heat exchanger between monoethylen glycol (20% mix) and Helium.

CHAPTER SIX

6. Conclusions and Discussion

6.1 Scope of research

The present research helped establish a stable integrated mathematical model for dynamic as well as adiabatic analysis. This is an invaluable tool to analyze complex Stirling systems with good accuracy. This paves the way for further work in the area including performance prediction, design optimization and parametric study. The study also helped identify flaws and suggest improvements in existing designs. Aided by mathematical model, it is possible to analyze the feasibility and performance of a few novel systems which hold potential for CHP applications and can incorporate Stirling technology.

Conversion of IC engines into Stirling engine:

Construction of Stirling engines is a cost intensive process requiring precision machining for any realistic output. Efforts are on to convert an internal combustion engine into a Stirling engine. IC engines are compact, robust, and relatively cheap (because they are mass produced). Ease of parts availability, excellent sealing and ability to withstand high pressure due to robust construction add to the appeal. This gives us the freedom to run the Stirling cycle at higher pressure thereby corresponding to an increased work output. An IC gasoline RC aircraft engine is selected. It is a 2-stroke twin cylinder inline engine. Two such engines can be used to construct a 4 cylinder Stirling engine wherein one of the twin cylinder engines acts as hot end and the other as cold end.

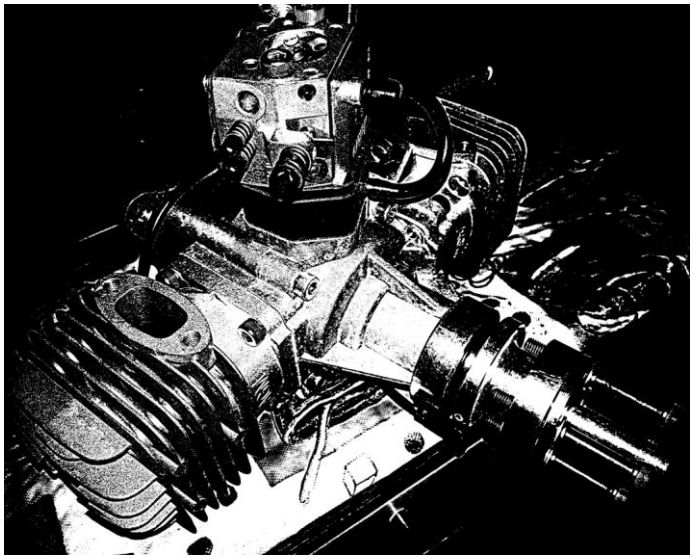

Figure 80 Two cylinder inline gasoline RC aircraft engine for conversion into Stirling engine

6.2 Keys to using the integrated code

The integrated mathematical model is stable and is capable of predicting and analyzing results for a wide variety of Stirling engine configurations. The following points are useful for tuning power output in an engine with the code:

Power output decreases if:

→ Operating frequency decreases

→ Viscous damping at displacer/hot end piston and power piston increases

→ Mass of displacer and power piston decreases

→ Spring damping coefficient of power piston decreases

→ Spring damping coefficient at displacer/hot end piston increases

BIBLIOGRAPHY

[1] 'Key World Energy Statistics 2014', International Energy Agency, 2014.

[2] R. Stirling, Improvements for diminishing the consumption of fuel and in particular, an engine capable of being applied to the moving of machinery on a principle entirely new. British Patent 5456 (1817).

[3] Musings from the Chiefio. *China: Where Money Turns to Coal.* [Online]

http://chiefio.wordpress.com/2009/02/25/china-where-coal-turns-to-money/.

[4] Caleb C. Lloyd, 'A Low Temperature Differential Stirling Engine for Power Generation', Master of Engineering Thesis, University of Canterbury, 2009.

[5] Wikipedia: Renewable Energy Sources and World Energy Consumption 2010

http://upload.wikimedia.org/wikipedia/commons/6/67/Total_World_Energy_Consumption_by_Source_2010.png

[6] Wikipedia: *Renewable Energy* - http://en.wikipedia.org/wiki/File:Ren2006.png.

[7] Global Energy Statistical Yearbook 2014, Enerdata. https://yearbook.enerdata.net/#renewable-data-in-world-primary-consumption-shares-by-region.html

[8] Evan Hughes, "Biomass cofiring: Economics, policy and opportunities", Biomass and Bioenergy 19 (2000) 457 – 465, Pergamon, Elsevier Science Ltd.

[9] Kolin, Ivo. *Stirling Motor - History, Theory, Practice.* Dubrovnik: Zagreb University Publications, Ltd., 1991.

[10] Power Cycles for Electricity Generation

http://www.powerfromthesun.net/Book/chapter12/chapter12.html

[11] William R. Martini, 'Stirling Engine Design Manual', September 2004.

[12] "Stirling Engines - Mechanical Configurations." *Ohio University*. N.p., Apr. 2010. Web. 23 Mar. 2014:

http://www.ohio.edu/mechanical/stirling/engines/engines.html

[13] Keveney, M. "Two Cylinder Stirling Engine." 2000: http://www.animatedengines.com/vstirling.html

[14] "Beta Type Stirling Engines." *Ohio University*. N.p., Apr. 2010. Web. 23 Mar. 2014: http://www.ohio.edu/mechanical/stirling/engines/beta.html

[15] "Gamma Type Stirling Engines." *Ohio University*. N.p., Apr. 2010. Web. 23 Mar. 2014: http://www.ohio.edu/mechanical/stirling/engines/gamma.html

[16] Chen et al., "Design of a Stirling Engine for Electricity Generation", Bachelor of Science Thesis, Worcester Polytechnic Institute, March 2014.

[17] West, C.D. 1986. Principles and Applications of Stirling Engines. New York: Van Reinhold.

[18] Walker, G. 1980. Stirling Engines. Oxford: Clarendon Press.

[19] Berchowitz, D. M. 1986. Stirling Cycle Engine Design and Optimization. Ph.D. dissertation. University of Witwatersrand, Johannesburg, South Africa.

[20] Burden, R.L., and J.D. Faires. 1989. Numerical Analysis. 4th ed. Boston: PWS-KENT Publishing Co.

[21] Kankam, M.D., and J.S. Rauch. 1991. Comparative Survey of Dynamic Analyses of Free-Piston Stirling Engines. IECEC, Boston/NASA TM-I04491.

[22] Steidel, R.F. 1971. An Introduction to Mechanical Vibrations. New York: John Wiley & Sons, Inc.

[23] Urieli, I. and D.M. Berchowitz. 1984. Stirling Cycle Engine Analysis. Bristol, GB: Adam Hilger Ltd.

[24] Klotter, K., and E. Kreyszig. 1960. On a Special Case of Self-Sustained Oscillations. Journal of Applied Mechanics.

[25] Nayfeh, Ali Hasan and Dean T. Mook. 1979. Nonlinear Oscillations. New York: John Wiley and Sons, Inc.

[26] Yan-Quian, Ye. and Others. 1986. Theory of Limit Cycles. Translations of Mathematical Monographs. Vol. 66. Providence, Rhode Island: American Mathematical Society.

[27] Redlich J.S., and D.M. Berchowitz. 1985. Linear Dynamics of Free Piston Stirling Engines. In Proc. Instn. Mech. Engrs., by the Institute of Mechanical Engineers. Vol. 199. N. A3 (March): 203-13.

[28] Finkelstein, Theodor and Organ, Allan J. *Air Engines.* Suffolk: Professional Engineering Publications, 2001.

[29] Hargreaves, C.M. *The Philips Stirling Engine.* Amsterdam: Elsevier Science Publishers, 1991.

[30] Harrigan, R. W. and Stine, W. B. *Power From The Sun.* s.l.: John Wiley and Sons, Inc., 1985.

[31] Stirling and Hot Air Engine Home Page. *Solar Stirling Engines.* http://www.stirlingengines.org.uk/gifs/sunpower/mcd.gif.

[32] Pure Energy Systems. *World's largest solar installation to use Stirling engine technology:* http://pesn.com/2005/08/11/9600147_Edison_Stirling_largest_solar/

[33] Los Alamos National Laboratory. *Acoustic Stirling Heat Engine.* http://www.lanl.gov/mst/engine/

[34] A. Felix Regin, S.C. Solanki, J.S. Saini, An analysis of a packed bed latent heat thermal energy storage system using PCM capsules: Numerical investigation, *Renewable Energy* 34 (2009) 1765–1773.

[35] Zhengguo Zhang, Xiaoming Fang , Study on paraffin/expanded graphite composite phase change thermal energy storage material , *Energy Conversion and Management*, Volume 47, Issue 3, February 2006, Pages 303-310

[36] Ahmet Sarı, Ali Karaipekli**,** Thermal conductivity and latent heat thermal energy storage characteristics of paraffin/expanded graphite composite as phase change material, *Applied Thermal Engineering***,** Volume 27, Issues 8-9, June 2007, Pages

1271-1277

[37] S. Pabis; M. Jaros, The First Period of Convection Drying of Vegetables and the Effect of Shape-dependent Shrinkage, *Biosystems Engineering* (2002) 81 (2), 201 to 211

[38] P. Sathiamurthi, PSS. Srinivasan, Design and Development of Waste Heat Recovery System for air Conditioning Unit**,** European Journal of Scientific Research, Vol.54 No.1 (2011), pp.102-110

[39] *Goran G. Jankes, Nikola D. Tanasi, Mirjana S. Stanmani, And Vuk M. Adzi*, Waste heat potentials in the drying section of the paper machine in umka cardboard mill, *Thermal Science*, Year 2011, Vol. 15, No. 3, pp. 735-747

[40] F. Meunier , "Theoretical performances of solid adsorbent cascading cycles using the zeolite-water and active carbon-methanol pairs: four case studies", *Journal of Heat Recovery Systems*, Pages 491-498

[41] J. Ringler, M. Seifert, V. Guyotot , W. Hübner, Rankine Cycle for Waste Heat Recovery of IC Engines, *SAE International Journal of Engines,* October 2009 vol. 2 no. 1 67-76

[41] T Shudo1, K Toshinaga1, Combustion control for waste-heat recovery system in internal combustion engine vehicles: Increase in exhaust-gas heat by combustion phasing and its effect on thermal efficiency factors, *International Journal of Engine Research,* April 1, 2010 vol. 11 no. 2, pp 99-108.

[42] P. S. Bundela, Vivek Chawla, Sustainable Development through Waste Heat Recovery, *American Journal of Environmental Sciences*, Volume 6, Issue 1, Pages 83-89

[43] Amrit Om Nayak, G. Ram Kumar, T. Manoj, R. Vinod, Comparative Study Between Experimental Analysis and CFD Software Analysis of PCM material in Thermal Energy Storage System, *International Journal of Chemical Engineering and Applications,* Vol.2, No. 6, Pages 400 – 407, December 2011 (ISSN 2010-0221)

[44] M. Gowtham, Amrit Om Nayak, T. Manoj, G. Ram Kumar, Design and analysis of biomass drying unit with waste heat recovery and storage, *Procedia Engineering, Elsevier,* Volume 38, 2012, Pages 1161–1165

[45] COMSOL website: http://www.comsol.com/multiphysics/nonisothermalflow/

[46] Nayak A. O. et al., 'Simulation studies of Solar water heater with Vapor Adsorption material', proceedings of *'International Conference on Simulation Modeling and Analysis'*, held jointly by Amrita University and National Institute of Technology at Coimbatore, Tamil Nadu, India in December 2011

[47] Tiina E. K. Jarvinen, Henrik Holmberg, Pekka Ahtila, Theoretical Potential to Convert Excess Heat into Mechanical Work in the Finnish Industry, *Chemical Engineering Transactions,* Volume 35, 2013, Pages 253 – 258

[48] R. Gheith et al., 'Study of the regenerator constituting material influence on a gamma type Stirling engine', Journal of Mechanical Science and Technology 26 (4) (2012) 1251~1255

[49] Nayak A. O. et al., 'Simulation studies of solar water heater with Vapor Adsorption material', proceedings of International Conference on Simulation Modelling and Analysis, jointly held by National Institute of Technology, Calicut, India and Amrita University, Coimbatore India, December 2011.

[50] Nitish Hirve, 'Thermodynamic analysis of a Stirling engine using second order isothermal and adiabatic models for application in micropower generation system', MSME thesis, University of Washington, March, 2015.

[51] William R. Martini, 'Stirling Engine Design Manual', Second Edition, 1983.

[52] Jose Martinez, 'Some mathematical models to describe the dynamic behavior of the B-10 free-piston Stirling engine', Master of Science in Mechanical Engineering Thesis, Ohio State University, 1994.

[53] Graham Walker, 'Stirling Engines', 1980.

[54] Nayak A. O. et al., 'Ocean Thermal Energy Stirling Power Plant (OTE-SPP), Proceeding of World Congress on Engineering 2012, London, UK.

[55] Nayak A. O. et al., 'Modified Stirling Engine with Multiple Pistons', 3161/CHE/2012, Office Journal of the Patent Office, India, Issue No: 42/2012, October 2012.

[56] Timoumi et al., 'Design and performance optimization of GPU-3 Stirling engines', Energy 33 (2008) 1100–1114, Science Direct, Elsevier.

[57] Johannes Matthias Strauss, 'Direct Piston Displacement Control of Free Piston Stirling Engines', Dissertation work for Doctor of Philosophy degree in Faculty of Engineering, Stellenbosch University, December 2013.

APPENDIX

A. Stirling energy flow diagram

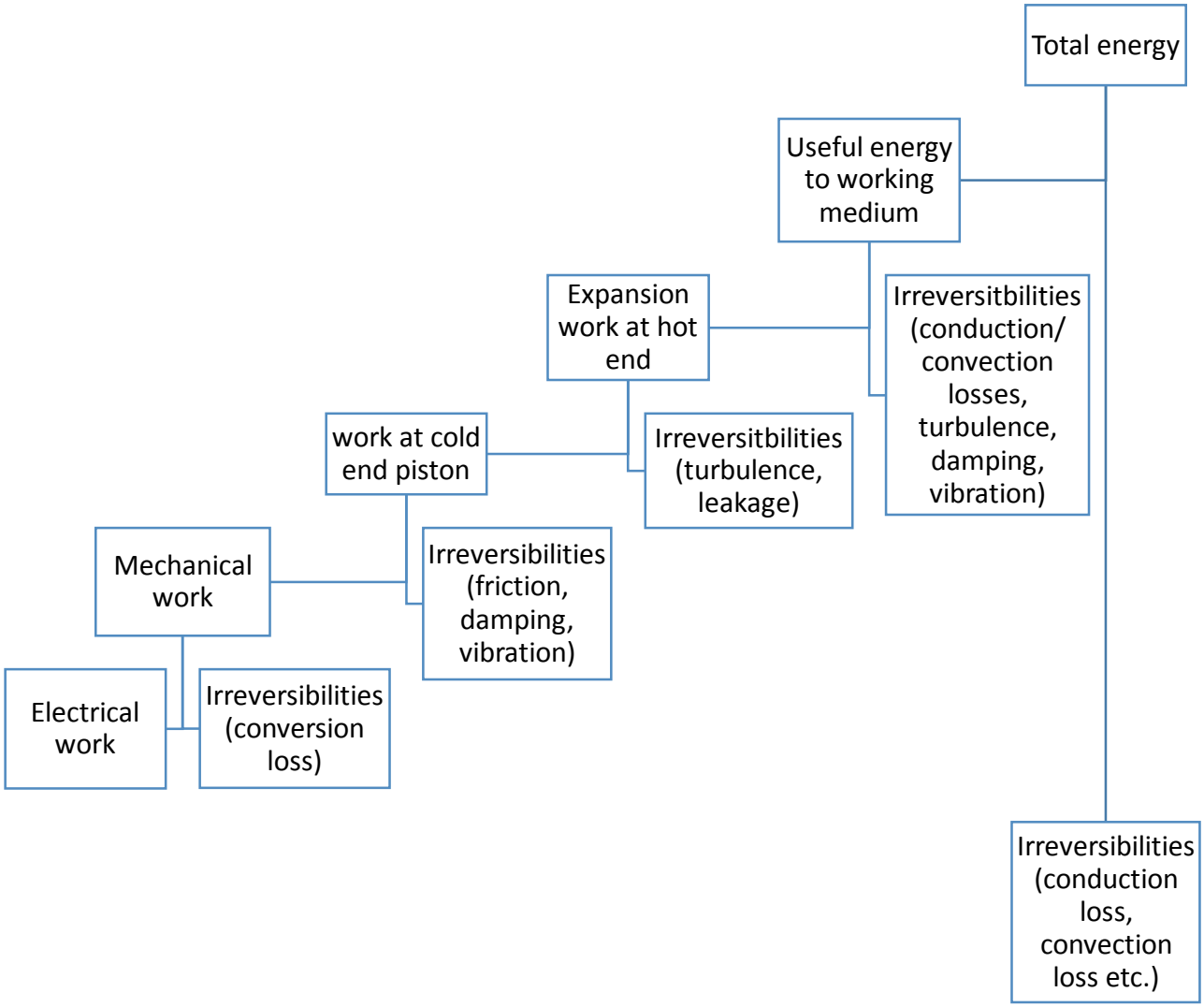

The above flow chart is a simple energy flow diagram representing a Stirling system where useful energy and possible irreversibilities at different stages have been shown.

B. MATLAB code integrating dynamic and thermodynamic analysis

[Adiabatic analysis subroutine]

```
%ADIABATIC ANALYSIS

%Nomenclature

% Ve(j,i)=Maximum Hot end volume,
% Vhe=Hot end heat exchanger volume
% Vhd=hot end dead volume
% Vc(j,i)=Cold end volume
% Vc(j,i)e=cold end heat exchanger volume
% Vc(j,i)d=cold end dead volume
% Vd=cold end maximum displacer volume
% Vp=cold end maximum piston volume
% Vr=regenerator volume

% The=hot end heat exchanger temperature
% Tce=cold end heat exchanger temperature
% Tr=regenerator temperature
% Te=expansion space temperature
% Tc=compression space temperature
% me=expansion space mass
% meh=hot end heaat exchanger mass
% mr=regenerator mass
% mc=compression space mass
% mec=cold end heat exchanger mass
% p=instantaneous pressure
% r=Co/Cv for the working gas
% R=gas constant;
% f=crank angle
% AL=phase lag

%Define constant values

R=2.0679*1000;
r=1.666666672;
Cp=5.1926*1000;
Cv=3.1156*1000;
Power=zeros(1,90);
efficiency=zeros(1,90);
clearance=zeros(1,90);
```

```
m=input('Enter the crank angle increment in degrees : ');
k=input('\nEnter number of iterations : ');
AL=pi/180*90;

%Set engine dimensions

% totalv=740;
% vupper=740;
% lbyd=0.5;
% Di=7;
% Do=1.5*Di;
% s=Di*lbyd;
% Dpis=6;
% Lp=Dpis*lbyd;
% h=0.5;              %clearance
% Ld=5;               %displacer height
% Li=s+Ld;            %inner cylinder height
% Lo=Li+(2*h);        %outer cylinder height
% Lr=0.5*Lo;          %Regenerator height
% Ltop=(Lo-Lr)/2;     %hot & cold end heat exchanger heights
                      % area=pi/4*Do*Do;

Vhe=input('Enter hot end heat exchanger volume in cm3: ');
Vce=input('Enter cold end heat exchanger volume in cm3: ');
Vr=input('Enter regenerator section volume in cm3: ');

%Set initial conditions
Th=input('Hot end heat exchanger temperature in K: ');
Tk=input('Cold end heat exchanger temperature in K: ');
Tr=(Th-Tk)/log(Th/Tk);

angle=input('Enter the total crank angle (in degrees): ');
n=(angle/m)+1;
cyc=angle/360;

p=zeros(k,n);
Ve=zeros(k,n);
Vc=zeros(k,n);
v=zeros(k,n);
Te=zeros(k,n);
Tc=zeros(k,n);
p(1,1)=input('\nInitial charging pressure in MPa: ');
```

```
W1=zeros(k,n);

%Volume arrays

Vem=input('Enter expansion end working volume in cm3: ');
Vp=input('Enter compression end working volume in cm3: ');
Vcm=Vem;
Vd=Vem+Vp;
Ved= input('Enter expansion space dead volume in cm3: ');
Vcd= input('Enter compression space dead volume in cm3: ');

Ve(1,1)=(Vd/2*(1-cos(m*pi/180)));   %Start with displacer
at topmost position
Vc(1,1)=(Vd/2*(1+cos(m*pi/180))+Vp/2*(1-cos((m*pi/180)-
(AL))));
Vpiston=zeros(k,n);
Vcompression=zeros(k,n);
v=zeros(k,n);
v(1,1)=Vc(1,1)+Ve(1,1)+Vr+Vhe+Vce;
v(2,1)=v(1,1);

%Mass arrays

Dmc=zeros(k,n);
gAck=zeros(k,n);
gAkr=zeros(k,n);
gArh=zeros(k,n);
gAhe=zeros(k,n);
Dmce=zeros(k,n);
Dmr=zeros(k,n);
Dmhe=zeros(k,n);
mce=zeros(k,n);
mhe=zeros(k,n);
mr=zeros(k,n);
me=zeros(k,n);
mc=zeros(k,n);
meact=zeros(k,n);

%Work and Heat arrays

DQk=zeros(k,n);
Qk=zeros(k,n);
DQr=zeros(k,n);
```

```
Qr=zeros(k,n);
DQh=zeros(k,n);
Qh=zeros(k,n);
DW=zeros(k,n);

%Other arrays

f=zeros(k,n);
fd=zeros(k,n);
dexp=zeros(k,n);
dcomp=zeros(k,n);
num=zeros(k,n);
den=zeros(k,n);
Dp=zeros(k,n);

Tck=Tc(1,1);
The=Th;

term=r*((Vce/Tck)+(Vr/Tr)+(Vhe/The));

M=(p(1,1)*(Ve(1,1)+Ved)/R/Th)+(p(1,1)*(Vc(1,1)+Vcd)/R/Tk)+(
p(1,1)*Vr/R/Tr)+(p(1,1)*Vhe/R/Th)+(p(1,1)*Vce/R/Tk);
mr(1,1)=(p(1,1)*Vr/R/Tr);
mhe(1,1)=(p(1,1)*Vhe/R/Th);
mce(1,1)=(p(1,1)*Vce/R/Tk);
mc(1,1)=(p(1,1)*(Vc(1,1)+Vcd)/R/Tk);

Te(1,1)=Th;
Tc(1,1)=Tk;

for j=1:k
    Ve(j,1)=(Vd/2*(1-cos(m*pi/180))); %Start with displacer
at topmost position
    Vc(j,1)=(Vd/2*(1+cos(m*pi/180))+Vp/2*(1-cos((m*
    pi/180)-(AL))));
    Vpiston(j,1)=Vp/2*(1-cos((m* pi/180)-(AL)));
    Vcompression(j,1)=Vd/2*(1+cos(m*pi/180));
    v(j,1)=Vc(j,1)+Ve(j,1)+Vce+Vhe+Vr+Ved+Vcd;
    mr(j,1)=(p(j,1)*Vr/R/Tr);
    mhe(j,1)=(p(j,1)*Vhe/R/Th);
    mce(j,1)=(p(j,1)*Vce/R/Tk);
    mc(j,1)=(p(j,1)*(Vc(j,1)+Vcd)/R/Tc(j,1));
    me(j,1)=M-(mr(j,1)+mc(j,1)+mhe(j,1)+mce(j,1));
```

```
    Te(j,1)=p(j,1)*(Ve(j,1)+Ved)/R/me(j,1);
    Tck=Tc(j,1);
    The=Th;

for i=2:n
    fd(j,i)=i*m;
    f(j,i)=i*m*pi/180;
    Ve(j,i)=(Vem/2*(1-cos(f(j,i))));
    dexp(j,i-1)=Ve(j,i)-Ve(j,i-1);
    Vc(j,i)=(Vd/2*(1+cos(f(j,i)))+Vp/2*(1-cos(f(j,i)-AL)));
    dcomp(j,i-1)=Vc(j,i)-Vc(j,i-1);
    Vcompression(j,i)=Vd/2*(1+cos(f(j,i)));
    Vpiston(j,i)=Vp/2*(1-cos(f(j,i)-AL));
    v(j,i)=Vc(j,i)+Ve(j,i)+Vce+Vhe+Vr+Vcd+Ved;
    num(j,i)=-r*p(j,i-1)*(((dcomp(j,i-1))/Tck)+(((dexp(j,i-
    1))/The)));
    term=r*((Vce/Tck)+(Vr/Tr)+(Vhe/The));
    den(j,i)=((Vc(j,i)+Vcd)/Tck)+term+((Ve(j,i)+Ved)/The);
    Dp(j,i)=num(j,i)/den(j,i);

    p(j,i)=p(j,i-1)+Dp(j,i);

    Dmc(j,i)=(((p(j,i)*dcomp(j,i- 1))+(Vc(j,i)+Vcd)*
    Dp(j,i)/r))/(R*Tck);
    mc(j,i)=mc(j,i-1)+Dmc(j,i);
    mr(j,i)=(p(j,i)*Vr/R/Tr);
    mhe(j,i)=(p(j,i)*Vhe/R/Th);
    mce(j,i)=(p(j,i)*Vce/R/Tk);
    me(j,i)=M-(mc(j,i)+mr(j,i)+mhe(j,i)+mce(j,i));
    meact(j,i)=p(j,i)*Ve(j,i)/R/Te(j,i);

    Tc(j,i)=p(j,i)*(Vc(j,i)+Vcd)/R/mc(j,i);
    Te(j,i)=p(j,i)*(Ve(j,i)+Ved)/R/me(j,i);

    Dmce(j,i)=mce(j,i)*Dp(j,i)/p(j,i);
    Dmr(j,i)=mr(j,i)*Dp(j,i)/p(j,i);
    Dmhe(j,i)=mhe(j,i)*Dp(j,i)/p(j,i);

    gAck(j,i)=-Dmc(j,i);
    gAkr(j,i)=gAck(j,i)-Dmce(j,i);
    gArh(j,i)=gAkr(j,i)-Dmr(j,i);
    gAhe(j,i)=gArh(j,i)-Dmhe(j,i);
```

```
    if gAck(j,i)>0
        Tck=Tc(j,i);
        Tkr=Tk;
    else
        Tck=Tk;
        Tkr=Tk;
    end
    if gAhe(j,i)>0
        The=Th;
        Trh=Th;
    else
        The=Te(j,i);
        Trh=Th;
    end

    DW(j,i)=(p(j,i)+p(j,i-1))/2*(dcomp(j,i-1)+dexp(j,i-1));
    W1(j,i)=W1(j,i-1)+DW(j,i);

    DQk(j,i)=((Vce)*Dp(j,i)*Cv/R)-Cp*((Tck*gAck(j,i))-
    (Tkr*gAkr(j,i)));
    Qk(j,i)=Qk(j,i-1)+DQk(j,i);
    DQr(j,i)=(Vr*Dp(j,i)*Cv/R)-Cp*((Tkr*gAkr(j,i))-
    (Trh*gArh(j,i)));
    Qr(j,i)=Qr(j,i-1)+DQr(j,i);
end
    p(j+1,1)=p(j,n);
    Tc(j+1,1)=Tc(j,n);
end

disp('Compression ratio for the engine = ');
disp(max(v(:))/min(v(:)));
Qh(k,n)=W1(k,n)-Qk(k,n);
disp('Heat given per cycle in J = ');
disp(Qh(k,n)/cyc);
disp('Heat rejected per cycle in J = ');
disp(Qk(k,n)/cyc);
disp('Regenerator net heat per cycle in J = ');
disp(Qr(k,n)/cyc);
temp=(W1(k,n)+Qh(k,n)+Qk(k,n))/2;
disp('Work output per cycle in J = ');
disp((W1(k,n))/cyc);
disp('Efficiency of the engine in percentage = ');
```

```
disp((W1(k,n)/Qh(k,n))*100);
disp('Power for 41.67Hz operating frequency in W = ');
disp(W1(k,n)*41.67/cyc);
disp(mean(p(k,1:n)));
```

[Dynamic analysis subroutine]

```
%% DYNAMIC ANALYSIS
% Nomenclature
format long;
w_op=zeros(n,1);                              %operating
frequency of the system
rpm_op=zeros(n,1);                            %operating rpm of
the system
m_c=input('\nEnter total mass of stationary cylinder
components or casing in kg: '); %total mass of stationary
cylinder components in kg

t_design=input('\n\nEnter 1 for flywheel design or 2 for
spring based Stirling design: ');

if t_design == 1
        m_fly=input('\n\nEnter mass of flywheel in kg: ');
        K_const=input('\nEnter inertia constant of flywheel
       (depends upon shape of flywheel): ');
        r_fly=input('\nRadius of flywheel in metres: ');
        f_des=input('\nEnter design angular velocity in rps
        or design frequency in Hz:');
        cp_str=input('\nEnter cold end piston or power
        piston stroke in mm: ');
        hp_str=input('\nHot end piston stroke in mm: ');

%% hot end piston variables
w_hp=zeros(n,1);     %undamped natural resonance frequency
                     of hot end piston
Q_hp=zeros(n,1);      %stored hot end piston energy/energy
      loss per cycle at hot end piston oscillating at w_hp
Q_fly1=zeros(n,1);    %stored flywheel energy with respect
   to hot end piston/energy loss per cycle at flwyheel with
   respect to hot end piston(system at rpm_op)
k_hp=zeros(n,1);              %w_hp=sqrt(k_hp/m_hp)
dp=zeros(n,1);    %pressure variation obtained from
                  thermodynamic analysis
```

```
x_hp=zeros(n,1);  %array to store hot end position values
dx_hp=zeros(n,1); %array to store hot end piston position
                  change with increasing crank angle in metres
D_hp=input('\n\nEnter damping coefficient on hot end piston
     due to viscous forces: ');
D_fly1=input('\nEnter flywheel damping coefficient at hot
       end piston: ');
m_hp=input('\nEnter mass of hot end piston in kg: ');
dia_hp=input('\nEnter diameter of hot end piston in mm: ');
cl_hp=input('\nClearance at hot end piston in mm: ');

A_hp=pi/4*((dia_hp/1000).^2);  %displacer or hot end piston
                                cross-sectional area in m^2
x_hp(1,1)=hp_str/2000*(1+cos(0)); %initial hot end piston
                                   position

%mc from thermodynamic analysis

x_exp=zeros(n,1);   %array to store expansion space
                    displacement values
x_exp(1,1)=hp_str/2000*(1+cos(0))+cl_hp/1000;  %initial
                                    expansion space position
dx_exp=zeros(n,1);   %array t10o store expansion space
                     position change with increasing crank
                     angle in metres at cold end

k_eq1=(K_const*m_fly*r_fly*r_fly*f_des)/(hp_str/1000);
%Approximate equivalent spring stiffness in N/m for the
flywheel at hot end piston
p_eq1(1,1)=(k_eq1*dx_hp(1,1))/A_hp;       %approximate
equivalent spring pressure for the flywheel at hot end
piston
dp_eq1=zeros(n,1);  %array to store varying approximate
equivalent spring pressure for the flywheel at hot end
piston
alpha_p=zeros(n,1);  %thermal coupling between cold end
power piston and hot end piston

%total pressure(p) at each point or crank angle obtained
from thermodynamic analysis
%f(j,i) or phase difference is obtained from thermodynamic
analysis
```

```
%% cold end power piston

opt= input('\nExpected phase difference in degrees: ');
w_cp=zeros(n,1);     %undamped natural resonance frequency
of cold end power piston
Q_cp=zeros(n,1);     %stored cold end power piston
energy/energy loss per cycle at cold end power piston
oscillating at w_cp
Q_fly2=zeros(n,1); %stored flywheel energy with respect to
cold end power piston/energy loss per cycle at flwyheel
with respect to cold end power piston(system at rpm_op)
k_cp=zeros(n,1);     %w_cp=sqrt(k_cp/m_cp)
x_cp=zeros(n,1);     %array to store cold end power piston
                     position values
dx_cp=zeros(n,1);    %array to store cold end power piston
position change with increasing crank angle in metres

D_cp=input('\n\nEnter damping coefficient on cold end power
piston due to viscous forces: ');
D_fly2=input('\nEnter flywheel damping coefficient at cold
end power piston: ');
m_cp=input('\nEnter mass of cold end piston in kg: ');
dia_cp=input('\nDiameter of cold end piston in mm: ');
cl_cp=input('\nClearance at cold end piston in mm: ');

A_cp=pi/4*((dia_cp/1000)^2);  %power piston cross-sectional
                              area in m^2
x_cp(1,1)=cp_str/2000*(1+cos(opt)); %initial cold end power
                                    piston position

%mc from thermodynamic analysis

x_comp=zeros(n,1);  %array to store compression space
                    displacement values
x_comp(1,1)=hp_str/2000*(1+cos(0))+cp_str/2000*(1-cos(0-
AL))+cl_cp/1000;  %initial compression space position
dx_comp=zeros(n,1);     %array to store compression space
postition change with increasing crank angle in metres at
cold end

k_eq2=(K_const*m_fly*r_fly*r_fly*f_des)/(cp_str/1000);
%Approximate equivalent spring stiffness in N/m for the
flywheel at cold end power piston
```

```
p_eq2(1,1)=(k_eq2*dx_cp(1,1))/A_cp; %approximate equivalent
spring pressure for the flywheel at cold end power piston
dp_eq2=zeros(n,1);   %array to store varying spring
                     pressure at power piston
alpha_t=zeros(n,1);  %thermal coupling between hot end
          piston motion and cold end power piston force
alpha=zeros(n,1);    %|alpha_t*alpha_p|

f=zeros(n,1);
fd=zeros(n,1);

str_ratio=zeros(n,1); %Stroke ratio = |Xd/Xp| where Xd is
is the amplitude of the displacer and Xp is the amplitude
of the power piston
phi=zeros(n,1);          %phase angle
phi_d=zeros(n,1);        %phase angle degree

POW=zeros(n,1);    %Engine power

%% Calculations

q=input('\n\nEnter the required taylor series order: ');
syms x
tay_f=exp(x);
tf=taylor(tay_f,x,'Order', q);
tf_v=matlabFunction(tf);
x=m*pi/180;
t_v=feval(tf_v,sqrt(-1)*x);

for i=2:n
    fd(i,1)=i*m;
    f(i,1)=i*m*pi/180;
    dp(i)=(p(k,i)-p(k,i-1))*10^6;

    %hot end piston
    x_exp(i,1)=hp_str/2000*(1+cos(f(i,1)))+cl_hp/1000;
    %instantaneous x_exp
    dx_exp(i,1)=x_exp(i,1)-x_exp(i-1,1);
    x_hp(i,1)=hp_str/2000*(1+cos(f(i,1))); %instantaneous
                                           x_hp
    dx_hp(i,1)=x_hp(i,1)-x_hp(i-1,1);
    p_eq1(i,1)=(k_eq1*dx_hp(i,1))/A_hp;    %instantaneous
                                           p_eq1
```

```
    dp_eq1(i,1)=p_eq1(i,1)-p_eq1(i-1,1);
    k_hp(i,1)=abs(A_hp*((dp(i)/dx_hp(i))-
    ((dp_eq1(i)/dx_hp(i))))-((m_hp/m_c)*(dp(i)/0.00005))-
    ((dp_eq1(i)/dx_hp(i))));
    w_hp(i)=real(sqrt(k_hp(i,1)/m_hp));
    Q_hp(i)=real((w_hp(i)*m_hp)/(2*pi*D_hp));
    Q_fly1(i)=real((w_hp(i)*m_hp)/(2*pi*D_fly1));

    %cold end power piston

    x_comp(i,1)=hp_str/2000*(1+cos(f(i,1)))+cp_str/2000*(1-
    cos(f(i,1)-AL))+cl_cp/1000;    %instantaneous x_comp
    dx_comp(i,1)=x_comp(i,1)-x_comp(i-1,1);
    x_cp(i,1)=cp_str/2000*(1+cos(opt+f(i,1)));
    %instantaneous x_cp
    dx_cp(i,1)=x_cp(i,1)-x_cp(i-1,1);
    p_eq2(i,1)=(k_eq2*dx_cp(i,1))/A_cp;   %instantaneous
                                          p_eq2
    dp_eq2(i,1)=p_eq2(i,1)-p_eq2(i-1,1);
    k_cp(i,1)=abs(A_cp*((dp(i)/dx_cp(i)))-
    ((dp_eq2(i)/dx_cp(i)))-((m_cp/m_c)*(dp(i)/0.00005))-
    ((dp_eq2(i)/dx_cp(i))));
    w_cp(i)=sqrt(k_cp(i,1)/m_cp);
    Q_cp(i)=(w_cp(i)*m_cp)/(2*pi*D_cp);
    Q_fly2(i)=(w_cp(i)*m_cp)/(2*pi*D_fly2);

%operating frequency or rpm

w_op(i)=real((((w_cp(i)*w_hp(i))*((Q_hp(i)*Q_fly1(i))*((Q_f
ly2(i)+Q_cp(i)))+(Q_cp(i)*Q_fly2(i))*(Q_fly1(i)+Q_hp(i))))/
((w_cp(i)*w_hp(i)*Q_fly1(i)*(Q_fly2(i)+Q_cp(i)))+(w_hp(i)*Q
_cp(i)*Q_fly2(i)*(Q_fly1(i)+Q_hp(i))))));
    rpm_op(i)=60*w_op(i);

    % Engine parameters

    alpha_p(i,1)=abs(A_hp*((dp(i)/dx_cp(i)))-
    ((m_cp/m_c)*(dp(i)/0.00005)));
    alpha_t(i,1)=abs(A_cp*((dp(i)/dx_hp(i)))-
    ((m_hp/m_c)*(dp(i)/0.00005)));
    alpha(i)=abs(alpha_t(i,1)*alpha_p(i,1));
    str_ratio(i)=abs((alpha_p(i,1)/k_hp(i,1))*(((1-
    ((w_op(i)/w_hp(i))^2))^2)+(w_op(i)/(2*pi*w_hp(i))*
```

```
    ((1/Q_hp(i))))^2)^(-1/2));
    phi(i,1)=abs(atan((w_op(i)/(2*pi*w_hp(i))*
    ((1/Q_hp(i)))/(((((w_op(i))^2)/((w_hp(i))^2))-1)))));
    phi_d(i,1)=90-(phi(i)*(180/pi));

    X_d(i)=x_hp(i)/(t_v);
    X_p(i)=x_cp(i)/(t_v);

POW(i)=abs(((mean(w_op(i))*me(alpha_t(i))/2)*max(X_d(i))*ma
x(X_p(i)))*sin(max(phi(i))));

end

disp('Power output per cycle from engine in Watts = ');
disp((sum(POW))/cyc);
disp('Average operating frequency of engine in rpm= ');
disp(mean((w_op*60),1));
disp('Stroke-ratio of engine = ');
disp(mean(str_ratio,1));
disp('Optimal Phase difference between displacer and power
piston in degrees = ');
disp(max(phi_d));

elseif( t_design == 2 )

     d_str=input('\nEnter displacer stroke in mm: ');
     p_str=input('\nEnter power piston stroke in mm: ');
     cl_d=input('\nClearance at displacer in mm: ');
     cl_p=input('\nClearance at power piston in mm: ');

%% displacer variables

w_d=zeros(n,1);    %undamped natural resonance frequency of
                   displacer at hot end
Q_d=zeros(n,1);    %stored displacer energy/energy loss per
                   cycle at displacer oscillating at w_d
D_d=input('\n\nEnter damping coefficient on displacer due
to viscous forces: '); %Damping on displacer due to viscous
                       forces
D_s1=input('\nSpring damping coefficient at displacer : ');
%Spring damping coefficient at displacer
lda1=input('\nEnter angle between displacer spring and
horizontal in radians: ');  %angle between displacer spring
                            and horizontal in radians
```

```
del1=(sin(lda1))^2;     %spring orientation coefficient at
                        displacer
Q_s1=zeros(n,1);  %stored spring energy at displacer/energy
   loss per cycle at spring of displacer oscillating at w_d
m_d=input('\nEnter mass of hot end displacer in kg: ');
                          %mass of hot end displacer in kg
k_d=zeros(n,1);                          %w_d=sqrt(k_d/m_d)
dia_d=input('\nEnter displacer diameter in mm : ');   %70
A_d=pi/4*((dia_d/1000)^2);   %displacer cross-sectional
                             area in m^2
dp=zeros(n,1);          %pressure variation obtained from
                        thermodynamic analysis
x_d=zeros(n,1);   %array to store displacer position values
x_d(1,1)=d_str/2000*(1+cos(0)); %initial displacer position
dx_d=zeros(n,1);  %array to store displacer position change
          with increasing crank angle in metres at hot end

%mc from thermodynamic analysis

x_e=zeros(n,1);    %array to store expansion space
                   displacement values
x_e(1,1)=d_str/2000*(1+cos(0))+(cl_d/1000);  %initial
                                  expansion space position
dx_e=zeros(n,1);  %array to store expansion space postition
   change with increasing crank angle in metres at cold end

n_s=input('\n\nEnter the number of springs attached to the
displacer: ');  %1 number of springs attached to displacer
k_s=input('\nSpring stiffness at displacer in N/m : ');
%550 spring stiffness in N/m
p_s(1,1)=(k_s*dx_d(1,1))/A_d; %spring pressure at displacer
dp_s=zeros(n,1);    %array to store varying spring pressure
                    at displacer
alpha_p=zeros(n,1);    %thermal coupling between piston and
                       displacer
%total pressure(p) at each point or crank angle obtained
from thermodynamic analysis
%f(j,i) or phase difference is obtained from thermodynamic
analysis
%% power piston

opt= input('\nExpected phase difference in degrees: ');
w_p=zeros(n,1);    %undamped natural resonance frequency of
```

```
                    power piston at cold end
Q_p=zeros(n,1); %stored power piston energy/energy loss per
                cycle at power piston oscillating at w_p
D_p=input('\n\nEnter damping coefficient on cold end power
piston due to viscous forces: ');  %Damping on power piston
                                   due to viscous forces
D_s2=input('\nEnter spring damping coefficient at cold end
power piston: ');    %Spring damping coeff. at power piston
lda2=input('\nEnter angle between cold end power piston
spring and horizontal in radians: ');    %pi/2 angle
between power piston spring and horizontal in radians
del2=(sin(lda2))^2;  %spring orientation coefficient at
power piston
Q_s2=zeros(n,1);        %stored spring energy at power
piston/energy loss per cycle at spring of power piston
oscillating at w_p
m_p=input('\nEnter mass of cold end power piston in kg: ');
%mass of cold end power piston in kg
k_p=zeros(n,1);                        %w_p=sqrt(k_p/m_p)

dia_p=input('\nEnter cold end power piston diameter in mm:
');
A_p=pi/4*((dia_p/1000)^2);   %power piston cross-sectional
                             area in m^2
x_p=zeros(n,1);     %array for power piston position values
x_p(1,1)=p_str/2000*(1+cos(opt));    %initial power piston
                                     position
dx_p=zeros(n,1);   %array to store power piston position
change with increasing crank angle in metres at cold end
%mc from thermodynamic analysis

x_c=zeros(n,1);         %array to store compression space
                        displacement values
x_c(1,1)=d_str/2000*(1+cos(0))+p_str/2000*(1-cos(0-
AL))+(cl_p/1000);  %initial compression space position
dx_c=zeros(n,1);        %array to store compression space
postition change with increasing crank angle in metres at
cold end

n_s2=input('\n\nEnter number of springs attached to cold
end power piston: ');    %number of springs attached to
                         power piston
```

```
k_s2=input('\nEnter spring stiffness at cold end power
piston in N/m: ');          %spring stiffness in N/m
p_s2(1,1)=(k_s2*dx_p(1,1))/A_p; %displacer spring pressure
dp_s2=zeros(n,1);     %array for varying spring pressure at
                      power piston

alpha_t=zeros(n,1);   %thermal coupling between displacer
                      motion and power piston force
alpha=zeros(n,1);                       %|alpha_t*alpha_p|
f=zeros(n,1);
fd=zeros(n,1);
goc=zeros(n,1);             %General oscillation criterion
str_ratio=zeros(n,1);       %Stroke ratio = |Xd/Xp| where Xd
is the amplitude of the displacer and Xp is the amplitude
of the power piston
phi=zeros(n,1);                  %phase angle
phi_d=zeros(n,1);                %phase angle degree
POW=zeros(n,1);                  %Engine power

%% Calculations
q=input('\n\nEnter the required taylor series order: ');
syms x
tay_f=exp(x);
tf=taylor(tay_f,x,'Order', q);
tf_v=matlabFunction(tf);
x=m*pi/180;
t_v=feval(tf_v,sqrt(-1)*x);

for i=2:n
    fd(i,1)=i*m;
    f(i,1)=i*m*pi/180;
    dp(i)=(p(k,i)-p(k,i-1))*10^6;

    %displacer
    x_e(i,1)=d_str/2000*(1+cos(f(i,1)))+(cl_d/1000);
    %instantaneous x_e
    dx_e(i,1)=x_e(i,1)-x_e(i-1,1);
    x_d(i,1)=d_str/2000*(1+cos(f(i,1))); %instantaneous x_d
    dx_d(i,1)=x_d(i,1)-x_d(i-1,1);
    p_s(i,1)=(k_s*dx_d(i,1))/A_d;     %instantaneous p_s
    dp_s(i,1)=p_s(i,1)-p_s(i-1,1);
    k_d(i,1)=abs(A_d*((dp(i)/dx_d(i))-(n_s*del1*
```

```
    (dp_s(i)/dx_d(i))))-((m_d/m_c)*(dp(i)/0.00005))-(n_s*
    del1*(dp_s(i)/dx_d(i))));
    w_d(i)=real(sqrt(k_d(i,1)/m_d));
    Q_d(i)=real((w_d(i)*m_d)/(2*pi*D_d));
    Q_s1(i)=real((w_d(i)*m_d)/(2*pi*D_s1));

    %power piston
    x_c(i,1)=d_str/2000*(1+cos(f(i,1)))+p_str/2000*(1-
    cos(f(i,1)-AL))+(cl_p/1000);    %instantaneous x_c
    dx_c(i,1)=x_c(i,1)-x_c(i-1,1);
    x_p(i,1)=p_str/2000*(1+cos(opt+f(i,1)));
                                        %instantaneous x_p
    dx_p(i,1)=x_p(i,1)-x_p(i-1,1);
    p_s2(i,1)=(k_s2*dx_p(i,1))/A_p;   %instantaneous p_s2
    dp_s2(i,1)=p_s2(i,1)-p_s2(i-1,1);
    k_p(i,1)=abs(A_p*((dp(i)/dx_p(i)))-(n_s2*del2*
    (dp_s2(i)/dx_p(i)))-((m_p/m_c)*(dp(i)/0.00005))-
    (n_s2*del2*(dp_s2(i)/dx_p(i))));
    w_p(i)=sqrt(k_p(i,1)/m_p);
    Q_p(i)=(w_p(i)*m_p)/(2*pi*D_p);
    Q_s2(i)=(w_p(i)*m_p)/(2*pi*D_s2);

    %operating frequency

w_op(i)=real((((w_p(i)*w_d(i))*((Q_d(i)*Q_s1(i))*((Q_s2(i)+
del2*Q_p(i)))+(Q_p(i)*Q_s2(i))*(Q_s1(i)+del1*Q_d(i))))/((w_
p(i)*w_d(i)*Q_s1(i)*(Q_s2(i)+del2*Q_p(i)))+(w_d(i)*Q_p(i)*Q
_s2(i)*(Q_s1(i)+del1*Q_d(i))))));

    %General oscillation criterion
    alpha_p(i,1)=abs(A_d*((dp(i)/dx_p(i)))-((m_p/m_c)*
    (dp(i)/0.00005)));
    alpha_t(i,1)=abs(A_p*((dp(i)/dx_d(i)))-((m_d/m_c)*
    (dp(i)/0.00005)));
    alpha(i)=abs(alpha_t(i,1)*alpha_p(i,1));

goc(i)=abs(m_d*m_p*(w_op(i)+w_d(i))*(w_op(i)+w_p(i))*
sqrt(((w_op(i)-w_d(i))^2)+((w_d(i)/(4*pi))*((1/Q_d(i))+
(del1/Q_s1(i)))^2))*sqrt(((w_op(i)-w_p(i))^2)+
((w_p(i)/(4*pi))*((1/Q_p(i))+(del2/Q_s2(i)))^2)));
    if (alpha(i)-goc(i)>=0)
       semilogy(fd(i),alpha(i)-goc(i));
```

```
        %checking for damped system characteristics
        title('General oscillation criterion Vs. Crank angle
        in degrees');
        xlabel('Crank angle in degrees');
        ylabel('Oscillation condition - log scale to base
        10');
        hold on
    end

    str_ratio(i)=abs((alpha_p(i,1)/k_d(i,1))*
    (((1-((w_op(i)/w_d(i))^2))^2)+(w_op(i)/(2*pi*w_d(i))*
    ((1/Q_d(i))+(del1/Q_s1(i))))^2)^(-1/2));

phi(i,1)=abs(atan((w_op(i)/(2*pi*w_d(i))*((1/Q_d(i))+(del1/
Q_s1(i)))/(((((w_op(i))^2)/((w_d(i))^2))-1)))));
    phi_d(i,1)=90-(phi(i)*(180/pi));

    X_d(i)=x_d(i)/(t_v);
    X_p(i)=x_p(i)/(t_v);

POW(i)=abs(((mean(w_op(i))*max(alpha_t(i))/2)*max(X_d(i))*m
ax(X_p(i)))*sin(max(phi(i))));
end

disp('Power output per cycle from engine in Watts = ');
disp((sum(POW))/cyc);
disp('Average operating frequency of engine in Hertz= ');
disp(mean(w_op,1));
disp('Stroke-ratio of engine = ');
disp(mean(str_ratio,1));
disp('Optimal Phase difference between displacer and power
piston in degrees = ');
disp(mean(phi_d));
end
```

C. Drafting and manufacturing photos of engine

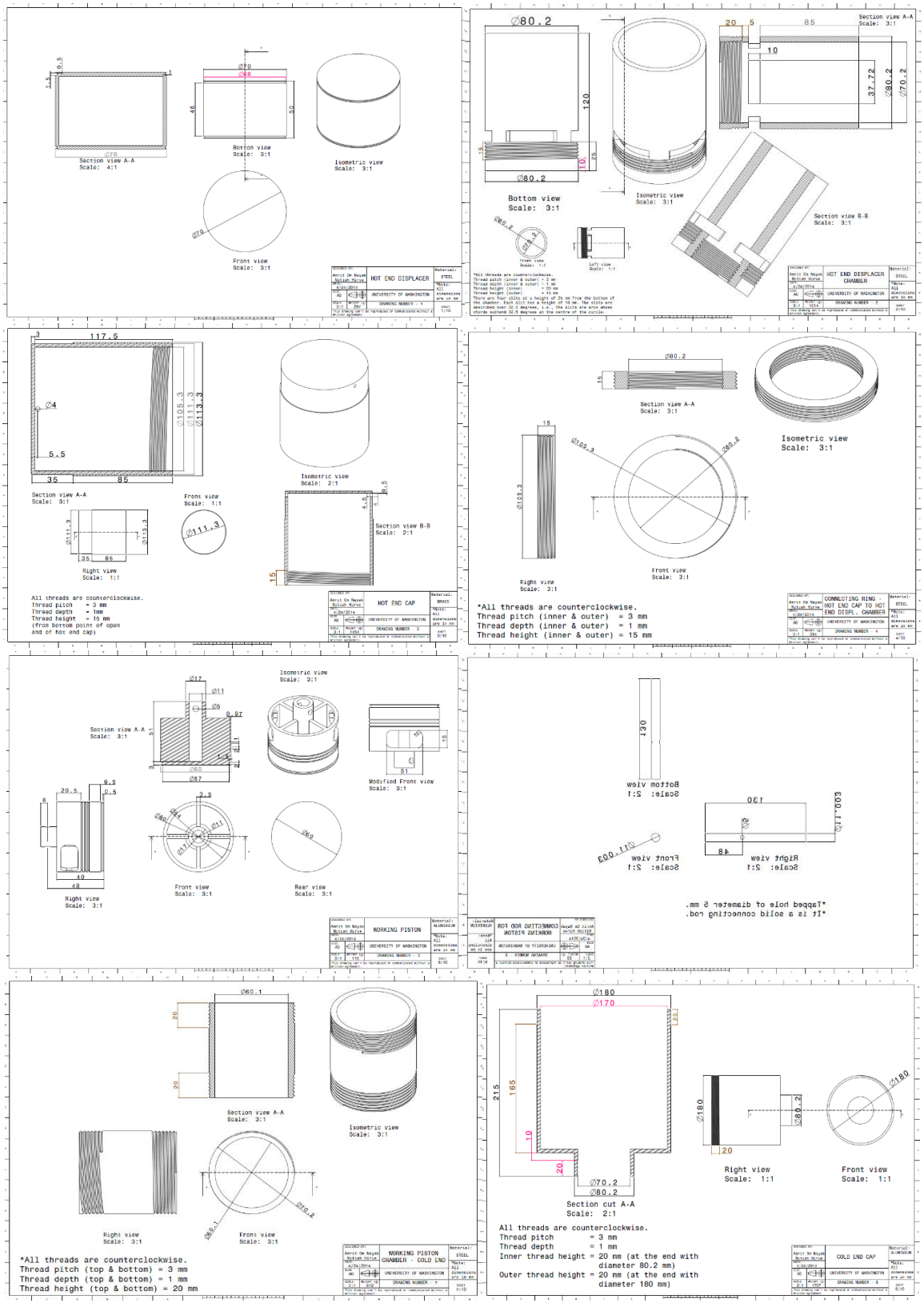

Figure 81 Design and manufacturing photos of free piston Stirling engine parts

Figure 82 Photographs of the modified engine